Nitrate budget and cycling in the east China seas revealed by stable nitrogen isotopes

Dissertation

with the aim of achieving a doctoral degree

at the Faculty of Mathematics, Informatics and Natural Sciences

Department of Earth Sciences

at Universität Hamburg

submitted by

Shichao Tian

Hamburg, 2022

Department of Earth Sciences

Date of Oral Defense: 13 04, 2022

Reviewers: Prof. Kay-Christian Emeis
                                         Dr. Birgit Gaye

Members of the examination   Chair: Prof. Kay-Christian Emeis
commission: Deputy chair: Dr. Birgit Gaye
                                         Dr. Thomas Pohlmann
                                         Dr. Niko Lahajnar
                                         Dr. Kirstin Dänke

Chair of the Subject Doctoral   Prof. Dr. Hermann Held
Committee Earth System Sciences:

Dean of Faculty MIN: Prof. Dr. Heinrich Graener

Eidesstattliche Versicherung | Declaration on Oath

Hiermit erkläre ich an Eides statt, dass ich die vorliegende Dissertationsschrift selbst verfasst und keine anderen als die angegebenen Quellen und Hilfsmittel benutzt habe.
|
I hereby declare upon oath that I have written the present dissertation independently and have not used further resources and aids than those stated.

Ort,den | City,date   Unterschrift | Signature

Abstract

The east China seas comprise one of the broadest continental shelves around the world and have experienced increasing input of anthropogenic reactive nitrogen (N_r) in recent decades. The supply of nutrients, markedly that of N_r, via fluvial and atmospheric transport has strongly increased in parallel with the growing population. The excess N_r created numerous ecological problems, such as increasing incidences of macroalgae blooms, harmful algae blooms, and more frequent occurrence of low oxygen regions near the estuaries. The cycling of N_r in the east China seas therefore is a potentially important ecosystem function mitigating effects of anthropogenic nitrogen inputs. Therefore, it is crucial to quantify the N_r input to this region, and to determine the quantities of nitrogen eliminated in and exported from it.

Samples of water, suspended matter and sediments were taken in the Bohai Sea (BHS) and Yellow Sea (YS) in spring (March and April) and summer (July and August) 2018. The Yellow River (YR) was sampled in May, July to November and Daliao River, Hai River, Luan River and Xiaoqing River were sampled in November 2018. In addition to nutrients, particulate organic carbon, the dual isotopes of nitrate ($\delta^{15}N$ and $\delta^{18}O$), nitrogen contents and $\delta^{15}N$ of suspended matter and sediments were determined in order to identify nitrogen sources and better constrain nitrogen budgets.

First, based on the available mass fluxes and isotope data, we propose an updated nitrogen budget of the BHS. Compared to previous estimates, it is more complete and includes the impact of interior cycling (nitrification) on the nitrate pool. The main nitrate sources are rivers contributing 19.2–25.6 % and the combined terrestrial runoff (including submarine fresh groundwater discharge of nitrate) accounting for 27.8–37.1 % of the nitrate input to the BHS while atmospheric input contributes 6.9–22.2 % to total nitrate. An unusually active interior nitrogen cycling contributes 40.7–65.3 % to total nitrate via nitrification. Nitrogen is mainly trapped in the BHS and mainly removed by sedimentation (70.4–77.8 %) and only very little is exported to the YS (only 1.8–2.4 %). At present denitrification is active in the sediments and removes 20.4–27.2 % of nitrate

from the pool.

Second, we compared the different seasonal dissolved inorganic nitrogen (DIN) variation between the north and south Yellow Sea Cold Water Masses (YSCWM). The nitrate concentration decreased from 2.41 ± 1.58 µmol L^{-1} in spring to 0.81 ± 0.61 µmol L^{-1} in summer in the northern part of the YSCWM. In contrast, nitrate increased from 5.49 ± 2.24 µmol L^{-1} to 7.58 ± 2.20 µmol L^{-1} in the southern part, accompanied by a decrease in $\delta^{15}N\text{-}NO_3^-$ and $\delta^{18}O\text{-}NO_3^-$ from values near 10.0 ‰ in the southern deep-water mass to values of about 5.0 ‰. The increasing nitrate concentration and decreasing $\delta^{15}N\text{-}NO_3^-$ and $\delta^{18}O\text{-}NO_3^-$ values of nitrate are indicative of nitrification that was a significant source of recycled nitrate in the southern part of YSCWM. To quantify this regenerated nitrate, we use a mixing model with end members of preformed nitrate in spring and regenerated nitrate in summer both, with their distinct dual isotope values. The values of $\delta^{15}N$ and $\delta^{18}O$ for regenerated nitrate were first constrained as 3.3 ‰ and 0.9 ‰, respectively. The results of the combined mass and isotope balance model suggest that in the southern YSCWM, in summer 65 % of the nitrate was regenerated and only 35 % was a residual of nitrate preformed in spring.

Our findings indicate that the northern part of YSCWM is a sink of N_r in the sub-thermocline water column, mainly because of denitrification in sediments. In contrast, the BHS and southern pool of YSCWM are a growing reservoir of regenerated terrestrial reactive nitrogen, the addition of which compensates for the removal by co-occurring sediment denitrification. The excess terrestrial nitrogen, delivered mainly by Changjiang River to the south YS and YR to the BHS, has already exhausted the attenuation capacity for N_r of those regions. In consequence, the BHS and southern YS are facing a higher ecological risk than the northern YS, when excess N_r discharge from Changjiang River and YR continues at present levels or even increases. A further eutrophication of the BHS and southern YS could induce water column hypoxia, as is increasingly observed in other marginal seas and seasonally off river mouths.

Zusammenfassung

Die ostchinesischen Meere befinden sich auf einem der weltweit breitesten Festlandsockel und haben in den letzten Jahrzehnten einen zunehmenden Eintrag von anthropogenem reaktivem Stickstoff (N_r) erfahren. Die Zufuhr von Nährstoffen, insbesondere von Nr, über fluviatilen und atmosphärischen Transport hat parallel zur wachsenden Bevölkerung stark zugenommen. Der Nr-Überschuss verursachte zahlreiche ökologische Probleme, wie z. B. zunehmendes Auftreten von Makroalgenblüten, schädliche Algenblüten und häufigeres Auftreten von Regionen mit niedrigem Sauerstoffgehalt in der Nähe der Flussmündungen. Der Kreislauf von Nr in den ostchinesischen Meeren ist daher eine potenziell wichtige Ökosystemfunktion, die die Auswirkungen anthropogener Stickstoffeinträge mildert. Daher ist es entscheidend, den Nr-Eintrag in diese Region zu quantifizieren und die daraus entfernten und exportierten Stickstoffmengen zu bestimmen.

Proben von Wasser, Schwebstoffen und Sedimenten wurden im Frühling (März und April) und Sommer (Juli und August) 2018 in der Bohai-See (BHS) und im Gelben Meer (YS) entnommen. Der Gelbe Fluss (YR) wurde im Mai, Juli bis November 2018 beprobt und die Flüsse Daliao, Hai, Luan und Xiaoqing wurden im November 2018 beprobt. Zusätzlich zu Nährstoffen und partikulärem organischem Kohlenstoff wurden die dualen Isotope von Nitrat ($\delta^{15}N$ und $\delta^{18}O$), Stickstoffgehalte und $\delta^{15}N$ von Schwebstoffen und Sedimenten bestimmt, um Stickstoffquellen zu identifizieren und Stickstoffbudgets besser abzuschätzen.

Auf der Grundlage der verfügbaren Massenflüsse und Isotopendaten wurde ein aktualisiertes Stickstoffbudget der BHS erstellt. Im Vergleich zu früheren Schätzungen ist dieses vollständiger und umfasst die Auswirkungen des inneren Stickstoffkreislaufs (Nitrifikation) auf den Nitratpool. Die wichtigsten Nitratquellen sind Flüsse, die 19,2–25,6 % beitragen, und der kombinierte terrestrische Abfluss (einschließlich submariner Grundwassereinleitungen von Nitrat), die 27,8–37,1 % des Nitrateintrags in das BHS ausmachen, während der atmosphärische Eintrag 6,9–22,2 % zum Gesamtnitrat beiträgt.

Ein ungewöhnlich aktiver innerer Stickstoffkreislauf trägt 40,7–65,3 % zum Gesamtnitrat durch Nitrifikation bei. Stickstoff wird hauptsächlich in der BHS gebunden und hauptsächlich durch Sedimentation entfernt (70,4–77,8 %) und nur sehr wenig in die YS exportiert (nur 1,8–2,4 %). Derzeit ist die Denitrifikation in den Sedimenten effektiv und entfernt 20,4–27,2 % des Nitrats aus dem Becken.

Die saisonalen Schwankungen des gelösten anorganischen Stickstoffs (DIN) und die Unterschiede zwischen den Kaltwassermassen des nördlichen und südlichen Gelben Meeres (YSCWM) wruden verglichen. Die Nitratkonzentrationen sanken von $2,41 \pm 1,58$ µmol L-1 im Frühjahr auf $0,81 \pm 0,61$ µmol L-1 im Sommer im nördlichen Teil des YSCWM. Im Gegensatz dazu stieg Nitrat von $5,49 \pm 2,24$ µmol L-1 auf $7,58 \pm 2,20$ µmol L-1 im südlichen Teil, begleitet von einer Abnahme von $\delta^{15}N$-NO_3- und $\delta^{18}O$-NO_3- von Werten nahe 10,0 ‰ im südlichen Teil Tiefenwassermasse auf Werte um 5,0 ‰ vom Frühjahr zum Sommer. Die zunehmende Nitratkonzentration und die abnehmenden $\delta^{15}N$-NO_3- und $\delta^{18}O$-NO_3-Werte von Nitrat weisen auf Nitrifikation hin, die eine bedeutende Quelle für recyceltes Nitrat im südlichen Teil des YSCWM war. Um dieses regenerierte Nitrat zu quantifizieren, verwenden wir ein Mischungsmodell mit Endgliedern des vorgeformten Nitrats im Frühjahr und regeneriertem Nitrat im Sommer mit ihren unterschiedlichen dualen Isotopenwerten. Die Werte von $\delta^{15}N$ und $\delta^{18}O$ für regeneriertes Nitrat wurden zunächst auf 3,3 ‰ bzw. 0,9 ‰ beschränkt. Die Ergebnisse des kombinierten Massen- und Isotopenbilanzmodells deuten darauf hin, dass im südlichen YSCWM im Sommer 65 % des Nitrats regeneriert wurden und nur 35 % den Nitratrest aus dem Frühjahr ausmachte. Unsere Ergebnisse zeigen, dass der nördliche Teil des YSCWM eine Senke von Nr in der subthermoklinen Wassersäule ist, hauptsächlich aufgrund von Denitrifikation in Sedimenten. Im Gegensatz dazu sind die BHS und der südliche Pool des YSCWM ein wachsendes Reservoir für regenerierten Stickstoff aus dem Landeintrag, dessen vermehrter Eintrag die Entfernung durch die Denitrifikation in den Sedimenten kompensiert. Der starke Eintrag des Stickstoffs vom Land, der hauptsächlich vom Changjiang-Fluss in die südlichen YS und durch gen Gelben Fluss in die BHS erfolgt, hat die Pufferkapazität für Nr dieser Regionen bereits erschöpft. Infolgedessen sind das BHS und das südliche YS einem höheren

ökologischen Risiko ausgesetzt als das nördliche YS, wenn der übermäßige Nr-Eintrag aus dem Changjiang-Fluss und dem Gelben Fluss auf dem derzeitigen Niveau anhält oder sogar zunimmt. Eine weitere Eutrophierung des BHS und des südlichen YS könnte eine Wassersäulenhypoxie induzieren, wie sie zunehmend in anderen Randmeeren und saisonal vor Flussmündungen beobachtet wird.

Table of contents

List of figures

Chapter 1

Chapter 2

Chapter 3

Appendix

Appendix 1

Appendix 3

Appendix 4

Appendix 5

Appendix 6

xvi

List of tables

Chapter 1

Table 1.1. N-Containing Species Important in the Global N Cycle (Zhang et al., 2020). 1

Chapter 2

Table 2.1. Sources and sinks and the corresponding $\delta^{15}N$ and $\delta^{18}O$ values of nitrate in the BHS 52

Table 2.2. Results of sensitivity tests on mass fluxes and isotopes. 55

Chapter 3

Table 3.1. Important parameters in central bottom waters in the Yellow Sea 68

Table 3.2. Comparison of regenerated $[NO_3^-]_r$ and observed nitrate $\Delta[NO_3^-]$ in nCW and sCW. 71

Appendix

Appendix 2

Table A2.1 Summary of results of Chapter 2 ci

Appendix 4

Table A4.1. Two end member values in Bohai Sea civ

Chapter 1 – Introduction

1.1.   The background of marine N cycling

Interest in the marine nitrogen (N) cycle has drawn and is going to draw more attention, because (i) humans have immensely accelerated the global nitrogen cycle, (ii) an obvious underestimation of marine N_2 fixation in the past, and (iii) uncertainties concerning the reaction of marine biology and the marine nitrogen cycle to future climate change (Gruber, 2008a). The reactive nitrogen (N_r, N compounds excluding N_2) is one of the limiting nutrients for life, controlling primary production of the ecosystem. It constitutes many of the biologically relevant macromolecules, such as proteins, nucleic acids and chlorophyll. N_r is an essential nutrient source of life on earth as only few organisms can fix dinitrogen directly from the large atmospheric dinitrogen pool. N_r can participate in redox chemistry with different chemical valence (Table 1.1), it acts as reductant when in the form of ammonium (NH_4^+) and nitrite (NO_2^-), whereas it acts as an oxidant when in the form of nitrate (NO_3^-), as molecular oxygen is scarce in some environments (Figure 1.1). Due to this chemical reactivity N can participate in biological reactions under different redox conditions.

Table 1.1. N-Containing Species Important in the Global N Cycle (Zhang et al., 2020).

form	Molecular formula	Redox state
Ammonium, ammonia	NH_4^+, NH_3	-3
Organic N	$R\text{-}NH_3$	-3
Hydrazine	N_2H_4	-2
Hydroxylamine	NH_2OH	-1
Dinitrogen	N_2	0
Nitrous oxide	N_2O	+1
Nitric oxide	NO	+2

Nitrite, nitrous acid	NO_2^-, NHO_2	+3
Nitrogen dioxide	NO_2	+4
Nitrate, nitric acid	NO_3^-, HNO_3	+5
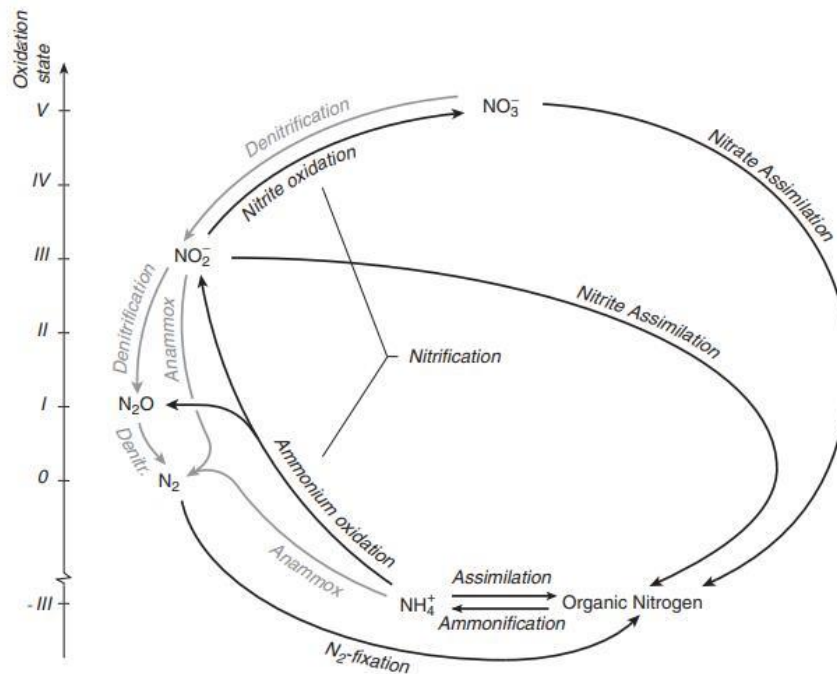
Figure 1.1. Major chemical forms and transformations of nitrogen in the marine environment. The various chemical forms of nitrogen are plotted versus their oxidation state. Processes shown in grey occur in anoxic environments only (Gruber, 2008a).
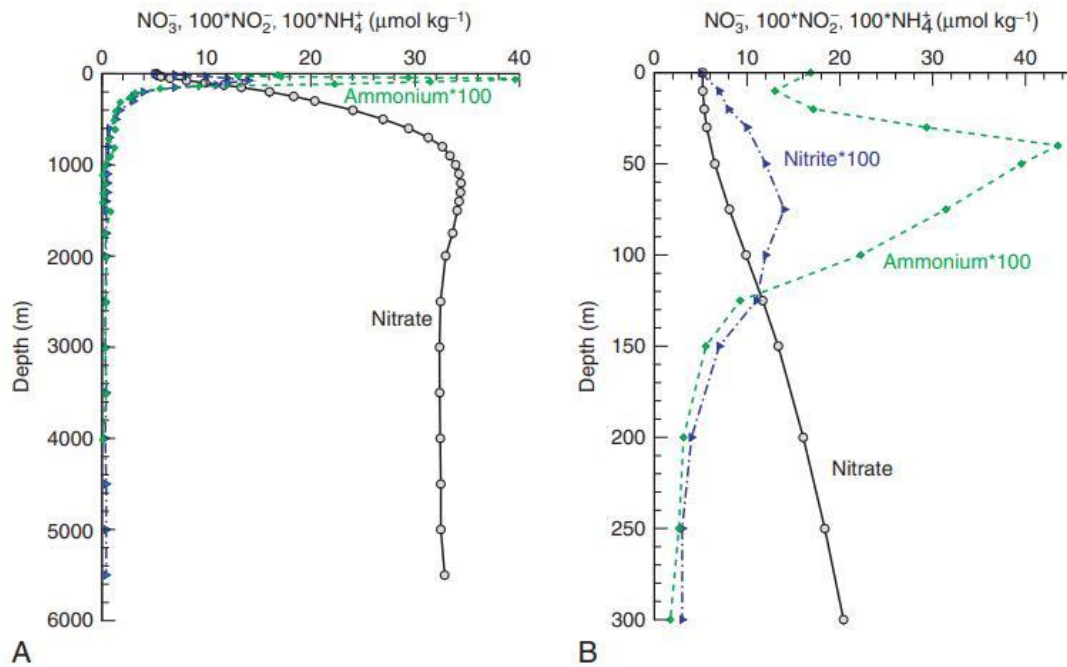
Figure 1.2. Global mean profiles of NO_3^-, NO_2^- and NH_4^+ in the ocean (Gruber, 2008a).
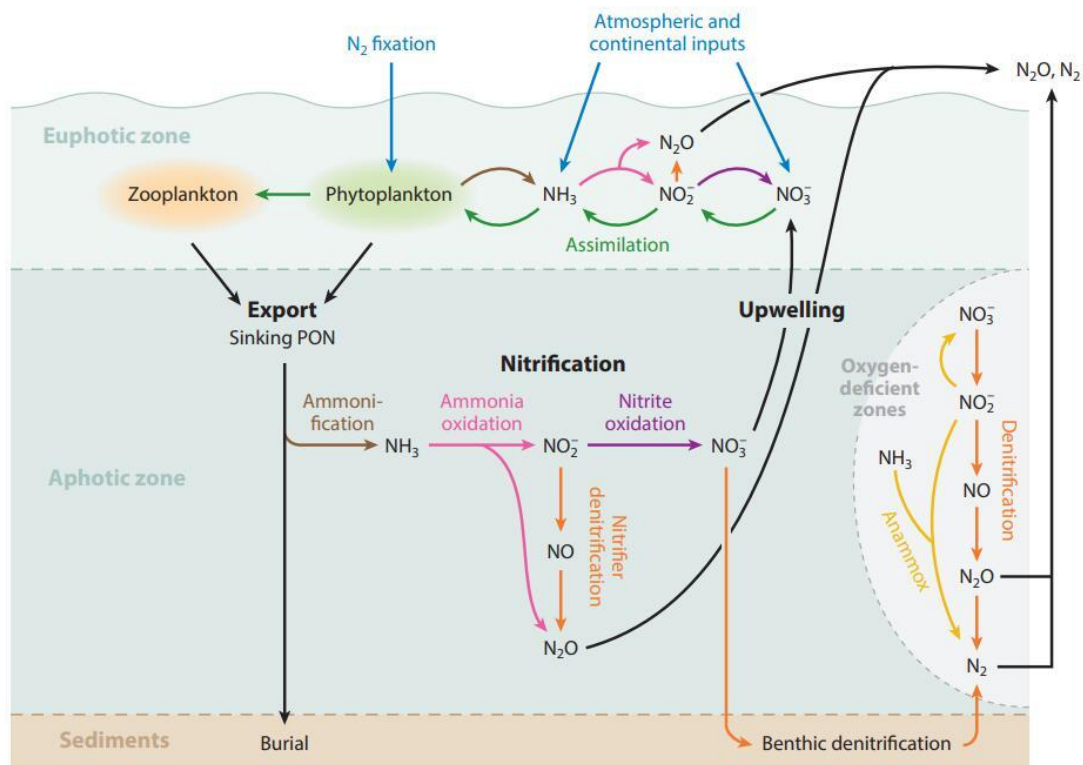
Figure 1.3. Overview of the marine N cycle, with internal cycling processes, sources and sinks (Casciotti, 2016).

The amount of N_r has constantly grown in the earth system since the invention of the Haber-Bosch process, namely by input of additional artificially fixed N_r. In 2001, it had already doubled the natural terrestrial sources of N_r of 63Tg N yr^{-1} (Fowler et al., 2013). Almost half of the human population at the beginning of the twenty-first century depends on fertilizer N for their food (Erisman et al., 2008). The anthropogenic perturbation of N_r had already induced a series of problems. The leakage and volatilization of these artificial N_r has strongly impacted the aquatic system including limnic and marine ecosystems. Differing from the "carbon dioxide problem", the "N problem" is regarded as more local and immediate as it is biologically required and as an environmental redox intermediate (Zhang et al., 2020).

Dissolved inorganic nitrogen (DIN) accounts for over half of the predicted total nitrogen export in Europe and southern Asia, and anthropogenic sources dominate the export of DIN (Seitzinger et al., 2005). In the ocean, the reservoir of N_r was estimated as 6.6×10^5 Tg (Gruber, 2008b) and the primary form of N_r in the ocean is NO_3^-, while NO_2^- and NH_4^+ generally have lower concentrations (Figure 1.2). The N_r reservoir is largely controlled by biological processes which can be divided into two "aspects" (Zhang et al., 2020): (1) The budget of N_r mainly controlled by input by N fixation and output by denitrification and associated microbial processes; (2) the internal cycling of N_r including transformation between different forms, such as assimilation, ammonification, and nitrification. These two aspects of biogeochemical processes constitute cycling in the ocean system (Figure 1.3).

1.2. Biogeochemistry settings of the Chinese marginal seas

The continental margin contributes >10-15 % to the global primary productions and > 40 % of the global carbon sequestration despite its small area (Muller-Karger et al., 2005; Jahnke, 2010; Levin et al., 2015a). Human activities are concentrated near coastal cities and heterogeneously impact on the continental margins via nutrient inputs, freshwater extraction, fishing, construction, species introductions, and contamination, among others (Levin et al., 2015a). Marginal seas are part of the continental margin systems connecting the land and the vast ocean. The Bohai Sea (BHS) and Yellow Sea (YS) are semi-enclosed basins located between the China mainland and Korean Peninsula; they are strongly affected by human activities due to growing industries on shore. Changes of hydrology, nutrient concentrations and sources, and resulting ecosystem responses have therefore progressively intensified during the last decades. The total load of Chinese major estuaries to coastal seas is about 9 % of the global river load for DIN and 1.5% of the global phosphate load, respectively (Smith et al., 2003; Liu et al., 2009a). In the year of 2018, the sea water quality became worse than Seawater Quality Standard Grade I of China (i.e. [DIN] $\geq$ 14.3 µmol L^{-1}) in the BHS and YS, especially in the big estuaries and coastal areas. The dominant indicators exceeding the standard were inorganic nitrogen and active phosphate (MEE, 2019). Below we

introduce the hydrology and biogeochemistry settings of the BHS, YS, and the related
big rivers.

1.2.1. The Bohai Sea

The Bohai Sea (BHS) is a semi-enclosed basin with a surface area of 77×10^3 km^2
and an average depth of 18 m (Su, 2001; Chen, 2009), it can be divided into the Bohai
Bay, the Liaodong Bay, the Laizhou Bay and the Central Bohai by region (Figure 1.4).
It exchanges salt water with the Yellow Sea (YS) through Bohai Strait and the Yellow
River (YR) is a major source of freshwater to BHS (Chen, 2009).
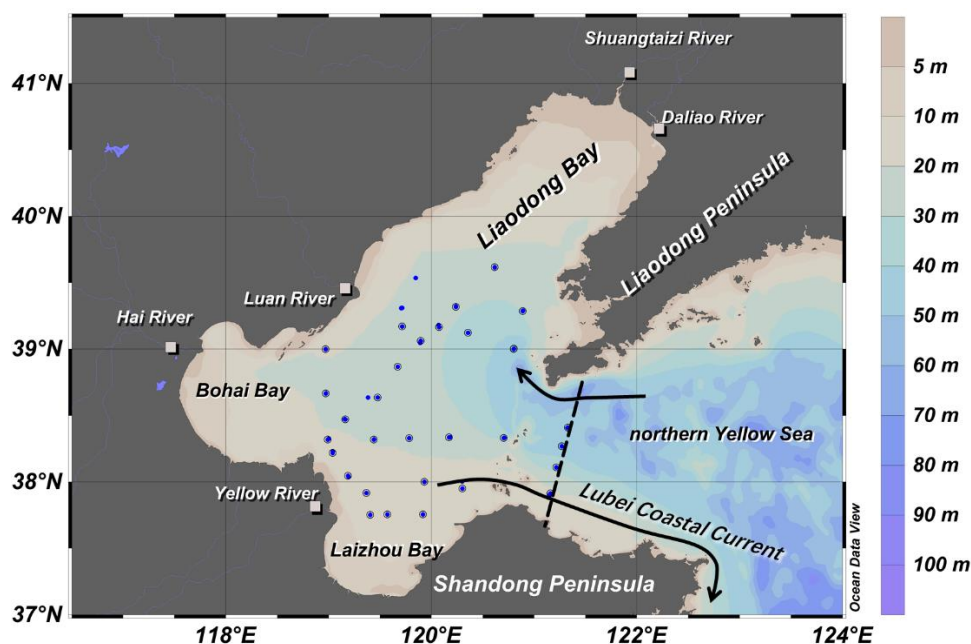
Figure 1.4. The geography and main currents of the Bohai Sea.

The population of the Circum-Bohai-Sea region is more than 200 million and 13
cities in this region exceed 1 million inhabitants. The BHS has been reported to have
received > 30 % of mainland China's total marine pollution, although it only constitutes
< 3 % of the total marine area of China (Xin et al., 2019). The 30 relatively large rivers
surrounding the BHS discharge 7.45×10^9 mol year^{-1} nitrate into it with a mean
concentration of 2.24 ± 2.11 mg L^{-1} (i.e. 160 ± 150 µmol L^{-1}) in discharge, which is

higher than those for most other rivers and watersheds around the world (e.g., Chang Jiang River, Mississippi River, and Bode Catchment) (Yu et al., 2021). The BHS thus is heavily impacted by human activities in one of the most densely populated terrestrial catchments of the world.

Rising anthropogenic activity in the catchment induced severe environmental changes in the BHS, including increasing salinity, temperature, concentrations of DIN and changes in stoichiometric nutrient ratios during the last fifty year (Zhao et al., 2002; Zhang et al., 2004; Ning et al., 2010; Wang et al., 2019; Xin et al., 2019). Many sources such as river discharge, atmospheric deposition, submarine groundwater, sewage and aquaculture pollution are responsible for the nutrient increase (Liu et al., 2017a; Wang et al., 2019; Wang et al., 2020a). The concentration of inorganic nitrogen in the central BHS has increased five-fold since the 1960s (Zhang et al., 2004), and the increase became even steeper since 2002 (Wang et al., 2018). DIN concentrations increased from 0.30 μmol L^{-1} to 3.55 μmol L^{-1} in the time from 1982–2009, while phosphate (from 0.76 μmol L^{-1} to 0.31 μmol L^{-1}) and silicate (26.6 μmol L^{-1} to 6.60 μmol L^{-1}) concentrations significantly decreased, so that N/P increased about 30 times (Zhang et al., 2004; Liu et al., 2011).

Phytoplankton nutrient limitation in the BHS switched from nitrogen to phosphorus in the period of the 1980s to the 1990s and this limitation pattern persists until the present day (Liu et al., 2009a; Xu et al., 2010; Wang et al., 2019). Harmful algal blooms (HABs) and phytoplankton growth occurred in the BHS in the 2000s frequently (Fu et al., 2016; Song et al., 2016b), both eutrophic and over proportional increase of nitrogen rather than phosphorus caused increased productivity, loss of biodiversity, and proliferation of HABs (Wang et al., 2021). The seasonal variations in nutrient concentrations and the N/P ratio are determined by physical–biological coupled processes (Ding et al., 2021).

1.2.2. The Yellow Sea

The YS with an area of about 380×10^3 km^2 and an average depth of 44 m is a semi-closed marginal sea surrounded by mainland China and the Korean peninsula. It

connects to the BHS in the northwest by the narrow Bohai Strait and with the East China Sea (ECS) in the south.

In the YS, water is a mixture of two end members, the isotopically light, freshwaters from precipitation and river runoff and the isotopically heavy, saline waters originated from a Kuroshio branch (Kang et al., 1994) and the water masses can be classified into the coastal waters and central YS waters (Figure 1.5) (Sun et al., 2013; Li et al., 2015a; Guo et al., 2020a). Currents in the coastal area are named Lubei Coastal Current (LCC), Subei Coastal Current (SCC), Yellow Sea Coastal Current (YSCC), Korean Coastal Current (KCC) which generally flow southward and are strong in the wintertime. In contrast the Taiwan Warm Current (TWC) flows northward and almost fades away when it enters the YS. In the central YS, Yellow Sea Warm Current (YSWC) prevails in wintertime, it is a sub-branch of the Kuroshio Current (KC). Yellow Sea Cold Water Mass (YSCWM) appears in summertime in the same central deep trough. Besides, Changjiang Diluted Water (CDW) connects the Changjiang Estuary to the central YS in summer. The invasion of CDW, TWC and YSWC are the principal driving forces of YS circulation (Guo et al., 2020a), coastal currents are more like the compensate currents.
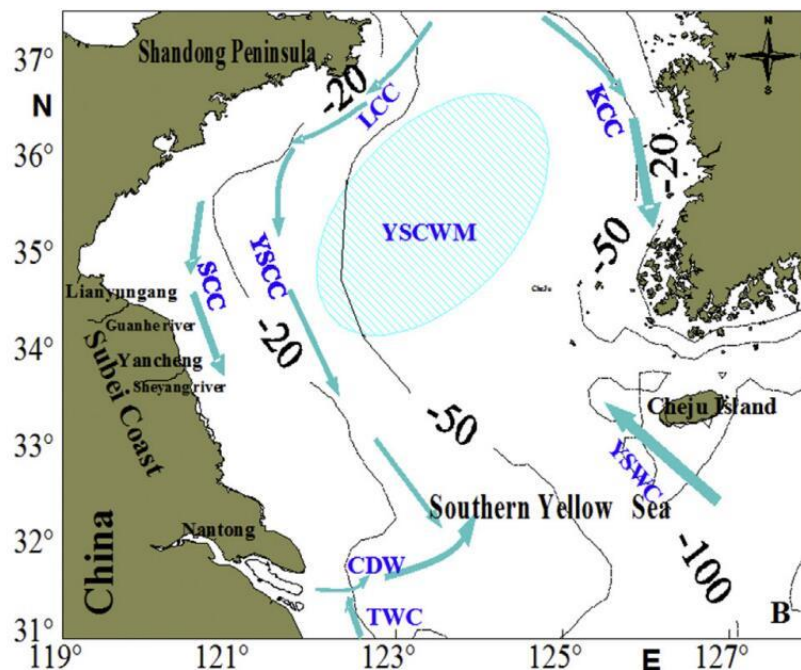
Figure 1.5. The main currents in the Yellow Sea (Li et al., 2015a)

The concentrations of NO_3^- and DIN in the southern YS have continuously increased from the 1980s (Wei et al., 2015; Yang et al., 2018a). DIN varied between 1.12 to 10.2 μmol L^{-1} during 1998-2008 with a slight increase, whereas phosphate varied between 0.04 to 0.73 μmol L^{-1} but without a clear trend in the years of sampling (Fu et al., 2012). For almost two decades a trend of increasing DIN concentrations during the pre-bloom period as well as a positive correlation between the *prolifera* biomass and DIN concentrations were observed (Li et al., 2017b). The most rapid increase of NO_3^-- and DIN occurred after the mid-1990s (Wei et al., 2015) and the level of the annual NO_3^- concentration in 2012 was over 5 times that of 1984 (Li et al., 2015a). The increased input of anthropogenic N_r in the last decades resulted in a shift from N-deficiency to P-deficiency in the YS and ECS (Wei et al., 2015; Guo et al., 2020a; Moon et al., 2021). A large upward spike in the N/P ratio was apparent in 2008, and the DO concentration decreased sharply in the same year (Li et al., 2015a).

The increase of the N_r in the YS can be ascribed to two sources, namely the anthropogenic input (terrestrial) and the outer shelf (marine) input. Terrestrial N inputs are strongly concentrated in areas close to river mouths and those confined regions with mariculture production (Wang et al., 2020b), whereas N increase in areas off the estuaries is due to enhanced atmospheric deposition and the input of outer shelf water (Zheng and Zhai, 2021). Marine or on-land aquaculture (Li et al., 2015a; Wang et al., 2020a), submarine ground water (SGD) (Liu et al., 2017b), sewage (Yang et al., 2018a), and atmospheric deposition (Shi et al., 2012; Qi et al., 2013; Yang et al., 2018a; Qi et al., 2020) all contributed to the enhanced N concentrations and increased N/P ratios in the YS. The total nitrogen inputs to BHS and YS increased rapidly from 1.0 to 4.1 Tg year^{-1} during 1970–2010 (Wang et al., 2020b). China's river N export was reported as the largest N source in BHS, YS and ECS, whereas riverine input of Korea was suggested to have a weaker impact on the YS (Moon et al., 2021).

The second source is advection from the adjacent ocean. Yellow Sea Warm Current (YSWC) is an asymmetric upwind flow and intrudes into the central YS along the western side of the YS trough from winter to early spring (Lin and Yang, 2011) and the YSWC is thus considered as a nutrients transporter. It originates from the northward Kuroshio branch current (Cheju Warm Current) and the Taiwan Warm Current in the northern part of the ECS (Lin and Yang, 2011). YSWC has high salinity and nutrient concentrations (Liu et al., 2015b; Liu et al., 2015c), supplying nutrients to the southern YS (Jin et al., 2013). The spring bloom in the YS is an important phenomenon occurring annually, and caused by the nutrient enriched YSCW exposed to enhanced irradiance in spring (Hyun and Kim, 2003; Liu et al., 2015c). The DO saturation values of surface waters in the southern YS generally exceed 100 %, indicating that phytoplankton photosynthesis plays a more important role than seawater temperature in the observed DO increase during the spring (Wei et al., 2010b; Xue et al., 2012). Thus, YSWC plays an important roles in the distribution of nutrients, phytoplankton biomass and also community structure in the central YS, specifically, diatoms and dinoflagellates are abundant in the YSCC, but the cyanobacteria and prasinophytes show opposing trends

(Liu et al., 2015b).

The Yellow Sea Cold Water Mass (YSCWM) fills the central YS trough in summer, it is located in the YS deep trough. The Yellow Sea Trough with a water depth of 70–100 m stretches north from the southeastern YS and extends northwestward into the BHS (Su et al., 2013), YSCWM forms due to the unique basin topography and the impact of both the seasonal evolution of the thermocline and the circulation system in the YS (Zhang et al., 2008a), water of YSCWM could not be distinguished from other waters by determination of the oxygen isotope of seawater (Kang et al., 1994). However, the ecosystem of the central YS was different from the other regions in the southern YS (Liu et al., 2015c), it is isolated from the direct influence of major river inputs so that the internal remineralized nutrients would play important roles instead (Chen et al., 2012; Sun et al., 2013; Li et al., 2017a). YSCWM is also a significant nutrient reservoir to the euphotic zone in summer (Wei et al., 2010a; Su et al., 2013), it supplies nutrients to the euphotic layer by vertical diffusion and turbulent entrainment and upwelling at the boundary (Su et al., 2013; Wang et al., 2020c). The nutrients in the YSCWM were suggested to be regenerated by decomposition of organic matter. A strong linkage of hypoxia and acidification with organic matter mineralization and stratification was observed in the YSCWM (Guo et al., 2020b). The accumulation of nutrients in it was also suggested to be the source of the spring phytoplankton bloom for the following year (Sun et al., 2013). The YSWCM seems to mainly act as a pool of nitrate but with low ammonium concentrations. The ammonium is mainly regenerated and taken up in the euphotic layer (Li et al., 2015a).YSCWM is also a sink of nitrate (Liu et al., 2003a; Duan et al., 2016) due to benthic processes rather than to water column denitrification (Zhang et al., 2018).

Overall, in the YS, YSWC and the CDW are the major sources of water supply in winter/early spring and in early summer, respectively (Jin et al., 2013). Regionally, excessive DIN introduced by terrestrial runoff and anthropogenic activities resulted in the potential for P limitation of primary production in coastal areas (Yuan et al., 2014; Guo et al., 2020a). The accelerated nutrient import from the Kuroshio Current, the

western Pacific boundary current, under global warming conditions influences the nutrient inventory of the YS and is therefore a climate feedback mechanism (Wei et al., 2015; Zheng and Zhai, 2021).

1.2.3. The primary rivers

The primary rivers discharging to the BHS and YS are the Yellow River (YR) and Changjiang River (CJR), respectively. YR and CJR are the sixth and third longest rivers around the world, respectively, and their drainage basins comprise the most populated areas of the world.

The total annual water discharge of rivers into BHS is about 68.5×10^9 m^3 $year^{-1}$, of which the YR accounts for more than 75 % (Liu et al., 2011). In summer, the fresh water discharge of the YR results in spots of low salinity in the surface of the BHS (Yu et al., 2020). The catchment of YR supplies 2.6×10^8 kg $year^{-1}$ (i.e. 0.26 Tg yr^{-1}) of nitrate from nitrification of ammonium/urea-containing fertilizer to the YR (Liu et al., 2013). Water exchange time of the YR estuary is only 0.1–0.2 days (Liu et al., 2009a), which implies a fast transfer of nutrients into the open BHS and much of these nutrients are trapped in Laizhou Bay (Zhang et al., 2004). River sediment transport and anthropogenic wastewater discharge were two driving forces for the nitrogen dynamics and sedimentary organic carbon in large river plume and inner bay areas (Li et al., 2016).

Besides, YR is characterized by high turbidity. The drainage basin of the YR encompasses a broad range of geological tectonic features (Zhang et al., 1995), the Loess Plateau is the major source of suspended particles to the YR (Chen et al., 2005). This makes the river quite turbid after passing the Loess Plateau. Another distinctive feature of the YR is the human "water-sediment regulation". It is a very short period before the flood season, when during this man-controlled event aimed to enhance the inventory of the dams and clean the amount of particulate deposit in the lower reach. It is reported that 54 % of the total annual sediment flux happened during this period in 2009 (Wang et al., 2012). Although the sediment discharge of the YR is abundant, anthropogenic particles from the YR are mainly trapped in the river sediments and in

Bohai Bay (Gao et al., 2012).

Changjiang River (Yangtze River), the largest river in China, discharges on average 9.25×10^{11} m^3 of water per year into the ECS, of which about 20 % is advected into the YS (Fan and Song, 2014; Liu et al., 2020). CJR input, Changjiang Diluted Water (CDW), is transported southward in winter and northward in summer (Fan and Song, 2014), it is a main nutrient source of the YS in summertime (Jin et al., 2013). During a longer period of 1900-2010, the CJR N flux input to the YS and ECS increased from 337 to 5896 Gg N year^{-1} (i.e. 0.3 and 5.9 Tg N year^{-1}) by model simulation (Liu et al., 2018). The area of highest nutrient concentrations appeared in the south or southwestern part of the southern YS during the 1980s-2012 (Li et al., 2017b). This supply of CDW is suggested the lead to major oxygen consumption and even hypoxia, inducing up to 70 % of the total DO consumption of the CJR estuary (Zhou et al., 2021), besides, it also partially accounts for the magnitude of macroalgal blooms in the southern YS in recent years (Li et al., 2017b).

1.3.   Nitrogen and oxygen stable isotopes in marine biogeochemistry

1.3.1.   The general settings of nitrogen and oxygen stable isotopes

The use of the N and O isotope ratio is a natural tracer for marine N cycle processes. Two stable isotopes of N are ^{14}N and ^{15}N with atomic masses of 14 and 15, respectively, ^{14}N is abundant with 99.67 % of total N in nature. Oxygen (O) has the three stable isotopes ^{16}O, ^{17}O and ^{18}O with abundances of 99.8 %, 0.03 % and 0.2 %, respectively. The ^{15}N : ^{14}N ratio and ^{18}O : ^{16}O are typically reported using the "delta" notation:

$$\delta^{15}N(‰) = (\frac{^{15}N : ^{14}N_{sample}}{^{15}N : ^{14}N_{air}} - 1) \times 1000 \quad (1.1)$$

$$\delta^{15}O(‰) = (\frac{^{18}O : ^{16}O_{sample}}{^{18}O : ^{16}O_{VSMOW}} - 1) \times 1000 \quad (1.2)$$

N_2 in air is the N isotope reference, O in VSMOW (Vienna Standard Mean Ocean Water) is the O isotope reference (Altabet, 2006; Casciotti, 2016).

Physical, chemical, and biological processes discriminate between isotopes of particular elements and this is referred to as isotopic fractionation (Casciotti, 2016). The isotopic fractionation is normally including the "equilibrium" and "kinetic" fractionation, the latter is not reversible and typically thought to dominate the fractionation in the ocean during the biochemical conversions of N. Enzymatic isotope fractionation arises from small differences in the rates of reactions containing heavy and light isotopes (Casciotti, 2016). The kinetic isotope effect (ε) is an amplitude of this isotopic fractionation:

$$^{15}\varepsilon(‰) = (1 - \frac{^{15}k}{^{14}k}) \times 1000 \quad (1.3)$$

where ^{14}k and ^{15}k are the rate coefficients of the reaction for ^{14}N- and ^{15}N-containing reactant, respectively. This isotopic fractionation results in predictable differences between the isotope ratio of the substrate and the product of a reaction. Usually, the products of an enzymatic reaction are depleted in heavy isotopes due to preferential reaction of the light isotope containing molecules. The ε can also be represented as:

$$^{15}\varepsilon = \delta^{15}N_{substrate} - \delta^{15}N_{product} \quad (1.4)$$

where $\delta^{15}N_{substrate}$ and $\delta^{15}N_{product}$ denotes the delta value of substrate and product. Normally, the products always have lower $\delta^{15}N$ than substrate.

Most of the fractionation effects can be generalized by two simplified models: the Rayleigh model for a closed system and the steady-state model for an open system (Mariotti et al., 1981; Altabet and Francois, 1994; Altabet, 2006; Casciotti, 2016; Sigman and Fripiat, 2019). In both models, the degree of consumption of the reactant

N pool (f) is a key variable, and the $\delta^{15}N$ of the initial reactant N pool ($\delta^{15}N_{initial}$) and the kinetic isotope effect (ε) are the two central isotopic parameters.

In a closed system with depletion of substrate and matching accumulation of the product over time, with the transformation proceeding at a constant rate and without resupply to the N pool, the Rayleigh equations describes the change in isotope ratio as a function of the fraction of the remaining substrate (f):

$$\delta^{15}N_{reactant} = \delta^{15}N_{initial} - \varepsilon\{\ln(f)\} \quad (1.5)$$

$$\delta^{15}N_{instantaneous} = \delta^{15}N_{reactant} - \varepsilon \quad (1.6)$$

$$\delta^{15}N_{accumulated} = \delta^{15}N_{initial} + \varepsilon\{f/(1-f)\} \times \ln(f) \quad (1.7)$$

where f is the fraction of the reactant remaining, $\delta^{15}N_{initial}$ is the delta value of the initial reactant N pool, and ε is the kinetic isotope effect of the transformation.

In an open system, continued replenishment of substrate is matched by removal of the product. In this situation, the rate of the gross supply of reactant N equals the sum of the rates of the product N generated and the residual reactant N exported. The steady state model is used to quantify uptake processes where supply and uptake are occurring simultaneously, such as consumption of nitrate by denitrification:

$$\delta^{15}N_{reactant} = \delta^{15}N_{initial} + \varepsilon \times (1-f) \quad (1.8)$$

$$\delta^{15}N_{product} = \delta^{15}N_{initial} - \varepsilon \times (f) \quad (1.9)$$
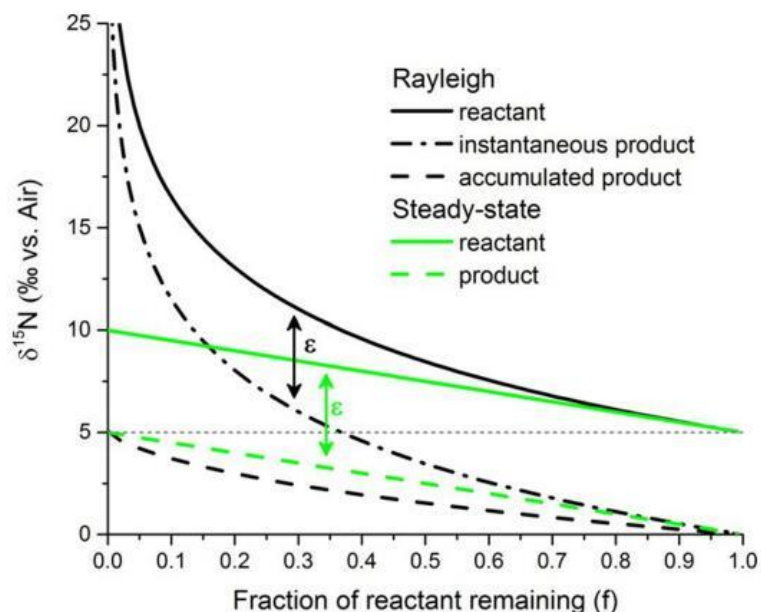
Figure 1.6. Simple models of N isotope changes associated with the consumption of a substrate (f) (Sigman and Fripiat, 2019).

The schematic diagram of the two models is shown in Figure 1.6. These equations are simplified, approximate forms of the full expressions. They are typically adequate, but their error is greater for higher consumption (lower f) and higher ε.

1.3.2. Isotope values and fractionation effects of primary N transformation processes

The global N_r budget is controlled by N fixation and denitrification (and anammox), while other biogeochemical processes such as assimilation for inorganic N, remineralization of organic N and nitrification of ammonium are attributed to the "internal cycling" of N_r (Sigman and Boyle, 2000; Brandes and Devol, 2002). Likewise, the $\delta^{15}N$ pool is impacted by the relative balance between N fixation and denitrification, internal processes only redistribute $\delta^{15}N$ in different forms and different regions, but do not affect the $\delta^{15}N$ of the global N pool (Figure 1.7) (Liu and Kaplan, 1989; Liu et al., 1996; Sigman et al., 1997; Wu et al., 1997). The deep ocean mean value of $\delta^{15}N$ and

δ^{18}O is 5.0 ‰ and 2.0 ‰, respectively, which is the result of balanced input and output of N (Sigman and Boyle, 2000; Sigman and Fripiat, 2019). In the marginal seas, the N pool and δ^{15}N are also influenced by inputs of anthropogenic sources via terrestrial discharge (river and submarine ground water) and atmospheric deposition.
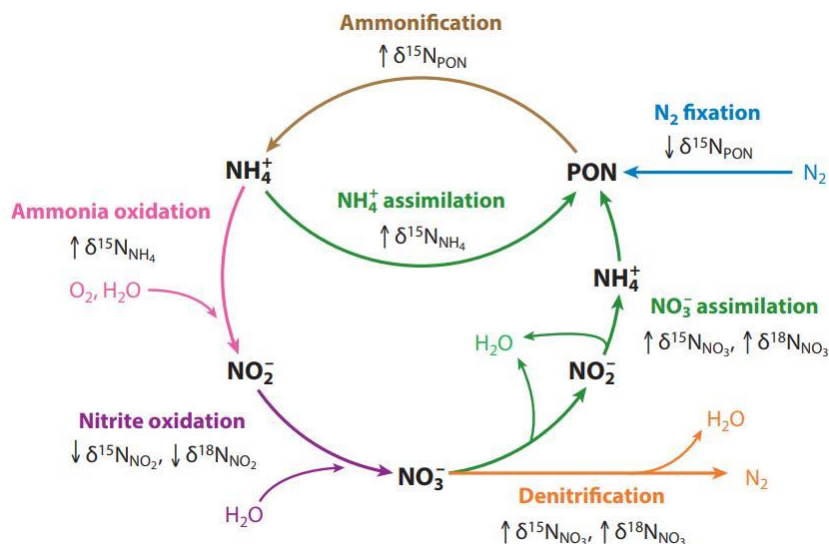
Figure 1.7. Overview of schematic N and O fractionation processes in the microbial N cycle and effects on the isotope values (Casciotti, 2016).

N fixation is normally catalyzed by cyanobacteria and other microorganisms able to convert N_2 into biomass N (Karl et al., 2002; Gruber, 2004). The cyanobacteria (blue-green algae) *Trichodesmium* is the dominant N fixer in the ocean, δ^{15}N averages of it are between -2 ‰ to 0.5 ‰ (Minagawa and Wada, 1986; Carpenter et al., 1997). Given that δ^{15}N of dissolved N_2 is about 0.7 ‰ higher than atmospheric N_2 (0 ‰ by definition) due to equilibrium isotopic fractionation between dissolved and gas phase N_2, yielding a fractionation effect of *Trichodesmium* of around 2 ‰. Simply, the δ^{15}N of fixed N is close to δ^{15}N of N_2, the average δ^{15}N of -1% was suggested to be the value of N fixation (Sigman and Fripiat, 2019), the subsequent remineralization of this biomass supplies new N with δ^{15}N close to 0 ‰ to the dissolved fixed N pools in the surface and subsurface ocean.

In addition to N fixation, other inputs of N_r to the marine environment are terrestrial runoff and atmospheric deposition. These inputs have been influenced by anthropogenic activities. A preindustrial mean $\delta^{15}N$ of 4 % for terrestrial runoff and 0 % for atmospheric deposition in the open ocean has been suggested although with large uncertainties (Sigman and Fripiat, 2019). In the contrast, the $\delta^{15}N$ of nitrate and atmospheric NO_x in the polluted river normally has relatively high values, but also depends on the composition of pollutants (see Sect. 1.3.3). The distinctive signals of different anthropogenic sources can allow source tracking by N (and O) isotopes (Figure 1.8).
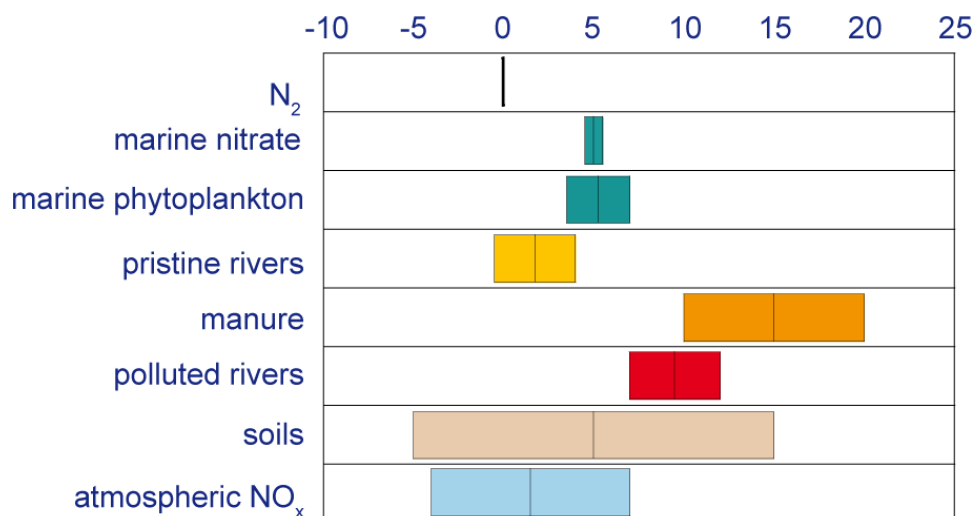
Figure 1.8. $\delta^{15}N$ ranges in of different N sources (Dähnke and Emeis, unpublished; after Sigman et al. (2005); Kendall et al. (2007); Jung (2015)).

Denitrification is the major N loss process of N_r in the ocean (Brandes and Devol, 2002). It occurs in the water column and in sediments with different isotopic effects on both $\delta^{15}N$ and $\delta^{18}O$ (Sigman et al., 2003). Active denitrification is reported to happen at DO < 4 μmol L^{-1} (Sigman et al., 2005). Water column denitrification has an isotope effect between 20 ‰ and 30 ‰ (Liu and Kaplan, 1989; Brandes et al., 1998; Voss et al., 2001) leaving the $\delta^{15}N$-NO_3^- increasingly enriched as denitrification proceeds. The

fractionation effects during denitrification of N ($^{15}\varepsilon$) and O ($^{18}\varepsilon$) are suggested to be 1:1 (Granger et al., 2008; Karsh et al., 2012). In contrast to water column denitrification, denitrification in sediments leads to little increase in the $\delta^{15}N$ of water column nitrate. Although fractionation effect is observed on organism scale, the expression of this is minimized by the nearly complete consumption of nitrate within sediment pore waters (Sigman et al., 2001; Brandes and Devol, 2002; Lehmann et al., 2004; Sigman and Fripiat, 2019).

The internal cycling generally includes the assimilation and remineralization (including ammonification and nitrification) of N_r. Different forms of N_r are assimilated with distinct isotope effects, moreover, complete or incomplete assimilation have different imprints on the N and O isotopes. Under conditions of complete assimilation of nitrate which normally happens in the stable stratified tropics and the subtropical gyres, organic N has the same $\delta^{15}N$ as its inorganic N source. The incomplete assimilation normally found in polar and upwelling regions, leaves an enhanced $\delta^{15}N$ in the residual nitrate pool (Sigman and Boyle, 2000; DiFiore et al., 2009). The most important sources of combined N for phytoplankton is nitrate, the lab results indicated that $^{15}\varepsilon$ of eukaryotic phytoplankton have a range of 5 ‰-7 ‰, normally with equivalent discrimination of N and O (Montoya and McCarthy, 1995; Granger et al., 2004; Granger et al., 2008). Field estimates suggested the $^{15}\varepsilon$ of 4 ‰-7 ‰ (Sigman and Fripiat, 2019), studies in the YS and ECS proposed an approximately 5 ‰ for $^{15}\varepsilon$ (Umezawa et al., 2013; Liu et al., 2017c; Wu et al., 2019; Liu et al., 2020). $^{15}\varepsilon$ of ammonium assimilation can reach 27 ‰ when ammonium concentrations are high, however, in most regions of the ocean ammonium has very low concentrations so that this fractionation factor is not obtained and $^{15}\varepsilon$ is 0 ‰ -1 ‰ at these low ammonium concentration; a $^{15}\varepsilon$ value of 4 ‰ is reached when ammonium concentration is 5 μmol L^{-1} (Hoch et al., 1992; DiFiore et al., 2009). All other N pools are smaller than the nitrate pool and their turnover is fast. Consequently, the isotopic discrimination associated with the assimilation of other N forms has less impact on N isotope distributions than of the assimilation of nitrate (Sigman and Fripiat, 2019).

Remineralization can be considered the combination of two steps: organic N ammonification and nitrification. Organic N degradation preferentially releases the light N back into the inorganic pool, resulting in the accumulation of ^{15}N in the residuals. However, the organic degradation includes many different reactions, the specific $^{15}\varepsilon$ of it is remained unclear, field studies suggested that the $^{15}\varepsilon$ of ammonification is less than 3 ‰ (Möbius and Dähnke, 2015; Sigman and Fripiat, 2019).

Nitrification also consists of two steps: ammonium oxidation and nitrite oxidation, catalyzed by different classes of bacteria. Isotope effects for ammonium oxidation reported from culture studies range from 14 ‰ to 38 ‰, with two marine nitrifiers yielding 14 ‰ and 19 ‰ (Casciotti et al., 2003; Arrigo, 2005; Altabet, 2006; Mariotti et al., 2006). Nitrite oxidation has the unusual "inverse" discrimination with a $^{15}\varepsilon$ of -12 ‰ (Casciotti, 2009) (Figure 1.7). During nitrification, one third of the O atoms are incorporated from dissolved oxygen and two thirds from ambient water. The strong O atom exchange between water and nitrite finally results in around five sixths of O atoms in newly nitrified nitrate originating from water (Mayer et al., 2001; Casciotti et al., 2010). Thus, the $\delta^{18}O$ is depending on value of water, dissolved oxygen and the isotopic effects involved with the nitrification reaction. This approach was used to track the source of nitrate in the rivers in northern Germany, the observed $\delta^{18}O-NO_3^-$ was in the range of 0.4 ‰ - 2.3 ‰, while the calculated value was 2 ‰ (Johannsen et al., 2008). In the open ocean, the empirical value of $\delta^{18}O$ in nitrified nitrate is around 1.1 ‰ higher than in ambient water (Sigman et al., 2009).

Overall, internal cycling of N_r has no effect on the ocean mean value of ^{15}N, but changes the distribution of ^{15}N in different areas and in different N components in some regions.

1.3.3. Isotope values of anthropogenic sources

Synthetic fertilizer is the main anthropogenic source of N_r. Since the invention of the Haber-Bosch process the amount of fixed nitrogen (120 Tg N year^{-1}) has constantly

grown and since 2010 it exceeds the natural terrestrial sources of reactive N of 63 Tg N year^{-1} (Fowler et al., 2013). Chinese agriculture has been using >25Tg N yr^{-1} as N fertilizers, mainly as urea and ammonium bicarbonate (IFA, 2005).

In general, synthetic fertilizers have a δ^{15}N-NO$_3^-$ average of 0 ‰ which is close to that of N$_2$. Manure and sewage have an average δ^{15}N-NO$_3^-$ value around 10 ‰ (Figure 1.9). Specifically, ammonium fertilizer, nitrate fertilizer and urea have δ^{15}N-NO$_3^-$ values of -4 ‰ to 4 ‰ (Xue et al., 2009) and δ^{18}O-NO$_3^-$ between 18 ‰ to 22 ‰ (Li et al., 2010; Dejwakh et al., 2012) Manure/sewage has δ^{15}N-NO$_3^-$ values ranging from 5 ‰ to 25 ‰ (Heaton, 1986; Aravena et al., 1993; Grischek et al., 1998; Liu et al., 2009b), but lacking δ^{18}O-NO$_3^-$ data.
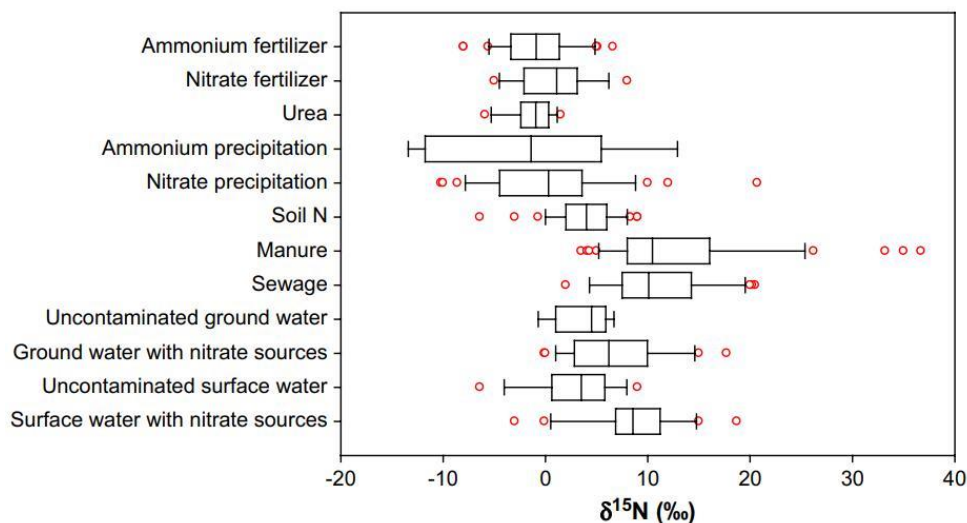
Figure 1.9. Box plots of δ^{15}N values of NO$_3^-$ from various sources and sinks (Xue et al., 2009).

The nitrate δ^{15}N- NO$_3^-$ values of PM2.5 (particulates that can be suspended in the air which have equivalent diameters of less than 2.5 microns) ranged from 3.5-17.8 ‰ in northern China, and values value increase with decreasing distance to urban areas (Zong et al., 2017; Fan et al., 2019; Zhang et al., 2019; Song et al., 2020). δ^{18}O-NO$_3^-$ range from 60 ‰ to 90 ‰, with values mostly around 80 ‰ (Zong et al., 2017; Chang et al., 2019; Kim et al., 2019; Liu et al., 2020; Song et al., 2020).

δ^{15}N measurements of dissolved and particulate N in pristine river systems range mostly from 0 to 5%. Anthropogenic inputs often increase the δ^{15}N of a system because they increase denitrification along the path of freshwater flow (Sigman and Fripiat, 2019). The polluted rivers in Europe have δ^{15}N and δ^{18}O of nitrate in the range of 7.8 ‰ to 16.2 ‰ and in the range of -0.1 ‰ to 3.2 ‰, respectively (Dähnke et al., 2008; Johannsen et al., 2008; Möbius and Dähnke, 2015). Rivers around the BHS have average value of δ^{15}N and δ^{18}O of nitrate is 11.4 ‰ ± 5.0 ‰ and 9.4 ‰ ± 7.2 ‰, respectively (Yu et al., 2021), the largest river (YR) discharging into the BHS has high δ^{15}N of nitrate with an average 12.3 ‰, but low δ^{18}O of nitrate with an average of -1.1 ‰ (Liu et al., 2013). The CJR, with wetter climate in its drainage basin in southern China, has relatively low δ^{15}N and δ^{18}O of nitrate of 2.1 ‰ to 6.6 ‰ and 0.6 ‰ to 3.9 ‰, respectively (Liu et al., 2009b; Chen et al., 2013; Yu et al., 2015; Wang et al., 2016; Liu et al., 2020; Zhong et al., 2020).

1.4. Research project and motivation

1.4.1. Background of the project

The main aim of the PhD project is to characterize nitrogen cycling with respect to the anthropogenic impact in Chinese marginal Seas, namely the BHS, YS and ECS. The project is part of the BMBF (Bundesministerium für Bildung und Forschung) funded joint project MEGAPOL. This project aims at tracking the signature and dispersal of pollutants in coastal seas of China. The work is carried out in cooperation with the project partners from the Helmholtz-Center Geesthacht, the Institute of Baltic Sea Research in Warnemünde, the Yantai Institute of Coastal Zone Research, the Second Institute of Oceanography (SIO), MNR, Hangzhou and the National Marine Environmental Monitoring Centre, MEE, Dalian.

1.4.2. Research motivations and questions

Worldwide, eastern Chinese waters belong to the ocean regions that are most strongly affected by human activities (Levin et al., 2015a). One important threat to these regions is anthropogenic input of nutrients. N_r, a major nutrient for terrestrial and

oceanic organisms, is used in fertilization and is also an end product of combustion processes. Among other effects, it causes eutrophication, alterations in species composition, and the expansion of bottom water hypoxia when it reaches the coastal ocean. In the aquatic environment, $\delta^{15}N$ of nitrate, nitrite and particulate nitrogen are widely used to characterize nitrogen sources and N-cycling because they are source-specific, or are characteristic of processes that lead to fractionation of nitrogen during biological processes.

Low $\delta^{15}N$ values are characteristic for the western Pacific and have been explained by high rates of nitrogen fixation (Gaye et al., 2009). Rivers impacted by anthropogenic activity, on the other hand, transport nitrate with elevated $\delta^{15}N$ to the coastal becoming assimilated by phytoplankton and buried as detritus in near coastal sediments. The $\delta^{15}N$ value in rivers of northern Germany are positively correlated with the amount of arable and urban land in the catchments (Johannsen et al., 2008). The high $\delta^{15}N$ of river nitrate is matched by high $\delta^{15}N$ of nitrate in surface sediments in the German Bight (Pätsch et al., 2010). But differing from rivers in Europe and although the BHS and YS receive high anthropogenic nutrient inputs from rivers with high $\delta^{15}N$ in nitrate, the $\delta^{15}N$ values in sediments near the river mouths of BHS and the northern YS are only slightly elevated over the marine background (Liu et al., 2009b; Liu et al., 2015a) (Figure 1.10). As yet it is unclear whether this is due to unprocessed artificial fertilizer input, nitrification regenerating isotopically depleted nitrate, atmospheric deposition, or N_2 fixation.
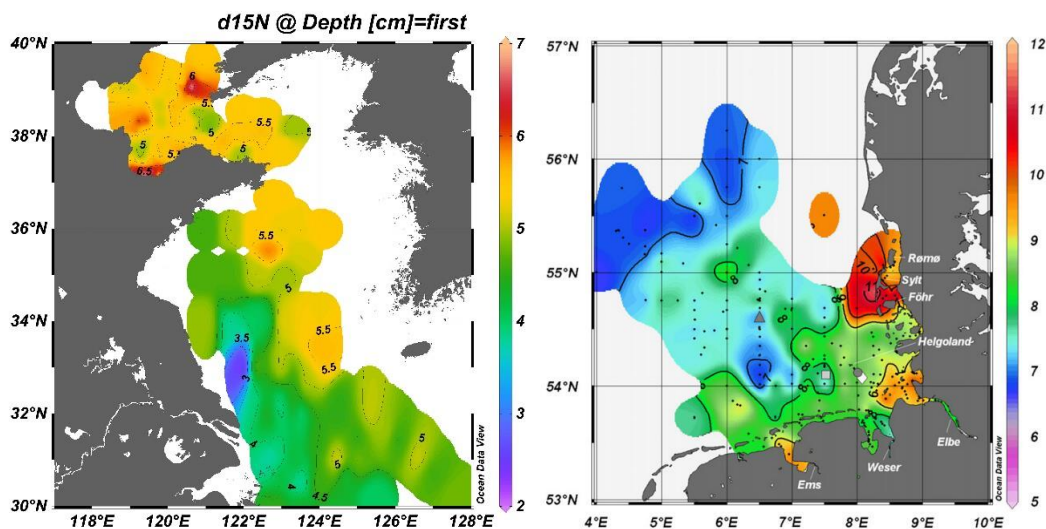
Figure 1.10 The distribution of $\delta^{15}N$ in surface sediment in the Bohai Sea and Yellow Sea (left), and in German Bight (right) (Serna et al., 2010). Notice the high $\delta^{15}N$ seaward of the German rivers estuaries.

We aim to examine these possible explanations: (i) The contribution of atmospheric deposition low in $\delta^{15}N$ values of N_r (Jia and Chen, 2010) may balance the nitrogen supply from polluted rivers (Liu et al., 2013), thus masking the high $\delta^{15}N$ signal from rivers. (ii) The high $\delta^{15}N$ of nutrient inputs from rivers may be not expressed in the particle-rich (and possibly light-limited) coastal zone due to incomplete nitrate utilization during biological assimilation. (iii) Processes of nutrient regeneration from sedimentary organic nitrogen of newly fixed atmospheric N_2 (nitrification) that preferentially produce ^{15}N-depleted ammonium and nitrate may be involved. These will to our knowledge be the first data on benthic nitrogen cycling based on stable N-isotopes, whereas solid data for the North and Baltic Seas are available. Balancing fluxes and N-isotopes in the river-coastal sea continuum as part of the project modelling activity will enable us to decide, which of the alternative explanations may best explain the evidence.

There are three main questions that will be addressed:

1) How is nitrate supplied to Chinese marginal seas and how is this reflected in

$\delta^{15}N$ of particulate nitrogen and of dissolved nitrate in river loads?

2) How does land-derived reactive nitrogen interact with the nitrate pool of the open ocean?

3) Can the biogeochemical impact of megacities on nitrate dynamics and sedimentary processes be quantified?

1.5. Thesis outline

In Chapter 2, we proposed a nitrate budget for the BHS. It is based on the available mass fluxes and isotope data and is thereby an updated nitrogen budget with processes better constrained by stable isotopic data than in previous mass-based budgets. The data presented in this chapter are based on sampled campaigns in spring and summer of 2018, by two expeditions in the BHS and YS on *R/V Dongfanghong 2*. This part is an individual manuscript submitted to the journal *Biogeosciences* and is waiting for the final decision after major revision.

In Chapter 3, we compared the different seasonal DIN alteration between north and south Yellow Sea Cold Water Mass (YSCWM). It is the first time that the regenerated nitrate in the YS has been quantified by a combined mass and isotope balance model. The data presented in this chapter are based on sampling in spring and summer of 2018, during two expeditions in the BHS and YS on *R/V Dongfanghong 2* like of Chapter 2. This part is also an individual manuscript submitted to the journal *Frontiers in Marine Science* and waiting for the comments of peer review.

Chapter 4 summarizes the main conclusions of this thesis and outlines future work.

Chapter 2 – A nitrate budget of the Bohai Sea

2.1. Introduction

Reactive (N_r) is an essential nutrient of life on earth, but only few organisms can fix dinitrogen directly from the large atmospheric dinitrogen pool. Since the invention of the Haber-Bosch process the amount of fixed nitrogen (120 Tg N year^{-1}) has constantly grown and since 2010 exceeds the natural terrestrial sources of reactive N of 63 Tg N year^{-1} (Fowler et al., 2013). Hotspots of agricultural N fertilizer application shifted from the US and western Europe in the 1960s to eastern Asia in the early 21st century (Lu and Tian, 2017). In China, the Haber-Bosch process produces 37.1 Tg N year^{-1}, which is almost 3 times of the biological N fixation of 12.0 Tg N year^{-1}. An estimated 32.0 Tg N year^{-1} are produced for fertilizer (Gu et al., 2015) and China accounted for 29 % of the global ammonium production in 2018 (IFA, 2019). The leakage and volatilization of this man-made reactive nitrogen has strongly impacted limnic and marine ecosystems in China. Riverine reactive nitrogen discharged to the ocean from China was estimated at 5.4 Tg N year^{-1} (Gu et al., 2015). The total load of Chinese major estuaries to coastal seas was about 9 % of the global river load for DIN and 1.5 % of the global phosphate load, respectively (Smith et al., 2003; Liu et al., 2009a).

The Bohai Sea (BHS) is a semi-enclosed basin with a surface area of 77×10^3 km^2 and an average depth of 18 m (Su, 2001; Chen, 2009) that is heavily impacted by human activities in one of the most densely populated terrestrial catchments of the world. It exchanges salt water with the Yellow Sea (YS) through Bohai Strait and the Yellow River (YR) is a major source of freshwater to BHS (Chen, 2009). During the last fifty years, rising anthropogenic activity in the catchment induced severe environmental changes in the BHS, including increasing salinity, temperature, concentrations of dissolved inorganic nitrogen (DIN) and changes in stoichiometric nutrient ratios (Zhao et al., 2002; Zhang et al., 2004; Ning et al., 2010; Wang et al., 2019; Xin et al., 2019). DIN concentrations increased from 0.30 µmol L^{-1} to 3.55 µmol L^{-1} in the time from

1982–2009, while phosphate (from 0.76 µmol L^{-1} to 0.31 µmol L^{-1}) and silicate (26.6 µmol L^{-1} to 6.60 µmol L^{-1}) concentrations significantly decreased, so that N/P increased about 30 times (Zhang et al., 2004; Liu et al., 2011). Phytoplankton nutrient limitation in the BHS switched from nitrogen to phosphorus in the period of the 1980s to the 1990s and this limitation pattern persists until the present day (Liu et al., 2009a; Xu et al., 2010; Wang et al., 2019).

The total annual water discharge of rivers into BHS is about 68.5×10^9 m^3 year^{-1}, of which the YR accounts for more than 75 % (Liu et al., 2011). Water exchange time of the YR estuary is only 0.1–0.2 days (Liu et al., 2009a), which implies a fast transfer of nutrients into the open BHS and much of these are trapped in Laizhou Bay (Fig. 1) (Zhang et al., 2004). The atmospheric deposition of nitrate (3.42 × 10^9 mol year^{-1}) in BHS was modelled to be less than riverine nitrate (7.25 × 10^9 mol year^{-1}), while more ammonium was supplied from atmospheric deposition (6.15 × 10^9 mol year^{-1}) than from riverine input (0.93 × 10^9 mol year^{-1}) in the 1990s (Zhang et al., 2004). BHS nitrate budgets reported during the last two decades were not completely constrained, because crucial data, such as groundwater discharge or nitrification, were not available (Liu et al., 2003b; Zhang et al., 2004; Liu et al., 2009a; Liu et al., 2011). There are few published nutrient data from the BHS over the last decade, and the terms in the N_r budget of BHS concerning the quantities of N_r generated or eliminated by biogeochemical cycling within the basin have not been addressed.

The nitrogen budget and in particular the internal sources and sinks of nitrate can be constrained with a mass-based and dual stable-isotope approach based on ^{15}N and ^{18}O of nitrate. The combination of data permits tracking of nitrate and quantification of internal cycling of inorganic nitrogen (Montoya et al., 2002; Sigman et al., 2005; DiFiore et al., 2006; Wankel et al., 2006; Sugimoto et al., 2009; Emeis et al., 2010). Stable isotopes of reactive nitrogen have been used to explore nitrogen sources in the eastern Chinese seas (Umezawa et al., 2013; Wang et al., 2016; Liu et al., 2017c; Li et al., 2019a; Wu et al., 2019; Liu et al., 2020; Yu et al., 2021) and the Changjiang Estuary (Chen et al., 2013; Yu et al., 2015; Wang et al., 2017; Yang et al., 2018b).

For this study, we analyzed water, suspended matter and sediments in the Bohai

Sea sampled during the spring and summer seasons for nutrient concentrations, carbon and nitrogen contents, dual isotopes (^{15}N and ^{18}O) of nitrate and ^{15}N of particulate nitrogen. The aim of the study is to characterize and quantify N_r sources and sinks, in particular those from internal cycling processes that have not been included in previous budgets (Liu et al., 2003b; Zhang et al., 2004; Liu et al., 2009a; Liu et al., 2011) to track the fate of N_r in the present Bohai Sea. The observation data presented here are the basis for a combined mass and isotope balance model, results of which will be a basis for future studies on the rising impact of fast-growing mega-cities in the BHS catchment and their possible impact on the adjacent YS.

2.2. Materials and methods

2.2.1. Sample collection

Research cruises were carried out by R/V *Dongfanghong 2* in spring and summer 2018 with 24 sampling sites in April and 25 sites in August, respectively (Figure 2.1). Water samples were taken from several depths by 12 L Niskin bottles attached to a CTD rosette (911plus, Seabird, USA). The water samples were filtered using nucleopore polycarbonate filters (0.4 µm) with plastic Nalgene filtration units. The filtered water was collected in Falcon PE tubes (45 mL), frozen immediately (-20 °C) and kept frozen until analyses in the home laboratory in Germany. Between 1 to 8 L of water were filtered through pre-weighted GF/F filters (0.7 µm, $\Phi = 47$ mm, Sigma Aldrich) which had been pre-combusted at 450 °C for 4 h. The filters were subsequently dried on board under 45 °C for 24 h. Surface sediments were taken with a box corer and surface samples were transferred into plastic bags with a metal spoon, frozen at -20 °C and were kept frozen until later analysis in the home lab.

YR water samples were taken from the Kaiyuan floating bridge in Lijin, located 44 km upstream of the river mouth. Samples were taken in the middle of the river course with a plastic reversing water sampler at 1 m under the surface. The water samples were filtered immediately for nutrient analysis and collection of suspended particles, and subsequently were stored frozen until delivered to the home laboratory. Samples were taken monthly in May, July to November from YR, and in November from Daliao River,

Hai River, Luan River and Xiaoqing River (Figure 2.1).
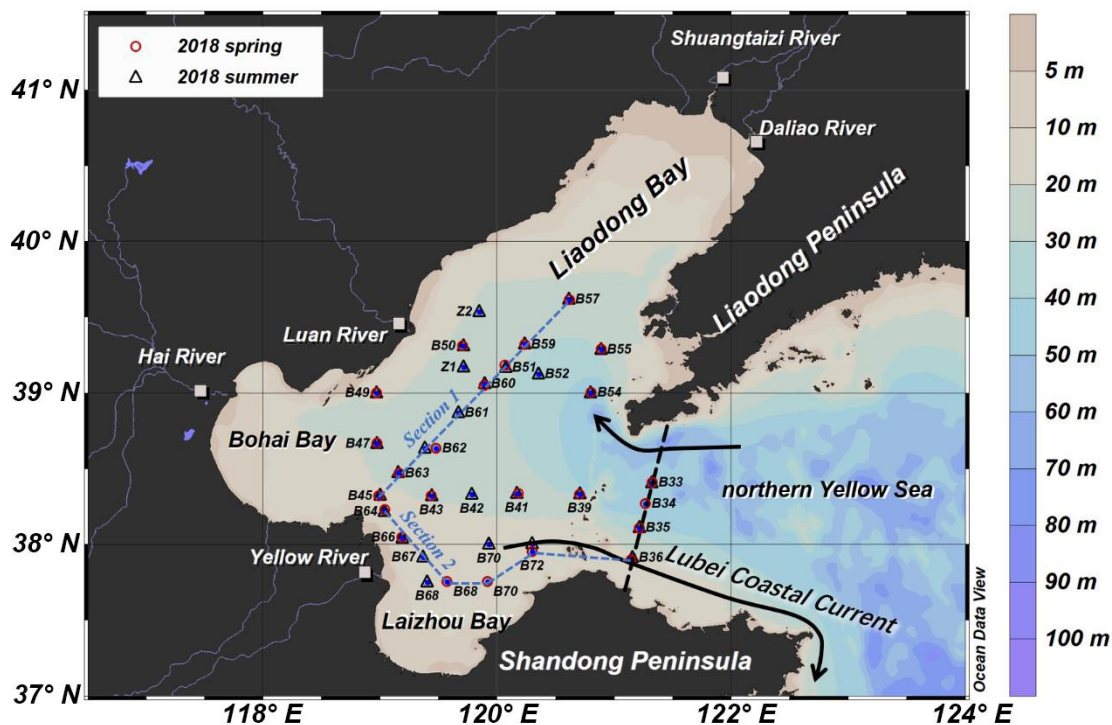
Figure 2.1 Sampling sites in Bohai Sea and rivers (Xiaoqing River not shown). Open red circles stand for sampling site in spring, open blue triangles stand for sampling sites in summer, names of the sites are marked nearby. Black arrows stand for the most significant currents flows in and out of the BHS. Blue dashed lines strand for two main sections, black dashed line stand for the boundary of our study area.

2.2.2. Measurements of nutrients and nitrate isotopes

Nutrient concentrations were measured with an AutoAnalyzer 3 system (Seal Analytics) using standard colorimetric methods (Grasshoff et al., 2009). The relative error of duplicate sample measurements was below 1.5 % for NO_x and phosphate concentrations, below 0.3 % for ammonium. The detection limit was < 0.05 µmol L^{-1} for NO_x, > 0.1 µmol L^{-1} for PO_4^{3-}, and > 0.013 µmol L^{-1} for ammonium.

$\delta^{15}N$ and $\delta^{18}O$ of nitrate ($\delta^{15}N = [(^{15}N/^{14}N)_{sample} / (^{15}N/^{14}N)_{standard}-1] \times 1000$ ‰, $\delta^{18}O = [(^{18}O/^{16}O)_{sample} / (^{18}O/^{16}O)_{standard}-1] \times 1000$ ‰,) were determined with the

denitrifier method (Sigman et al., 2001; Casciotti et al., 2002). Only the samples with nitrate concentrations > 1.7 µmol kg^{-1} were analyzed and $\delta^{15}N$ and $\delta^{18}O$ were analyzed in one sample run. Water samples were injected into a suspension of the denitrifier *Pseudomonas aureofaciens* with injection volumes adjusted to yield 10 nmol N_2O. The N_2O gas was purged by helium into a GasBench 2 (Thermo Finnigan) for purification. Afterwards the N_2O gas was analyzed by a Delta V Advantage and a Delta V Plus mass spectrometer. Samples were measured in duplicate and the two international standards IAEA-N3 ($\delta^{15}N–NO_3^- = +4.7$ ‰, $\delta^{18}O–NO_3^- = +25.6$ ‰) and USGS-34 ($\delta^{15}N–NO_3^- = -1.8$ ‰, $\delta^{18}O–NO_3^- = -27.9$ ‰) and an internal potassium nitrate standard were measured in each batch. The data were corrected by applying a bracketing correction (Sigman et al., 2009) and the standard deviations of the international and in-house standards was found to be ≤ 0.2 ‰ for $\delta^{15}N$ and ≤ 0.5 ‰ for $\delta^{18}O$. The standard deviations of duplicate samples were in the same range. Nitrite affects the results and was removed following the protocol of Granger and Sigman (2009) whenever $[NO_2^-]$ exceeded 5 % of the NO_x pool. In all other cases, we report combined (nitrite + nitrate) values.

2.2.3. Measurements of suspended matters and sediments

The tared GF/F filters were weighed to calculate the amount of suspended particulate matter (SPM) per liter of water. Total carbon and nitrogen concentrations in SPM and sediment samples were measured by a Euro EA 3000 (Euro Vector SPA) Elemental Analyzer, and SPM samples with high carbon and nitrogen contents and sediments were acidified to measure organic carbon content. The precision of total and organic carbon determination is 0.05 %, that of nitrogen is 0.005 %, and the standard deviations are less than 0.08 for total and organic carbon and 0.02 for nitrogen. Nitrogen isotope ratios were determined with a FlashEA 1112 coupled to a MAT 252 (Thermo Fisher Scientific) isotope ratio mass spectrometer. The precision of nitrogen isotope analyses is better than 0.2 ‰, and the standard deviation less than 0.03.

2.2.4. Measurements of dissolved oxygen

The dissolved oxygen (DO) samples were collected, fixed, and titrated on board following the Winkler procedure at an uncertainty level of < 0.5 %. A small quantity of NaN_3 was added during subsample fixation to remove possible interferences from nitrite (Wong, 2012). The DO saturation (DO %) was calculated from field-measured DO concentration divided by the DO concentration at equilibrium with the atmosphere which was calculated from temperature, salinity and local air pressure, as per the Benson and Krause Jr (1984) equation.

2.2.5. Hydrodynamic model of nutrient export from BHS to the Yellow Sea

The regional three-dimensional hydrodynamic Hamburg Shelf Ocean Model, HAMSOM (Backhaus, 1985), was applied in the East China Seas (23°–45° N, 117°–131° E) to calculate the water and nutrient transport through the Bohai Strait for the year 2018. The HAMSOM model has been applied to investigate the Bohai Sea physical circulation for several decades now and has been extensively validated in the Bohai Sea (Huang et al., 1999; Hainbucher et al., 2004; Jia and Chen, 2021). The spatial resolution of the model is 2' (approx. 3.7 km) with 20 layers in vertical direction, while the calculation time step is 3 minutes. The upper 50 m of the HAMSOM model are resolved by layers of 5 m thickness. The topography data (resolution of 2') were obtained from marine navigation charts. The meteorological forcing was derived from an hourly ERA5 dataset with a spatial resolution of 0.25° (CCCS, 2017). The open boundary SSH and the boundary T and S data and for the initial T and S fields were extracted from the daily Mercator-Ocean dataset (1/12 degrees) (Lellouche et al., 2019). 13 partial tides derived from the TPXO8-atlas v1 were superimposed to the SSH along the open boundary (Egbert and Erofeeva, 2002). The observed monthly river discharge were available for the two largest rivers, i.e., Changjiang and YR (China, 2015-2018), while the inputs for the remaining rivers were derived from the Watergap dataset (0.5°, monthly climatology) (Müller Schmied et al., 2014). The spin-up period of this model is 1 year.

Four sites on a north-south section through the Bohai Strait, i.e., B33, B34, B35,

and B36, have been selected to represent the open boundary of the BHS (Fig. 1). The simulated SSH and current velocities (west-east-component) were extracted along this section. In addition, nutrient concentrations were interpolated from the observed data at the four sites to the grid of the hydrodynamic model along the Bohai Strait section. Since the observational data just include spring and summer values, the mean value of nitrate in spring and summer had to be extrapolated to an entire year.

2.3. Results

2.3.1. Hydrological properties and nutrients

2.3.1.1. Hydrological properties

Averages of salinity and temperature in spring were 32.3 ± 0.5 (n = 72) and 4.7 ± 0.8 °C (n = 72), respectively, and the water column was vertically mixed (Figure 2.2 and Figure 2.3). The YR discharged relatively warm water and the lowest salinity was observed in the southeast of YR estuary (site B68, T > 6 °C, S < 31). Thus, the Yellow River Diluted Water (YRDW) is here defined as the water off the YR estuary with salinities lower than 31. In summer, averages of salinity and temperature were 31.6 ± 0.8 (n = 88) and 22.4 ± 4.2 °C (n = 88), respectively, and the surface layer was stratified. The YRDW extended to an even larger area than in spring caused by high river discharge. The YRDW turned northeast towards LiaoDong Bay into the central BHS in the surface layer (T > 27 °C, S < 31).

The water column oxygen concentrations (see Appendix A1) in the study area in spring and summer were 10.27–11.47 mg L and 3.84–8.86 mg L^{-1}, respectively, and thus much higher than the threshold for water column denitrification (0.15 mg L^{-1}). The detailed results of DO and other parameters are shown in Appendix A2.
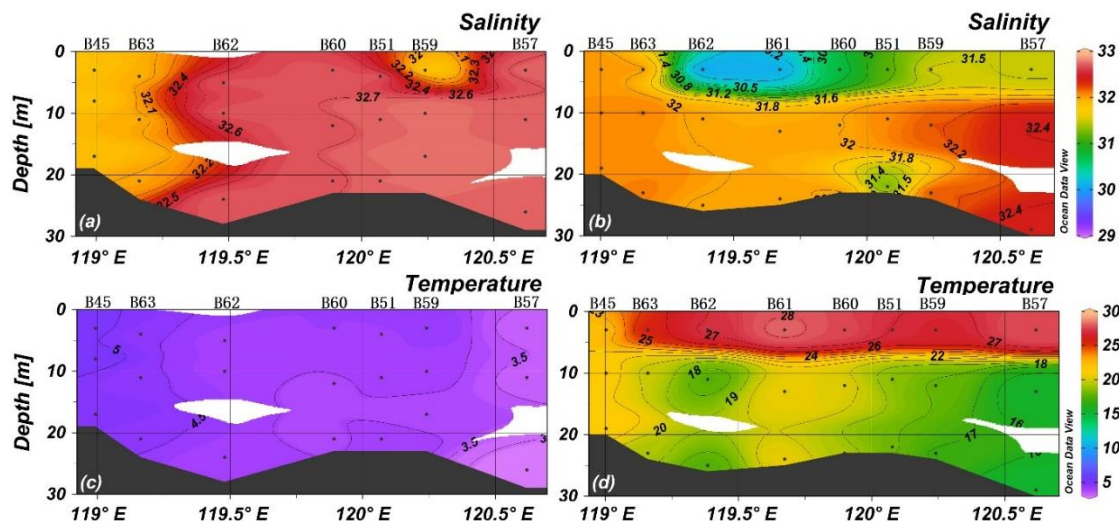
Figure 2.2. Temperature (°C) and salinity (psu) of section 1 of spring (a and c) and summer (b and d).
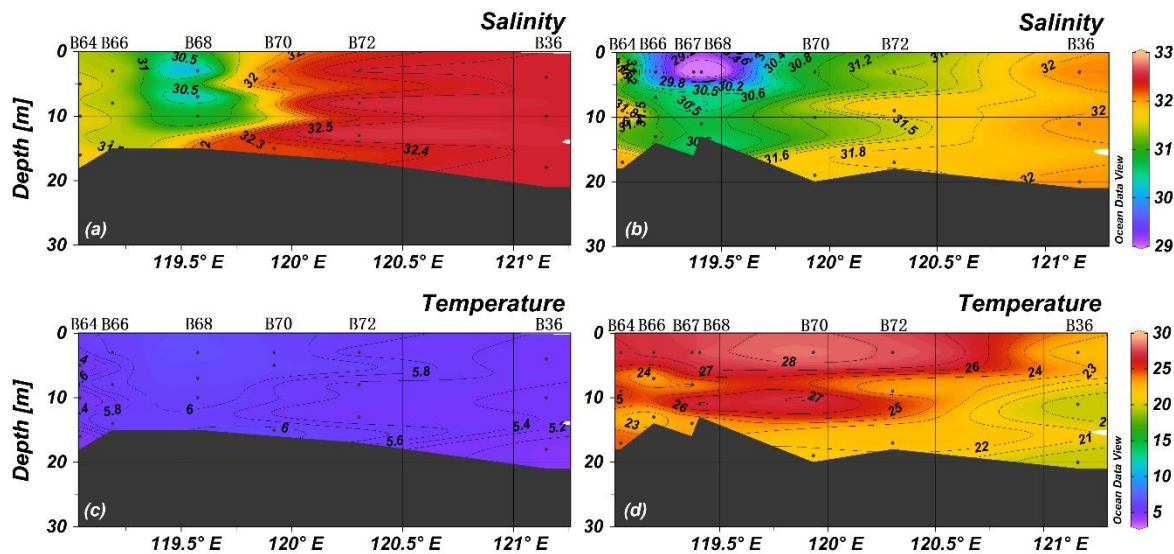
Figure 2.3. Temperature (°C) and salinity (psu) of section 2 of spring (a and c) and summer (b and d).

2.3.1.2. Nutrient concentrations and distributions

Nutrient concentrations in spring were almost vertically uniform, consistent with temperatures and salinities, and no distinct nutricline was observed (Figure 2.4). The YR discharge is indicated by a nitrate maximum at station B68 (31.0 μmol L^{-1}) and the lowest observed salinity. Concentrations of NH_4^+ were higher than 1 μmol L^{-1} and PO_4^{3-} concentrations were lower than 0.4 μmol L^{-1} adjacent to YR estuary, and PO_4^{3-} increased towards the central BHS (along section 1) and north of Shandong peninsula (along section 2). The average concentrations of NO_3^-, NO_2^-, NH_4^+ and PO_4^{3-} of all spring samples were 6.5 ± 5.8 μmol L^{-1}, 0.2 ± 0.2 μmol L^{-1}, 0.8 ± 0.5 μmol L^{-1}, and 0.4 ± 0.2 μmol L^{-1} (n = 72), respectively.

In summer, NO_3^- was almost depleted in the BHS except for stations B66 and B67 (included in section 2) located in the tongue of YRDW. NO_2^- and NH_4^+, concentration was higher than 2 μmol L^{-1} and 5.5 μmol L^{-1}, respectively, in the same area (Figure 2.5). In the central BHS (section 1), the upper 10 m water layer was nutrient depleted, while concentrations were high in the lower layer. The average concentrations of NO_3^-, NO_2^-, NH_4^+ and PO_4^{3-} of 1.9 ± 2.7 μmol L^{-1}, 0.8 ± 1.1μmol L^{-1}, 1.6 ± 1.9 μmol L^{-1} and 0.1 ± 0.1 μmol L^{-1} (n = 85), respectively.
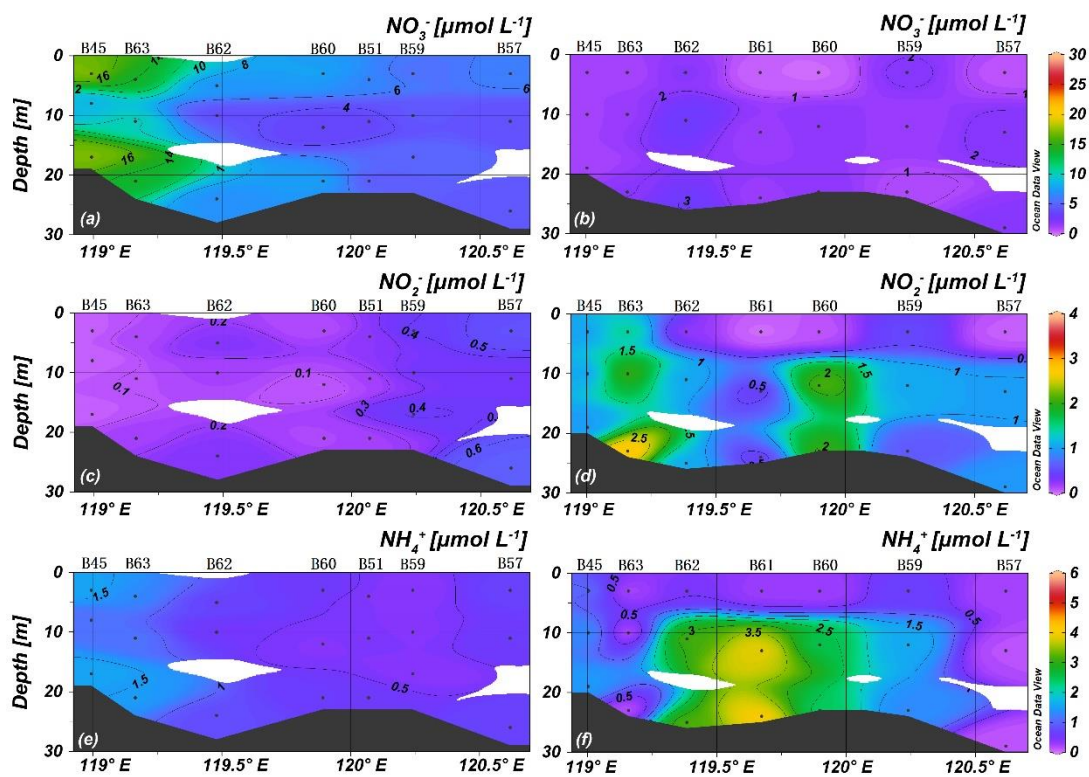
Figure 2.4. Nutrients of section 1 (µmol L^{-1}) of spring (a, c, and e) and summer (b, d, and f).
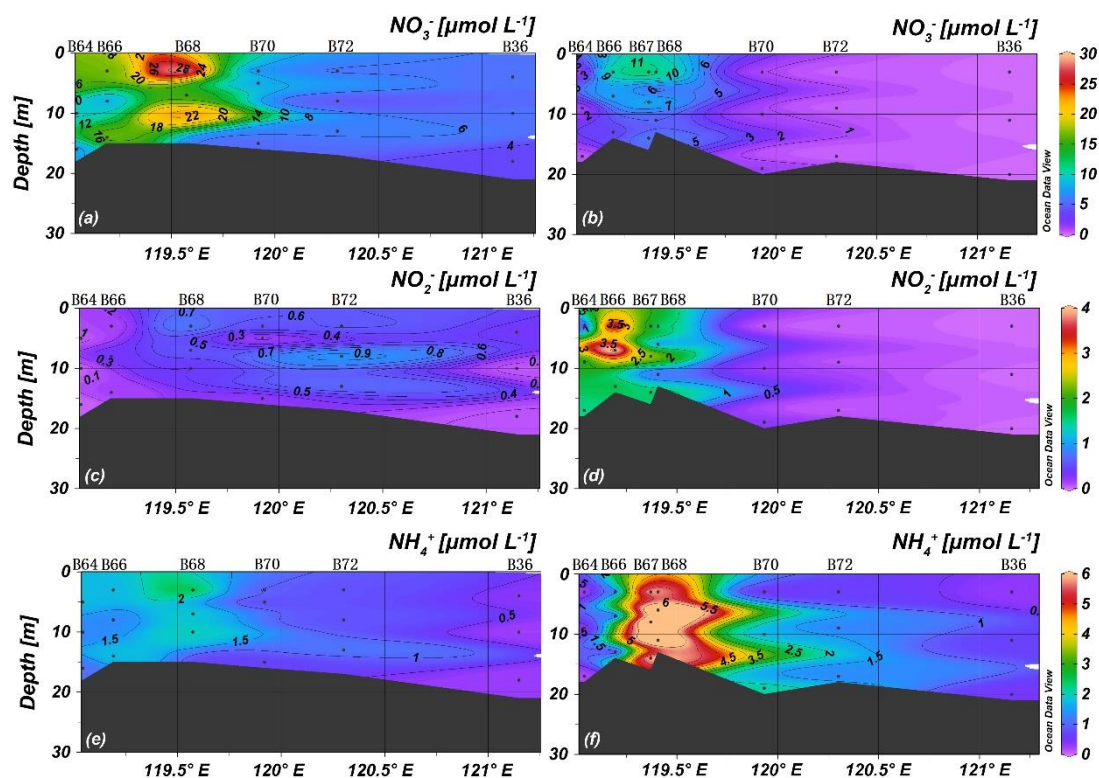
Figure 2.5. Nutrients of section 2 (μmol L^{-1}) of spring (a, c, and e) and summer (b, d, and f).

2.3.2. Dual isotopes of nitrate

In spring, the average values of δ^{15}N and δ^{18}O were 7.8 ± 1.4 ‰ and 12.0 ± 3.3 ‰ (n = 52), and δ^{15}N and δ^{18}O ranged between 5.6–10.5 ‰, and 5.0–20.0 ‰, respectively. δ^{15}N and δ^{18}O were both vertically homogenous, corresponding to the vertical profile of salinity, temperature, and nitrate. Relatively high δ^{15}N values were observed in the southwestern part of BHS including the areas adjacent to Bohai Bay and Laizhou Bay, which is consistent with high nitrate concentrations. The δ^{18}O was inversely related to δ^{15}N with low values near the YR estuary and high values in the northeast of the central BHS and north of Shandong peninsula (Figure 2.6 and Figure 2.7).

Due to the low nitrate concentration in summer, only a subset of samples could be

analyzed and most of these are from the YRDW that had $[NO_3^-] > 1.7$ µmol L^{-1}. The average values of $\delta^{15}N$ and $\delta^{18}O$ were 9.9 ± 3.5 ‰ (n = 23) and 8.7 ± 3.3 ‰ (n = 23), and ranged between 3.5–23.9 ‰ and 3.1–18.4 ‰, respectively. The mean value of $\delta^{15}N$ was higher than that of spring samples, whereas the $\delta^{18}O$ value was lower. Relatively high $\delta^{15}N$ and $\delta^{18}O$ values of 23.9 ‰ and 18.4 ‰ were registered in the surface water of YRDW (site B62) and decreased with water depths at increasing nitrate concentrations.
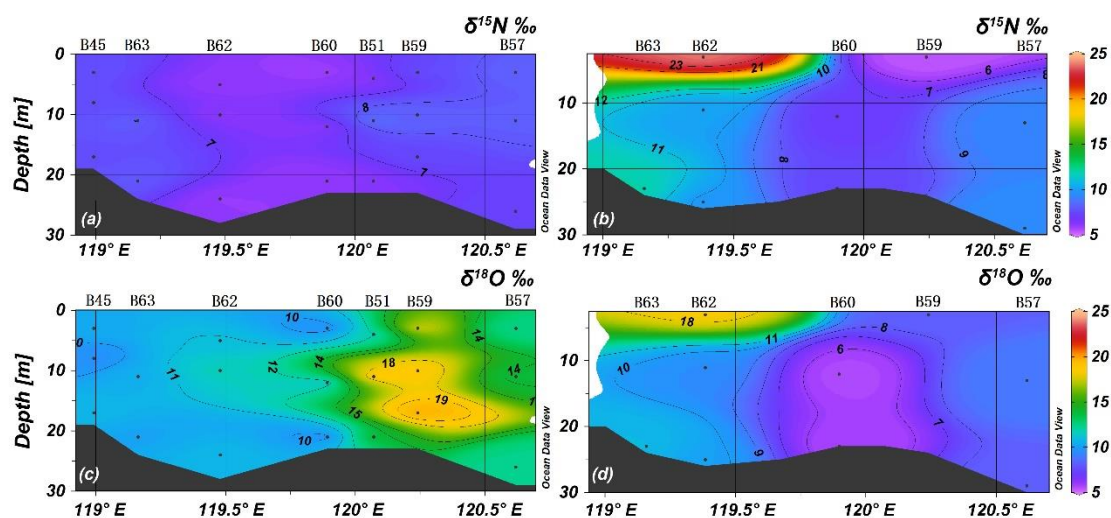
Figure 2.6. Nitrate isotopes (‰) of section 1 of spring (a and c) and summer (b and d).
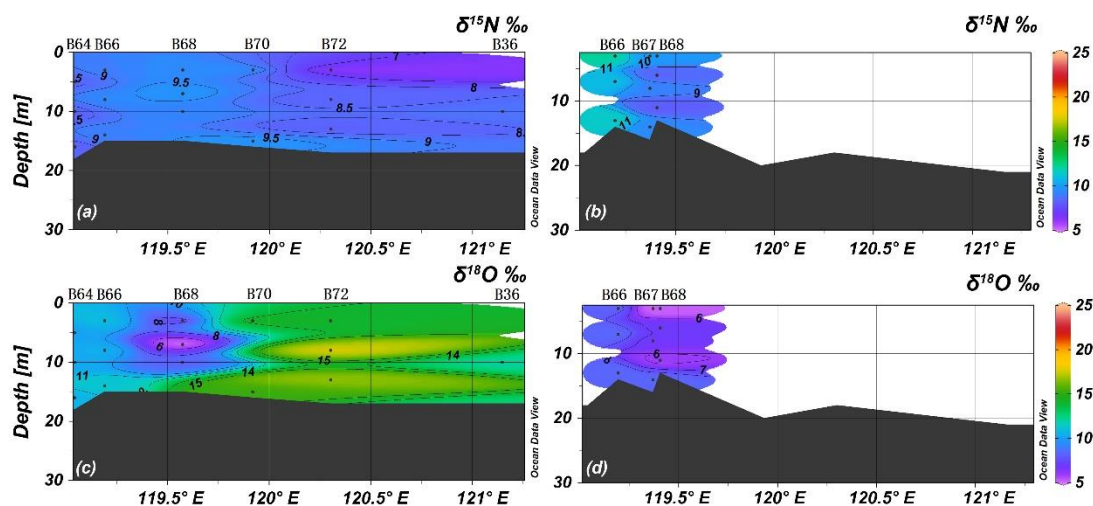
Figure 2.7. Nitrate isotopes (‰) of section 2 of spring (a and c) and summer (b and d).

2.3.3. Suspended particulate matter

In spring suspended particulate matter (SPM) concentrations were mostly vertically homogenous along both transects with high values (>15 mg L^{-1}) close to the YR mouth (see Appendix A3). C_{org} % and N % are anti-correlated with SPM concentrations and high values occurred in the central BHS and north of Shandong Peninsula. In summer SPM concentrations were significantly higher than in spring and maxima occurred in deep water off the YR (> 30 mg L^{-1}) and in the west part of the BHS. C_{org} % and N % maxima occur in surface waters in the eastern Laizhou Bay and the central BHS.

The average δ^{15}N of SPM in spring was 4.8 ± 0.9 ‰ (n = 14), with a maximum (> 6.10 ‰, n = 3) south of Luan River. The lowest values were observed in the southern Bohai Strait and northeast of YR estuary. The other samples varied in a narrow range of 3.9–4.7 ‰ (n = 11). In summer, the average of δ^{15}N was 5.7 ± 0.8 ‰ (n = 34) and ranged from 3.9 ‰ to 7.2 ‰. Systematic variation of δ^{15}N of SPM was barely discernable and only exhibited a weak decline from the YR mouth into the northeastern BHS (section 1) and into the Bohai Strait (section 2) (see Appendix A3), thus tracking

the salinity dilution gradient in the surface layer.

2.3.4.   The discharge of the Yellow River

The water discharge of the year 2018 determined at the Lijin hydrography station was 333.8×10^9 m^3 which was by 14 % higher than the multi-year average of 292.8×10^9 m^3 (1952-2015) (MWR, 2019). The monthly mean discharge was $27.80 \pm 20.21 \times 10^9$ m^3 per month (n = 12), which was higher than the multi-year average value by 14–51 %, indicating that in YR basin 2018 was a flood year. The water discharge maximum was from July to October (Figure 2.8). During May to November in 2018 (no value for June), the mass fluxes of nitrate, phosphate increased with the water discharge of YR, while the monthly fluxes of nitrite and ammonium exhibited an opposite tendency. δ^{15}N and δ^{18}O of YR nitrate ranged from 9.1–10.9 ‰ and 1.1–3.0 ‰, respectively. The monthly mass-weighted average value of δ^{15}N and δ^{18}O were 9.9 ‰ and 1.9 ‰, respectively. δ^{15}N and δ^{18}O were positively correlated (δ^{18}O = 1.04 × δ^{15}N - 8.43, R^2 = 0.85), as were δ^{15}N and the monthly mass flux of nitrate (R^2 = 0.63).
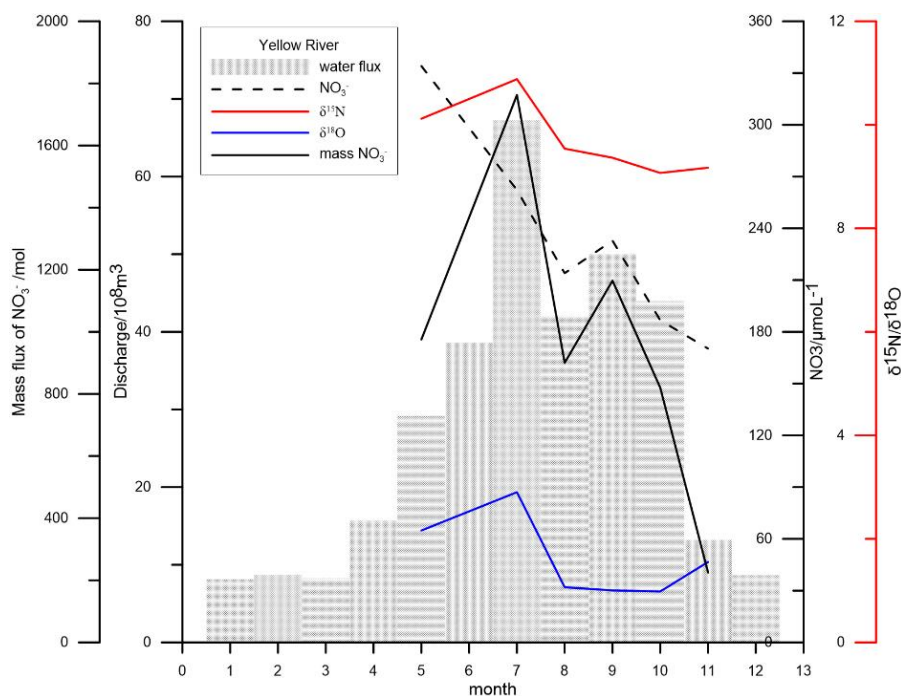
Figure 2.8. Monthly variation of water flux (shadowed bar), nitrate concentration (dashed line), mass flux of nitrate (solid line), and dual nitrate isotopes ($\delta^{15}N$ in upper red solid line and $\delta^{18}O$ in lower blue solid line) of YR in 2018. Water samples were monthly collected in May, July to November in Lijin, nitrate concentrations ($\mu mol\ L^{-1}$) and dual isotopes ($\delta^{15}N$ and $\delta^{18}O$, in per mil) were measured in home laboratory, monthly water flux data ($10^8\ m^3$)are according to the YR Sediment Bulletin 2018 (http://www.yrcc.gov.cn/nishagonggao/2018/index.html#p=20).

2.3.5. Nitrate exchange with the Yellow Sea

Based on current velocities and nutrient concentrations along the section crossing the Bohai Strait, the annual water and nitrate export from BHS to the YS in the year 2018 was calculated to 1.26×10^{-3} Sv (1 Sv=$10^6\ m^3\ s^{-1}$) and 0.9×10^9 mol year^{-1}, respectively. In this study, the exported nitrate are assumed with the average isotopes values of the BHS ($\delta^{15}N$ = 8.9 ‰ and $\delta^{18}O$ = 10.4 ‰).

Making use of the three-dimensional model (HAMSOM) results, it is also possible to determine a spatial distribution of the annual nutrient flux through the Bohai Strait section (Figure 2.9). Positive values represent a nutrient flux out of the Bohai Sea, while negative ones indicate a flux into the Bohai Sea. The strongest nutrient export occurs at the southern part of the Bohai Strait, while the major import takes place in the upper 15 m in the northern Bohai Strait (Figure 2.9).
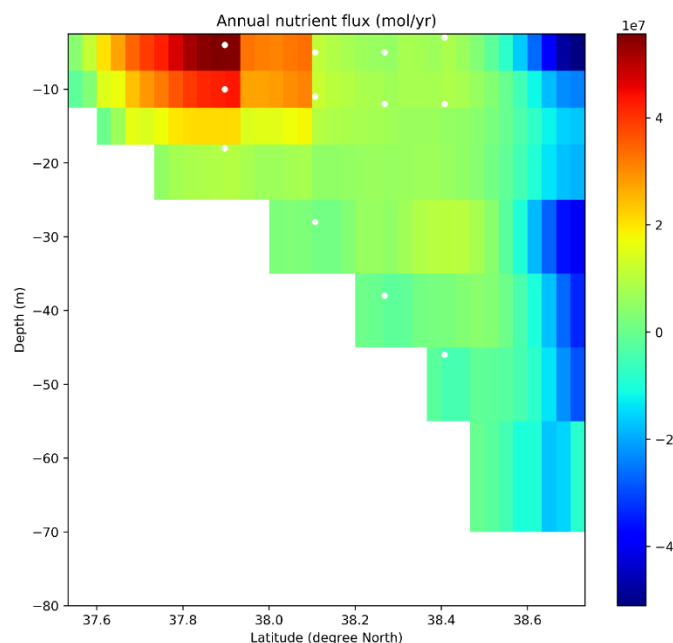
Figure 2.9. Simulated net fluxes of nitrate (mol year^{-1}) in the Bohai Strait of the year 2018. White dots are the sampling sites, the color bar is the flux of nitrate (10^7 mol year^{-1}), positive values stand for the export of nitrate from BHS to YS.

2.4. Discussion

2.4.1. The hydrographic and nutrients characteristics in spring and summer

The sampling in early spring occurred during a season of low biological activity so that nutrients behaved almost conservatively. YR discharged 333.8×10^9 m^3 water and 8.0×10^9 mol nitrate to the Bohai Sea in 2018, accounting for 85 % and 84 % of water and nitrate discharge of all large rivers in the Bohai Sea, respectively. As is indicated by the negative correlations of NO_3^- (r = -0.78, p < 0.01), and NH_4^+ (r = -0.79, p < 0.01) with salinity, the YR is one of the major sources of these nutrients in the BHS, whereas PO_4^{3-} is contributed by the inflow of saline waters from the YS as indicated by the positive correlation with salinity (r = 0.43, p < 0.01). Concentrations of nitrate were relatively high in the southern Bohai Strait but low in its northern part, suggesting that in spring nitrate-rich water flows out of Bohai Strait along the northern shore of

Shandong Peninsula in the LCC, while nitrate-depleted water flows in from the northern YS via the northern strait.

In summer, the water is stratified with the thermocline at about 8 m water depth and coinciding with halo- and nutriclines. Nutrients are depleted to trace amounts above the thermocline. In contrast to the other nutrients, phosphate concentrations did not increase with depth in the southwestern part of BHS (i.e. Bohai Bay and Laizhou Bay). Similar to the spring situation, salinity was weakly positively correlated with PO_4^{3-} (r = 0.29, p < 0.05) and NO_2^- (r = 0.32, p < 0.05), whereas it was negatively correlated with NO_3^- (r = -0.69, p < 0.01) and NH_4^+ (r = -0.37, p < 0.01), respectively. The average N/P ratio in BHS in spring and summer was 28.2 ± 38.2 and 86.9 ± 126.3, respectively, implying that productivity in BHS was phosphorus limited. Thus, diazotrophic N_2 fixation is excluded as a significant input of N_r because of high N:P ratios.

2.4.2. The main sources and sinks of nitrate in the BHS

Most of the external and internal sources of nitrate to the BHS are characterized by distinct dual isotope values. These fingerprints combined with mass flux estimates are in the following used to constrain the mass and isotope budget of nitrate in the BHS. Specifically, the role of internal cycling processes can thus be quantified, which were lacking in previous budgets. In the following, each of the sources and sinks is described, along with isotope composition or isotope fractionation associated with cycling processes.

2.4.2.1. Riverine inputs

The main input from this source of BHS N_r is from the YR and we calculated a nitrate input of YR of 7.95×10^9 mol year^{-1}, based on the annual average discharge (Yellow River Conservancy Commission of MWR, 2019) and the load-weighted nitrate concentration during our sampling period during the year 2018. The water discharge of the other 7 important rivers (Hai River, Shuangtaizi River, Daliao River, Luan River, Xiaoqing River, Daling River and Xiaoling River) sums up to 59.86×10^8 m^3 year^{-1}

(Ma et al., 2004; Zhang et al., 2004; Yu et al., 2018; MWR, 2019). Nitrate fluxes of these rivers were calculated based on water discharge and our nitrate measurements in YR, Hai River, Daliao River, Luan River and Xiaoqing River. Owing to a lack of data on nitrate concentrations of Shuangtaizi River, Daling River and Xiaoling River and considering that these rivers drain basins adjacent to Daliao River, we assume that nitrate concentration of these rivers were same as those of the Daliao River. The total riverine input of nitrate summed up to 9.49×10^9 mol.

The mass-weighted average annual values for $\delta^{15}N$ and $\delta^{18}O$ of nitrate in these rivers were 10.0 ‰ and 1.3 ‰, respectively, taken here to represent the river nitrate isotopic composition discharged into BHS.

2.4.2.2. Submarine groundwater input

The DIN supplied to BHS by submarine groundwater discharge (SGD) flux has been estimated to be 2–10 times the YR discharge (Peterson et al., 2008; Wang et al., 2015; Luo and Jiao, 2016). These fluxes of SGD are a mixture of submarine fresh groundwater discharge (SFGD) and recirculated saline groundwater discharge (RSGD) (Peterson et al., 2008; Liu et al., 2011; Liu et al., 2017a), but only the freshwater component is relevant as a source for the budget.

The latest estimates of SGD for the BHS are 10.0×10^9 m^3 year^{-1} (Liu et al., 2017a) and 19.1×10^9 m^3 year^{-1} (Wang et al., 2015), respectively. The nitrate concentration of SFGD is not documented, but the nitrate concentration of groundwater in YR Delta was 304.2 ± 254.2 µmol L^{-1} (Liu et al., 2011). For reducing the error of these indirectly measured data, we decided to use the value of 4.25×10^9 mol year^{-1} for the nitrate flux of SFGD, which is the averaged products of SFGD water fluxes and nitrate concentrations shown above. This value is only approximately 10 % of previous estimates of the input nitrate for SGD into BHS (Liu et al., 2011) due to the exclusion of RSGD.

Because of pollution and denitrification processes in soils, aquifers and groundwater (Soares, 2000; Chen et al., 2007; Zhang et al., 2013), the value of $\delta^{15}N$

and $\delta^{18}O$ of nitrate in SFGD is more enriched than those of river runoff and this is illustrated by the observed $\delta^{15}N$ value of 20.2 ± 9.0 ‰ (n = 19) of on-land groundwater near the YR delta (Chen et al., 2007). As there are as yet no reported $\delta^{15}N$ values of SFGD and RSGD inputs, we decided to take this value as the signal of nitrate $\delta^{15}N$ imported by SFGD into the BHS. There are no data available for $\delta^{18}O$ of nitrate of SFGD, and we will discuss possible constraints in the box model discussion (Sect. 2.4.3.2).

2.4.2.3. Atmospheric deposition

Combined atmospheric input by wet and dry deposition ranged from 3.14×10^9 mol year^{-1} to 3.42×10^9 mol yr^{-1} (Liu et al., 2003b; Zhang et al., 2004). We adopted the annual mass of NO_x deposition for China of 6.2 Tg year^{-1} (Zhao et al., 2017) and related this value to the area of the BHS, which results in an annual deposition of 3.6×10^9 mol year^{-1}. Owing to a lack of directly measured data for atmospheric NO_x the BHS, we adopt $3.42 \pm 2.29 \times 10^9$ mol year^{-1} (Zhang et al., 2004) as the atmospheric nitrate flux.

The nitrate $\delta^{15}N$ values of PM2.5 (fine particulate matter suspended in the air) ranged from 3.5–17.8 ‰ in northern China (Zong et al., 2017; Fan et al., 2019; Zhang et al., 2019; Song et al., 2020), whereas nitrate $\delta^{15}N$ of precipitation ranged from -2.5 to +0.9 ‰ (Zhang et al., 2008b; Chang et al., 2019; Kim et al., 2019; Li et al., 2019b). Assuming that PM2.5 is the main component of dry deposition we use a $\delta^{15}N$ value of 8.2 ‰ reported from Beihuangcheng island in Bohai Strait (Zong et al., 2017), while the wet deposition has a $\delta^{15}N$ value of -2.35 ‰ (Chang et al. (2019). Wet deposition in BHS was estimated as 54–68 % of total deposition (Liu et al., 2003b; Zhang et al., 2008b; Zhao et al., 2017), resulting in a mass-weighted average of BHS atmospheric deposition ranging from 1.03 –2.56 ‰, of which the arithmetic mean value of 1.80 ‰ is adopted here.

The nitrate $\delta^{18}O$ of PM2.5 in BHS ranged from 65.0–88.1 ‰ (seasonally) (Zong et al., 2017), the value in Beijing is 88.3 ± 6.9 ‰ (Song et al., 2020) and 57.80 ± 4.23 ‰ in cloud samples of Shandong (Chang et al., 2019). For nitrate $\delta^{18}O$ of dry deposition,

we thus assume a mean value of 80.5 ‰ and that wet deposition has a $\delta^{18}O$ of 57.8 ‰. These two estimates combined give a ratio of dry and wet deposition in the range of 65.8–68.0 ‰. The arithmetic mean value is 66.9 ‰, which we take to represent the $\delta^{18}O$ of nitrate deposited from the atmosphere to the BHS.

The ammonium deposited from the atmosphere is assimilated by phytoplankton and is subsequently entrained into the N cycle via remineralization and nitrification or is nitrified directly in the water. Thus, the nitrified atmospheric ammonium is included here as a source bearing on $\delta^{15}N$ of nitrate in the seawater. The ammonium deposition in BHS was 6.15×10^9 mol year^{-1}, which is more than the nitrate deposition of 3.42×10^9 mol year^{-1} (Zhang et al., 2004).

The atmospheric ammonium has low $\delta^{15}N$ values of -6.53 to -1.2 ‰ (Zhang et al., 2008b; Chang et al., 2019). Given that the $\delta^{15}N$ value of ammonium of the North China Plain is -1.2 ‰ ± 4.5 ‰ (Zhang et al., 2007), and that there is no obvious accumulation of ammonium in the surface layer in the observations, we assume that this isotope value is identical to the $\delta^{15}N$ value of nitrified atmospheric ammonium.

The $\delta^{18}O$ of nitrate from nitrification is roughly 1 ‰ higher than that of ambient H_2O (Casciotti et al., 2007; Casciotti et al., 2008b; DiFiore et al., 2009; Sigman et al., 2009). The $\delta^{18}O$ of H_2O in the BHS was reported as -0.67 ‰ ± 0.25 ‰ (n=10) (Wu, 1991; Kang et al., 1994) and thus the $\delta^{18}O$ of the newly nitrified nitrate should be approximately 0.3 ‰.

2.4.2.4. Benthic fluxes

A latest number of benthic reactive nitrogen loss including denitrification and annamox for the BHS and northern YS is 3.5×10^9 t N year^{-1} (Zhang et al., 2018). Combining the area of the BHS and assuming that 82 % benthic nitrogen loss was by denitrification, the denitrification flux calculates to 10.1×10^9 mol year^{-1}. Globally, the sediment denitrification rate varies in the range of approximately 0.5 to 2 mmol m^{-2} d^{-1} (Devol, 2015), which is equivalent to 14.1×10^9 mol year^{-1} to 28.2×10^9 mol year^{-1} in the BHS. We assume that diffusion is not accompanied by isotope fractionation (Devol,

2015), so that $\delta^{15}N$ and $\delta^{18}O$ of nitrate diffusing into the sediment are the same as the nitrate pool in BHS (8.9 ‰ and 10.4 ‰, respectively).

The processes of nitrogen cycling in sediments are complex and variable (Lehmann et al., 2004). The degradation of organic matter, nitrification and assimilation are acting under aerobic conditions, whereas denitrification, anammox and dissimilatory nitrate reduction to ammonium (DNRA) are observed under anaerobic conditions. When organic matter is degraded in the surface sediments, part of the produced ammonium diffuses into the overlying bottom water and subsequently is nitrified to nitrite and nitrate under aerobic condition. For our purpose only the ammonium nitrified bears on the seawater nitrate pool. The mean $\delta^{15}N$ value of sediment in BHS was 5.4 ‰ (n = 20), and according to the fractionation factor during organic matter remineralization of 2 ‰ (Möbius, 2013) and subsequent nitrification (see above), the $\delta^{15}N$ and $\delta^{18}O$ of nitrate efflux from the sediment are assumed to be 3.4 ‰ and 0.3 ‰, respectively.

2.4.2.5. Sedimentation

The mass flux of N_r sedimentation is unknown. In terms of the effects of N_r sedimentation on nitrate dual isotopes, phytoplankton organisms that assimilate nitrate from the dissolved phase are the main source of sinking particles, so that the N and O will be removed from the nitrate pool following the assimilation fractionation factor. Sinking particles in the BHS have a $\delta^{15}N$ of 5.2 ‰ ($\delta^{15}N_{sink}$) corresponding to the average values of spring and summer, which integrates multiple processes such as photosynthesis of phytoplankton, heterotrophic synthesis of bacteria, and heterotrophic degradation (remineralization).

There is no observed data of $\delta^{18}O$ of nitrate removed from the pool during assimilation ($\delta^{18}O_{sink}$), but this value can be estimate by the assimilation fractionation factor ($^{18}\varepsilon$). The per mil fractionation factors ε of N ($^{15}\varepsilon$) and O ($^{18}\varepsilon$) in nitrate during assimilation are generally assumed to be around 5 ‰, so that $^{15}\varepsilon : ^{18}\varepsilon = 1 : 1$. Here we adopt the average of $^{15}\varepsilon$ and $^{18}\varepsilon$ as 5 ‰ (DiFiore et al., 2009; Granger et al., 2010; Umezawa et al., 2013; Wang et al., 2016; Liu et al., 2017c; Wu et al., 2019), so that the

$\delta^{18}O$ of nitrate removed from the pool during assimilation ($\delta^{18}O_{sink}$) should be 5.0 ‰ according to the $\delta^{18}O$ (10.0 ‰) of the dissolved nitrate pool.

2.4.3.   The nitrate budget in the BHS

A box model of the nitrate budgets for the Bohai following the LOICZ approach (Zhang et al., 2004) balanced sources and sinks of nitrate in BHS and was updated by several other nitrate budgets for the BHS during last two decades (Liu et al., 2003b; Zhang et al., 2004; Liu et al., 2009a; Liu et al., 2011). All were, in general, not completely constrained because of a lack of data on some important source or loss terms. We here associate the nitrate isotope compositions of pools, sources, and sinks of nitrogen with a box model of the BHS nitrate in order to improve the understanding of nitrate cycling in the BHS. Finally, based on the combined mass and isotope box model informed by new data on the isotopic composition of nitrate, surface sediment, and suspended particulate nitrogen in the water column discussed above, we propose an updated N-budget that is internally consistent.

2.4.3.1.   The nitrate budget based on mass fluxes and corresponding δ15N values

The sources of nitrate for BHS are river inputs, submarine fresh groundwater input, atmospheric deposition, and remineralization. The most important sinks are net export to the YS, sediment denitrification and particulate matter sedimentation. Assuming the mass and N isotope of nitrate in the BHS are in steady–state, the sources and sinks of nitrate follow the Eq. 2.1 and Eq. 2.2:

$$(m_{atm} + m_r + m_N + m_{SFGD} + m_{ntr}) - (m_{net} + m_{sink} + m_{denitr}) = 0 \quad (2.1)$$

$$\begin{aligned}(\delta^{15}N_{atm}m_{atm} + \delta^{15}N_r m_r + \delta^{15}N_N m_N + \delta^{15}N_{SFGD}m_{SFGD} + \delta^{15}N_{ntr}m_{ntr}) \\ -(\delta^{15}N_{net}m_{net} + \delta^{15}N_{sink}m_{sink} + \delta^{15}N_{denitr}m_{denitr}) = 0\end{aligned} \quad (2.2)$$

where the terms m with different subscripts refer to the corresponding nitrogen mass fluxes, m_{atm} refers to atmospherically deposited nitrate, m_r refers to river nitrate, m_N refers to nitrified ammonium deposited from the atmosphere, m_{SFGD} refers to

nitrate in submarine fresh groundwater discharge, m_{ntr} refers to nitrification in the water column. In terms of sinks, m_{net} refers to the mass fluxes associated with net export of nitrate from BHS to the YS, m_{sink} refers to nitrate sedimenting from seawater as particulate N, and m_{denitr} refers to denitrification in the sediment. The unit of the mass fluxes is 10^9 mol. The "$\delta^{15}N$" refers to the $\delta^{15}N$ value of the N mass flux which with the same subscripts. As mentioned previously, the mass fluxes for m_N, m_{ntr}, m_{sink} and $\delta^{15}N_{ntr}$ are unknown and need to be constrained.

The range of $\delta^{15}N_{ntr}$ can be constrained by a simplified interior nitrate cycling model. Ammonium links particles and nitrate in this interior cycling, and there are two different sources of remineralised ammonium in seawater. One is ammonium diffusing from the sediment, the other is the ammonification of PN in the water column. The ammonium from remineralization through both processes is then nitrified in the water column and is a source of nitrate. The average $\delta^{15}N$ values of PN and sediments in the BHS in our study are 5.2 ‰ and 5.4 ‰, respectively. The fractionation factor of ammonification of PN and sediment as the first step of generating recycled nitrate are estimated to 3 ‰ (Sigman and Fripiat, 2019) and 2 ‰ (Möbius, 2013), respectively. The remineralised ammonium from PN and sediments thus should have $\delta^{15}N$ values between 2.2 ‰ and 3.4 ‰.

The ammonium concentrations in the BHS are low in the water column in spring and in the surface layer in summer, indicating that the ammonium from PN mineralization is most likely completely converted to nitrate, so that there is no fractionation effect for this step. Thus, the $\delta^{15}N$ value of newly nitrified nitrate from complete nitrification of ammonium generated by PN mineralization is 2.2 ‰. In the case of incomplete nitrification, especially under the thermocline in summer, the newly nitrified nitrate has a $\delta^{15}N$ of 0.2 ‰, given a net fractionation factor of nitrification (ammonium to nitrate) of 2 ‰ (Sigman and Fripiat, 2019). In our model below, the assimilation of ammonium originating from SPM remineralization was not included, as its proportion is unknown in the BHS. The simplified model may thus underestimate the input of ^{15}N-depleted nitrogen into the nitrate pool.

Ammonium diffusing out of the sediment will either be mixed into the euphotic

layer and subsequently assimilated by the phytoplankton, or nitrified in the water column. The accumulating of ammonium beneath the thermocline was a significant process in summer, as shown by the high nitrite and ammonium concentrations beneath the thermocline. The ratio of these two branching processes is not known in the BHS. If all of the ammonium from sediment is nitrified, the produced nitrate will have a $\delta^{15}N$ of 3.4 ‰ (see above). If the ammonium is only partially nitrified (especially in summer beneath the thermocline), the produced nitrate will have a $\delta^{15}N$ of 1.4 ‰ at a fractionation factor of nitrification of 2 ‰ (Sigman and Fripiat, 2019). Thus, the $\delta^{15}N$ value of the nitrate produced by nitrification ($\delta^{15}N_{ntr}$) of ammonium from sediment is in the range of 1.4 ‰ to 3.4 ‰.

Overall, combing the $\delta^{15}N$ ranges of PN- and sediment- originated nitrate, the range of $\delta^{15}N$ for newly nitrified nitrate is 0.2–3.4 ‰.

2.4.3.2. The coupled N and O budgets box model of nitrate

Because the nitrate mass fluxes m_N, m_{ntr}, and m_{sink}, cannot be segregated only based on N mass budgets and $\delta^{15}N$ values, we turn to the $\delta^{18}O$ values of the sources and sinks of nitrate for further constraints. Eq. 2.3 applies if we assume that the oxygen isotope composition of nitrate reflects the steady–state mass fluxes, as does $\delta^{15}N$ of the nitrate pool:

$$
\begin{aligned}
&(\delta^{18}O_{atm}m_{atm} + \delta^{18}O_r m_r + \delta^{18}O_N m_N + \delta^{18}O_{SFGD}m_{SFGD} + \delta^{18}O_{ntr}m_{ntr}) \\
&-(\delta^{18}O_{net}m_{net} + \delta^{18}O_{sink}m_{sink} + \delta^{18}O_{denitr}m_{denitr}) = 0
\end{aligned}
\quad (2.3)
$$

where the $\delta^{18}O$ subscripts refer to the nitrate mass flux with the same subscripts. The $\delta^{18}O$ of different sources and sinks are either fixed values or ranges of values in our own data, or those taken from the literature (Table 2.1).

According to Eq. 2.1, 2.2 and 2.3, the unknown mass fluxes m_N, m_{ntr} and m_{sink} can be solved by a set of ternary linear equations including the three unknown terms, when appropriate boundary values of $\delta^{15}N_{ntr}$ and $\delta^{18}O_{SFGD}$ are chosen. $\delta^{15}N_{ntr}$ ranged in 0.2 ‰ to 3.4 ‰ as discussed in Sect. 2.4.3.1, whereas $\delta^{18}O_{SFGD}$ is a crucial term without any data or literature constraint. As the only constraint, $\delta^{18}O_{SFGD}$ is expected to be

higher than the value of nitrate imported from the rivers ($\delta^{18}O_r = 1.3$ ‰) due to the fractionation associated with denitrification in the anaerobic aquifers (see Sect. 2.4.2.2). The results can be summed up in three different cases:

(1) When setting the value of $\delta^{15}N_{ntr}$ to 3.4 ‰, we obtain estimates for m_N that range from 0.00 to 4.83×10^9 mol yr^{-1}, for m_{ntr} in the range of 15.08 to 32.27×10^9 mol year^{-1} and m_{sink} in the range of 26.08–38.45×10^9 mol year^{-1}. The corresponding values of $\delta^{18}O_{SFGD}$ range from 1.3–15.9 ‰, and the upper range of $\delta^{18}O_{SFGD}$ yields $m_N = 0.0$ due to the assumption that any mass flux must be equal or greater than 0.

(2) When we choose a $\delta^{15}N_{ntr}$ value of $3.2 - 2.4$ ‰, respectively, to explore effects of the methodological error of $\delta^{15}N$ for our isotope method (0.2 ‰, see Sect. 2.2.2), again under the premise that the mass fluxes are positive numbers, results in m_N, m_{ntr} and m_{sink} estimates in a narrower range than when $\delta^{15}N_{ntr}$ is 3.4 ‰; these results are not shown.

(3) $\delta^{15}N_{ntr}$ values lower than 2.4 ‰ result in $\delta^{18}O_{SFGD}$ lower than 1.3 ‰, which is highly unlikely.

Thus, reasonable solutions only are reached when $\delta^{15}N_{ntr}$ is between 3.4 ‰ and 2.4 ‰. The results of the budget are shown in Figure 2.10 and Table 2.1, respectively.

atmospheric (m_{atm}) = 3.4
$\delta^{15}N_{atm}$ = 1.8 ‰
$\delta^{18}O_{atm}$ = 66.9 ‰

atmospheric (m_N) = 0.0–4.8
$\delta^{15}N_N$ = -1.2 ‰
$\delta^{18}O_N$ = 0.3 ‰

rivers (m_r) = 9.5
$\delta^{15}N_r$ = 10.0 ‰
$\delta^{18}O_r$ = 1.3 ‰

net export (m_{net}) = 0.9
$\delta^{15}N_{net}$ = 8.9 ‰
$\delta^{18}O_{net}$ = 10.4 ‰

Nitrate pool of BHS
NO_3^- = 5.82 × 10⁹ mol
$\delta^{15}N_{NO_3^-}$ = 8.9 ‰
$\delta^{18}O_{NO_3^-}$ = 10.4 ‰

SFGD (m_{SFGD}) = 4.3
$\delta^{15}N_{SFGD}$ = 20.2 ‰
$\delta^{18}O_{SFGD}$ = 1.3–15.9 ‰

Sedimentation (m_{sink}) = 26.1–38.5
$\delta^{15}N_{sink}$ = 5.2 ‰
$\delta^{18}O_{sink}$ = 5.0 ‰

Denitrification (m_{denitr}) = 10.1
$\delta^{15}N_{denitr}$ = 8.9 ‰
$\delta^{18}O_{denitr}$ = 10.4 ‰

Nitrification (m_{ntr}) = 15.1–32.3
$\delta^{15}N_{ntr}$ = 2.4–3.4 ‰
$\delta^{18}O_{ntr}$ = 0.3 ‰

Figure 2.10. The budgets and the corresponding dual isotope values of nitrate in the BHS 2018. The terms included are discussed in the text in Sect. 2.4.3. The unit of mass flux is 10⁹ mol year⁻¹.

Table 2.1. Sources and sinks and the corresponding $\delta^{15}N$ and $\delta^{18}O$ values of nitrate in the BHS

	Contributions	Mass fluxes 10^9mol NO_3^-	References	$\delta^{15}N$	References	$\delta^{18}O$	References
Sources							
Atmosphere (nitrate)	6.9–9.2 %	3.4	Zhang et al. (2004)	1.8 ‰	Assumption based on Liu et al. (2003b); Zhang et al. (2008b); Zhao et al. (2017); Zong et al. (2017); Chang et al. (2019), see Sect. 2.4.2.3	66.9 ‰	Assumption based on Liu et al. (2003b); Zhang et al. (2008b); Zhao et al. (2017); Zong et al. (2017); Chang et al. (2019); Song et al. (2020), see Sect. 2.4.2.3
Atmosphere (nitrified ammonium)	0.0–13.0 %	0.0–4.8	Assumption based on this study, see Sect. 2.4.2.3	-1.2 ‰	Assumption based on Sigman et al. (2005); Zhang et al. (2007), see Sect. 2.4.2.3	0.3 ‰	Assumption based on Wu (1991); Kang et al. (1994); Casciotti et al. (2007); Casciotti et al. (2008a); DiFiore et al. (2009); Sigman et al. (2009), see Sect. 2.4.2.3
Rivers	19.2–25.6 %	9.5	Assumption based on Ma et al. (2004); Zhang et al. (2004); Yu et al. (2018) and this study, see Sect. 2.4.2.1	10.0 ‰	This study	1.3 ‰	This study
SFGD	8.6–11.5 %	4.3	Assumption based on	20.2 ‰	Chen et al. (2007)	1.3–	Assumption based on

			Chen et al. (2007); Liu et al. (2011); Wang et al. (2015); (Liu et al., 2017a), see Sect. 2.4.2.2			15.9 ‰	this study, see Sect. 2.4.2.2 and 2.4.3.2
Nitrification	40.7–65.3 %	15.1–32.3	Assumption based on this study, see Sect. 2.4.3.2	2.4–3.4 ‰	Assumption based on Möbius (2013); Sigman and Fripiat (2019), see Sect. 2.4.3.2	0.3 ‰	Assumption based on Wu (1991); Kang et al. (1994); Casciotti et al. (2007); Casciotti et al. (2008a); DiFiore et al. (2009); Sigman et al. (2009), see Sect. 2.4.2.3
Sinks							
Net export	1.8–2.4 %	0.9	Assumption based on this study, see Sect. 2.3.5	8.9 ‰	Assumption based on this study, see Sect. 2.3.5	10.4 ‰	Assumption based on this study, see Sect. 2.3.5
Sedimentation	70.4–77.8 %	26.1–38.5	Assumption based on this study, see Sect. 2.4.3.2	5.2 ‰	Assumption based on this study, see Sect. 2.4.2.5	5.0 ‰	Assumption based on this study, see Sect. 2.4.2.5
Denitrification	20.4–27.2 %	10.1	Liu et al. (2011); (Zhang et al., 2018)	8.9 ‰	Assumption based on this study, see Sect. 2.4.2.4	10.4 ‰	Assumption based on this study, see Sect. 2.4.2.4

The mass flux of nitrate (m_N) originating from nitrification of atmospheric ammonium ranges from 0.00 to 4.83×10^9 mol year^{-1} and accounts for up to 79 % of the total ammonium deposition (6.15×10^9 mol year^{-1}; Zhang et al. (2004)). This in turn implies that most of the atmospherically deposited ammonium is directly assimilated rather than nitrified to nitrate. This agrees with phytoplankton preference to assimilate ammonium rather than nitrate (Glibert et al., 2016). The bulk of internal sources of nitrate originates from nitrification in the water column (from water column ammonification and ammonium diffusing from sediment). This single source (m_{ntr}) accounts for 40.7–65.3 % of the total sources of nitrate in BHS and appears to be much more important than in other coastal environments. For example, between 15–27 % of productivity was supported by nitrified ammonium in the seawater in Monterey Bay (Wankel et al., 2007). Likewise, nitrification supplied 34 % of the surface nitrate in eastern Hainan Island, which like Monterey Bay is also an upwelling area (Chen et al., 2020). This indicates that nitrate regeneration by nitrification may play a more important role in shallow and land-input dominated marginal seas than in upwelling dominated marine settings.

2.4.3.3. Assessment of model uncertainties

The uncertainties of the modeled nitrate mass and isotope budget lie essentially in some of the mass flux estimates and in possibly erroneous assumptions on values of $\delta^{15}N$ and $\delta^{18}O$ in some of the sources and sinks. In the sensitivity test, the three critical mass fluxes m_N, m_{ntr}, and m_{sink}, and the upper limit value of $\delta^{18}O_{SFGD}$ change correspondingly when only one single term or one group of terms change (i.e., mass flux or isotope value). Note that the lower limit of m_N and $\delta^{18}O_{SFGD}$ is fixed as 0 and 1.3 ‰, respectively, so that only the relative deviations of their upper limits are discussed below. The results are given in relative deviation to our best estimates in the budget. In addition, the widest ranges of mass fluxes and $\delta^{18}O_{SFGD}$ are covered when $\delta^{15}N_{ntr} = 3.4$ ‰ in the standard budget, thus we only compare the deviations when $\delta^{15}N_{ntr} = 3.4$ ‰.

River input of nitrate is 9.49×10^9 mol in the year 2018 as suggested above. Considering that the river fluxes are variable annually, we also adopt the multi-year average value (1952–2015) water discharge of YR of 292.8 km^3 instead of 333.8 km^3 in 2018 (MWR, 2019). Hence the annual nitrate discharge is 8.52×10^9 mol and is 10 % less than our preferred estimate; the resulting relative deviations are shown in Table 2. With respect to the isotope composition of the river nitrate, our observations suggest that the nitrate $\delta^{15}N$ and $\delta^{18}O$ of YR changed little during the sampling period. On the other hand, the average values of nitrate $\delta^{15}N$ and $\delta^{18}O$ for rivers are mass weighted instead of arithmetic mean values, so that a change of nitrate $\delta^{15}N$ and $\delta^{18}O$ for rivers

with low nitrate discharges would induce little change of the average values. Considering the wide variations of the riverine dual nitrate isotopes around the BHS (Yue et al., 2013; Yu et al., 2021), we tested situations where the dual nitrate isotope values of the smaller rivers are 0.5 and 2 times our observed values (Table 2: 0.5 $\delta^{15}N_r$ and $\delta^{18}O_r$, 2 $\delta^{15}N_r$ and $\delta^{18}O_r$). The results suggest that the budget is particularly sensitive to higher $\delta^{15}N_r$ and $\delta^{18}O_r$ than assumed in our preferred model.

We consider the mass flux of atmospheric deposition of nitrate to be reliable, because differences in estimates from previous studies are quite small. According to these previous estimates (Liu et al., 2003b; Zhao et al., 2017), we adopt the minimum and maximum in mass flux of 3.14×10^9 mol to 3.65×10^9 mol for uncertainty estimates. For $\delta^{15}N_{atm}$, we test the values 1.0 ‰ and 2.6 ‰ according to the variable proportion of wet/dry deposition with different $\delta^{15}N$ endmembers. Likewise, $\delta^{18}O_{atm}$ was varied in the range of 60.3 ‰ to 71.6 ‰.

The flux of SFGD into the BHS varies in the range of 2.68×10^9 mol to 5.82×10^9 mol, which is mainly due to the different SFGD water fluxes assumed in our budget. Only if m_{SFGD} is assumed to be $> 2.90 \times 10^9$ mol the results match our assumption. When $m_{SFGD} = 5.82 \times 10^9$ mol, the relative deviations are large (Table 2.2), implying that our budget is very sensitive to m_{SFGD}.

The flux of denitrification in the BHS has a confidence interval of 15 % (Zhang et al., 2018), resulting in the m_{denitr} to range from 8.57×10^9 mol to 11.60×10^9 mol. The results of tests with these two fluxes are shown in Table 2.2.

Overall, these tests indicate that m_N and $\delta^{18}O_{SFGD}$ vary by ±50 % and are particularly sensitive to uncertainties of the assumed endmembers, whereas the relative deviations of m_{ntr}, m_{sink} normally vary in the range of ±20 %. Uncertainties will be significantly reduced if any of these terms can be constrained by further empirical studies.

Table 2.2. Results of sensitivity tests on mass fluxes and isotopes.

Test	m_N	m_{ntr}	m_{sink}	$\delta^{18}O_{SFGD}$
$m_r = 8.52$	-28 %	-8 % to 14 %	-9 % to 1 %	-25 %
0.5 $\delta^{15}N_r$ and $\delta^{18}O_r$	-20 %	-8 % to 6 %	-7 % to 0	-18 %
2 $\delta^{15}N_r$ and $\delta^{18}O_r$	39 %	-11 % to 16 %	1 % to 13 %	37 %
$m_{atm} = 3.14$	5 %	-19 % to -7 %	-15 % to -9 %	4 %
$m_{atm} = 3.65$	-54 %	-9 % to 41 %	-10 % to 11 %	-49 %
$\delta^{15}N_{atm} = 1.0$ ‰	-40 %	-13 % to 18 %	-13 % to 0 %	-37 %
$\delta^{15}N_{atm} = 2.6$ ‰	-15 %	-3 % to 10 %	-5 % to 0 %	-14 %
$\delta^{18}O_{atm} = 60.3$ ‰	8 %	-27 % to 8 %	-18 % to -9 %	8 %
$\delta^{18}O_{atm} = 71.6$ ‰	-54 %	-8 % to 44 %	-9 % to 12 %	-49 %

m_{SFGD} = 5.82	116 %	-41 % to 46 %	1 % to 38 %	54 %
m_{denitr} = 8.57	13 %	6 % to 10 %	12 %	12 %
m_{denitr} = 11.60	-13 %	-10 % to -6 %	-12 %	-12 %

2.4.3.4. Biogeochemical implications of the box model

In other coastal eutrophic regions, such as the North Sea, a high $\delta^{15}N$ of river nitrate is reflected in a halo of high $\delta^{15}N$ in surface sediments in offshore areas (Pätsch et al., 2010). In the Bohai Sea, such an isotopic halo of river-borne eutrophication is not observed despite similar water exchange rates of 1–2 years (Serna et al., 2010; Li et al., 2015b) and similarly isotopically enriched river inputs. We speculate that the lack of a fingerprint of river nitrate in the $\delta^{15}N$ of sediments of BHS may be masked by active nitrification and atmospheric deposition that rapidly eradicate and homogenise spatial gradients.

Despite the uncertainties that are related to the box model approach, combining mass and isotope budgets of nitrate sources and sinks is clearly superior to solely nitrate mass balance considerations, especially when it comes to segregating the anthropogenic nitrate and the recycled nitrate inputs. It is of note that the BHS does not appear to pass on significant amounts of nitrate to the adjacent northern YS, so that the effects of excessive loading of this shallow mixing zone between land and ocean with anthropogenic nitrogen are yet mitigated by internal cycling processes.

2.5. Conclusions

Rivers contributed 19.2–25.6 % and the combined terrestrial runoff (including submarine discharge of nitrate with fresh groundwater) account for 27.8–37.1 % of the total nitrate input to the BHS. Atmospheric input contributes 6.9–22.2 % of nitrate to the BHS. Nitrification contributes 40.7–65.3 % of the total nitrate, indicating an unusually active interior nitrogen cycling of in the BHS. Nitrate was mainly trapped in the BHS and only very little was exported to the YS (only 1.8–2.4 %). Furthermore, nitrate was rather assimilated than exported to the YS along the main transport pathway Lubei Coastal Current, effectively retaining N_r in BHS. Sedimentation trapped 70.4–77.8 % of nitrate inputs, whereas denitrification was only active in the sediments that removed 20.4–27.2 % of nitrate from the pool. Seasonal biogeochemical variations were observed in the BHS in that dissolved inorganic nitrogen increased during summer under the thermocline, implying significant biological regeneration. If the interior cycling increases, for instance fueled by increased terrestrial and atmospheric N_r inputs, respiration coupled to organic matter and N recycling will increase and water-column hypoxia could consequently spread in the future and compromise ecosystems in the BHS. Whether this will invigorate water-column denitrification to balance the additional inputs is an open question, as is the capacity of BHS as a nitrate buffer

between the growing source of N_r on land and the open ocean.

3. Chapter 3 – Internal cycling of nitrogen in the Yellow Sea

3.1. Introduction

The small area of the coastal seas compared to the vast open ocean hosts around 20 % of all marine primary production (Jahnke, 2010) and plays a key role in processing nutrients and contaminants that enter the ocean via continental runoff and rivers (Levin et al., 2015b). River input and atmospheric deposition are the largest contributors and supply more than half of the reactive nitrogen (N_r) to the coastal sea areas (Voss et al., 2013). Anthropogenic activities have doubled or tripled N_r supply from natural processes at a global scale (Galloway et al., 2013), so that human activities on land are more and more impacting ecosystems in marginal seas (Levin et al., 2015b). An example are the seas bordering mainland China. The contribution of Chinese major estuaries to global coastal seas has been estimated at 5.4 Tg N yr^{-1} (Gu et al., 2015), which is about 10 % of the global river input for dissolved inorganic nitrogen (DIN) (Smith et al., 2003; Liu et al., 2009a). The increased input of anthropogenic N_r in the last decade resulted in a shift from N-deficiency to P-deficiency in the Yellow Sea (YS) and East China Sea (ECS) (Wei et al., 2015; Moon et al., 2021).

The YS with an area of about 3.8×10^5 km^2 and an average depth of 44 m is a semi-closed marginal sea surrounded by mainland China and the Korean peninsula. It connects to the Bohai Sea in the northwest by the narrow Bohai Strait and with the ECS in the south. Changjiang River (Yangtze River), the largest river in China, discharges on average 9.25×10^{11} m^3 of water per year into the ECS, of which about 20 % is advected into the YS (Fan and Song, 2014; Liu et al., 2020). Changjiang Diluted Water (CDW) is a main nutrient source of YS in summertime, while Yellow Sea Warm Current water (YSWC), the sub-branch of the Kuroshio Current, in wintertime is another major source (Jin et al., 2013). Regionally, excessive DIN introduced by terrestrial runoff and anthropogenic activities resulted in the potential for P limitation of primary production in the coastal areas (Yuan et al., 2014; Guo et al., 2020a). Globally, the accelerated nutrient import from the Kuroshio Current, the western Pacific boundary current, under global warming conditions also influences the nutrient inventory of the YS (Wei et al., 2015; Zheng and Zhai, 2021). The concentrations of nitrate and DIN in the southern YS have been continuously increasing from the 1980s (Li et al., 2015a; Wei et al., 2015; Wang et al., 2020b) and have been held responsible for increasing incidences of harmful algae blooms and macroalgal blooms in recent years (Li et al., 2017b; Wang et al., 2018; Xiao et al., 2019).

The Yellow Sea Cold Water Mass (YSCWM) fills the central YS trough and forms due to the unique basin topography and the impact of both the seasonal evolution of the thermocline and the circulation system in the YS (Zhang et al., 2008a). This water mass is a significant pool of nutrients, supplying them to the southern YS by vertical diffusion/upwelling processes (Su et al., 2013; Wei et al., 2016; Wang et al., 2020c). It is also a sink of nitrate (Liu et al., 2003a; Duan et al., 2016) due to benthic processes rather than to water column denitrification (Zhang et al., 2018).

Up to now, the portions of regenerated nitrate in the YSCWM have not been quantified, and the dynamics of internal nitrogen cycling are not clear. In our study, we measured the nutrients, dual stable isotopes of nitrate, and stable N-isotope composition of particulate and sedimentary nitrogen in two seasons in the YS. Results of the isotopic investigation quantify the shares of preformed and newly regenerated nitrate in the YSCWM. Seasonal comparison of DIN quantity and isotopic character in the northern and southern YSCWM furthermore give insights into how the regional and global nutrient sources affect the YSCWM in the central YS trough.

3.2. Materials and methods

3.2.1. Sample collection

Research cruises were carried out by R/V *Dongfanghong 2* in spring and summer 2018 with 42 sampling sites in April and 45 sites in August, respectively (Figure 3.1). Water samples were taken from several depths by 12 L Niskin bottles attached to a CTD rosette (911plus, Seabird, USA). The water samples were filtered using nucleopore polycarbonate filters (0.4 μm) with plastic Nalgene filtration units. The filtered water was collected in Falcon PE tubes (45 mL), frozen immediately (-20 ℃) and kept frozen until analyses in the home laboratory. Between 0.5 to 8 L of water were filtered through pre-weighed GF/F filters (0.7 μm, Φ = 47mm, Sigma Aldrich) which had been pre-combusted at 450 ℃ for 4 h. The filters were subsequently dried on board at 45 ℃ for 24 hours. Surface sediments were taken with a box corer and surface samples were frozen at -20 ℃ and were kept frozen until analysis in the home lab.
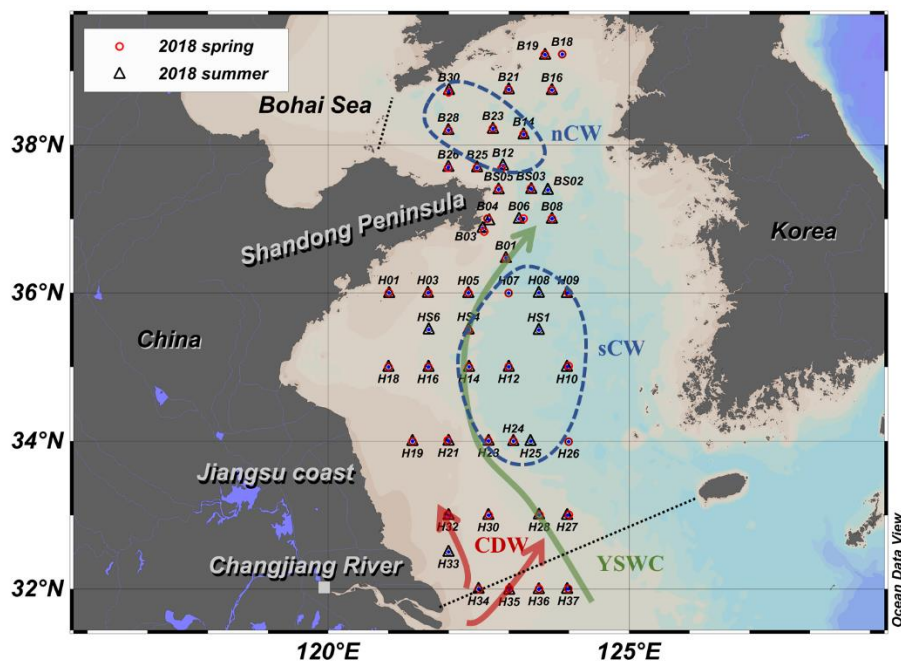
Figure 3.1. Sampling stations of spring and summer cruises are marked by red circles and black triangles, respectively. Note that most of the stations were sampled on both expeditions. The southern and northeastern boundary of the Yellow Sea is marked by the black dashed line. Yellow Sea Warm Current (YSWC) and Changjiang Diluted Water (CDW) are important external waters in spring and summer, respectively. These currents are drawn according to their general positions and our data of 2018. Sampling stations clustering in the north Cold Water mass (nCW) and south Cold Water (sCW) stations are marked by blue dashed lines, nCW and sCW are water masses defined in this study, they both are part of the Yellow Sea Cold Water Mass (YSCWM).

3.2.2. Measurements of nutrients and nitrate isotopes

Nutrient concentrations were measured with an AutoAnalyzer 3 system (Seal Analytics) using standard colorimetric methods (Grasshoff et al., 2009). The relative error of duplicate sample measurements was below 1.5 % for NO_x and phosphate concentrations, below 0.3 % for ammonium. The detection limit was < 0.5 µmol L^{-1} for NO_x, > 0.1 µmol L^{-1} for PO_4^{3-}, and > 0.013 µmol L^{-1} for ammonium.

$\delta^{15}N$ and $\delta^{18}O$ of nitrate ($\delta^{15}N = [(^{15}N/^{14}N)_{sample}/(^{15}N/^{14}N)_{standard}-1] \times 1000$ ‰, $\delta^{18}O = [(^{18}O/^{16}O)_{sample}/(^{18}O/^{16}O)_{standard}-1] \times 1000$ ‰) were determined with the denitrifier method (Sigman et al., 2001; Casciotti et al., 2002). Only the samples with nitrate concentrations > 1.7µmol L^{-1} were analyzed and $\delta^{15}N$ and $\delta^{18}O$ were analyzed in one sample run. Water samples were injected into a suspension of the denitrifier *Pseudomonas aureofaciens* with injection volumes adjusted to yield 10 nmol N_2O. The N_2O gas was purged by helium into a GasBench 2 (Thermo Finnigan) for purification. Afterwards the N_2O gas was analyzed by a Delta V Advantage and a Delta V Plus mass

spectrometer. Samples were measured in duplicate and the two international standards IAEA-N3 (δ^{15}N-NO$_3^-$ = +4.7 ‰, δ^{18}O-NO$_3^-$ = +25.6 ‰) and USGS-34 (δ^{15}N-NO$_3^-$ = -1.8 ‰, δ^{18}O-NO$_3^-$ = -27.9 ‰) and an internal potassium nitrate standard were measured in each batch. The data were corrected by applying a bracketing correction (Sigman et al., 2009) and the standard deviations of the international and in-house standards was found to be ≤ 0.2‰ for δ^{15}N and ≤ 0.5‰ for δ^{18}O. The standard deviations of duplicate samples were in the same range. Nitrite affects the results and was removed following the protocol of Granger and Sigman (2009) whenever [NO$_2^-$] exceeded 5 % of the NO$_x$ pool. In all other cases, we report combined (nitrite + nitrate) values.

3.2.3. Measurements of suspended matters and sediments

Loaded filters were weighed to calculate the amount of suspended particulate matter (SPM) per liter of water. Total carbon and nitrogen concentrations in SPM and sediment samples were measured by a Euro EA 3000 (Euro Vector SPA) Elemental Analyzer. Organic carbon was measured after acidifying samples for three times. The precision of total and organic carbon determination is 0.05 %, that of nitrogen is 0.005 %, and the standard deviations are less than 0.08 for total and organic carbon and 0.02 for nitrogen. Nitrogen isotope ratios were determined with a FlashEA 1112 coupled to a MAT 252 (Thermo Fisher Scientific) isotope ratio mass spectrometer. The precision of nitrogen isotope analyses is better than 0.2 ‰, and the standard deviation less than 0.03.

3.2.4. Measurements of dissolved oxygen

The dissolved oxygen (DO) samples were collected, fixed, and titrated on board following the Winkler procedure at an uncertainty level of < 0.5% (Xiong et al., 2020). A small quantity of NaN3 was added during subsample fixation to remove possible interferences from nitrite (Wong, 2012). The DO saturation was calculated from field-measured DO concentration divided by the DO concentration at equilibrium with the atmosphere which was calculated from temperature, salinity and local air pressure, as per the Benson and Krause Jr (1984) equation.

3.3. Results

3.3.1. Water masses

In spring the water column in the YS was vertically well mixed with salinity and temperature both decreasing northwards. The Yellow Sea Warm Current (YSWM) entered from the outer shelf northwestward into the central YS trough, transporting relatively warm and saline water (T > 7.0 °C, S > 32.5) and its northernmost tip reached 37° N (station B08) (Figure 3.1 and Figure 3.3a-d). The coastal water in the southern

YS (sYS) was characterized by relatively high temperatures and low salinities (T > 8.0 °C, S < 32.5). In the northern YS (nYS), temperatures decreased to around 4.0 °C to 6.0 °C and salinities were in the range of 32.2 to 32.5. Sea water in the YS can thus be roughly considered as a mixture of nutrient depleted nYS water with nutrient abundant YSWC and sYS coastal water (Figure 3.2).
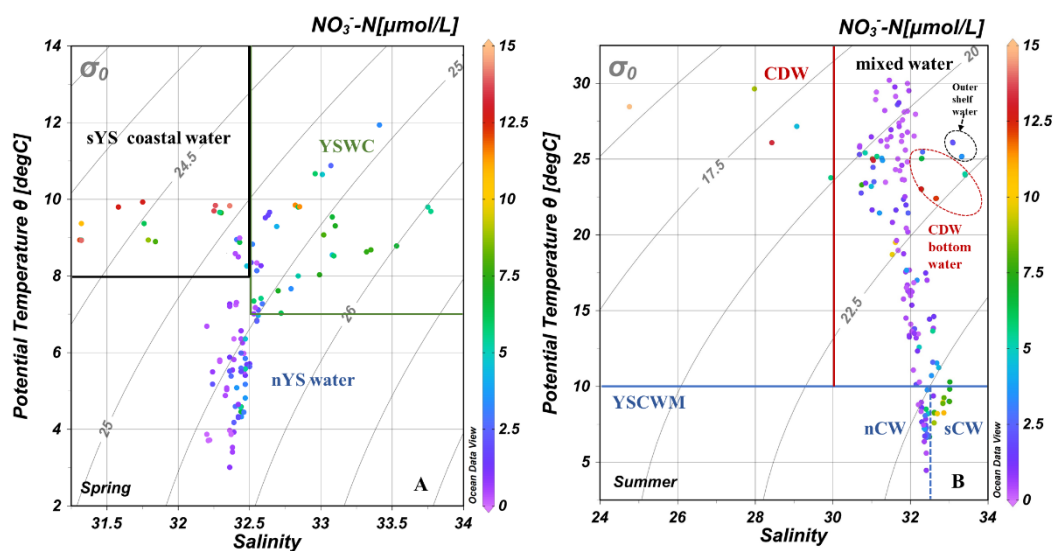
Figure 3.2. Water masses in the Yellow Sea in spring (A) and summer (B), note that the ranges of axes for spring and summer are different. sYS: south Yellow Sea, nYS: north Yellow Sea, YSWC: Yellow Sea Warm Current, CDW: Changjiang Diluted Water, YSCWM: Yellow Sea Cold Water Mass. nCW: north Cold Water mass, sCW: south Cold Water mass. In summer, the YSCWM can be divided into nCW and sCW located in nYS and sYS, respectively, with nitrate in nCW being lower than in sCW.
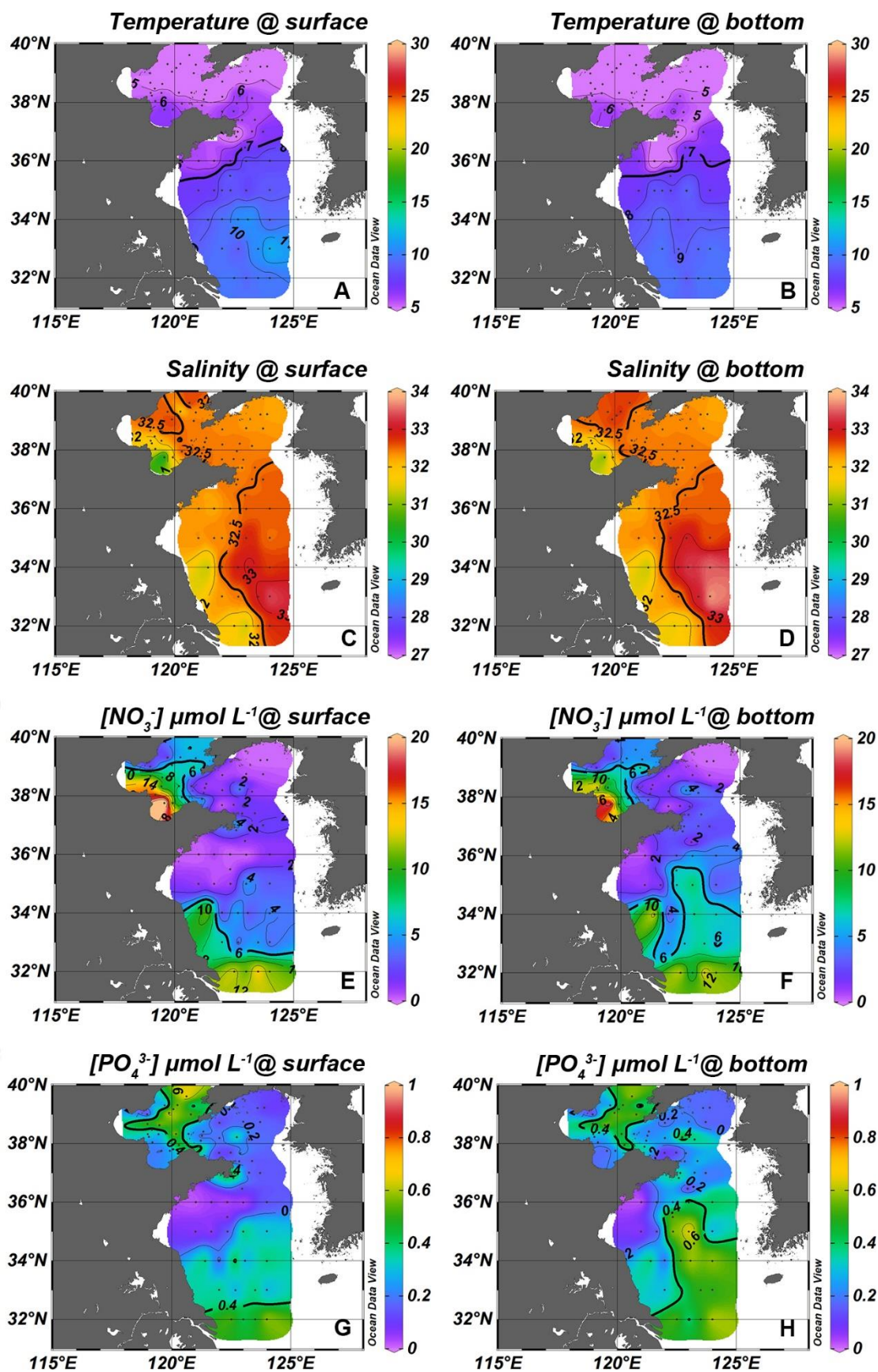
Figure 3.3. Patterns of temperature, salinity, nitrate and phosphate in spring. The left column are surface layers while the right column is the bottom layers.

In summer, the water column was stratified. The Yellow Sea Cold Water Mass (YSCWM; T < 10.0 °C) was found beneath the thermocline in the deep trough of the central YS (Figure 3.4b). The YSCWM can be divided into the northern Cold Water (nCW, 32.0 < S < 32.5) and southern Cold Water (sCW, 32.5 < S < 33.0) (Figure 3.2) While the nCW is mostly derived from the spring nYS water, the sCW inherited the features of the YSWC water (Figure A5.1). The upper layer of the YSCWM had relatively low salinities (31.0 < S < 32.0) and high temperatures (23.0 °C < T < 30.0 °C). Changjiang Diluted Water (CDW) in the southwest YS is characterized by low salinities and high temperatures (S < 30.0, T > 25.0) and appeared in the north and northeast of the Changjiang estuary.
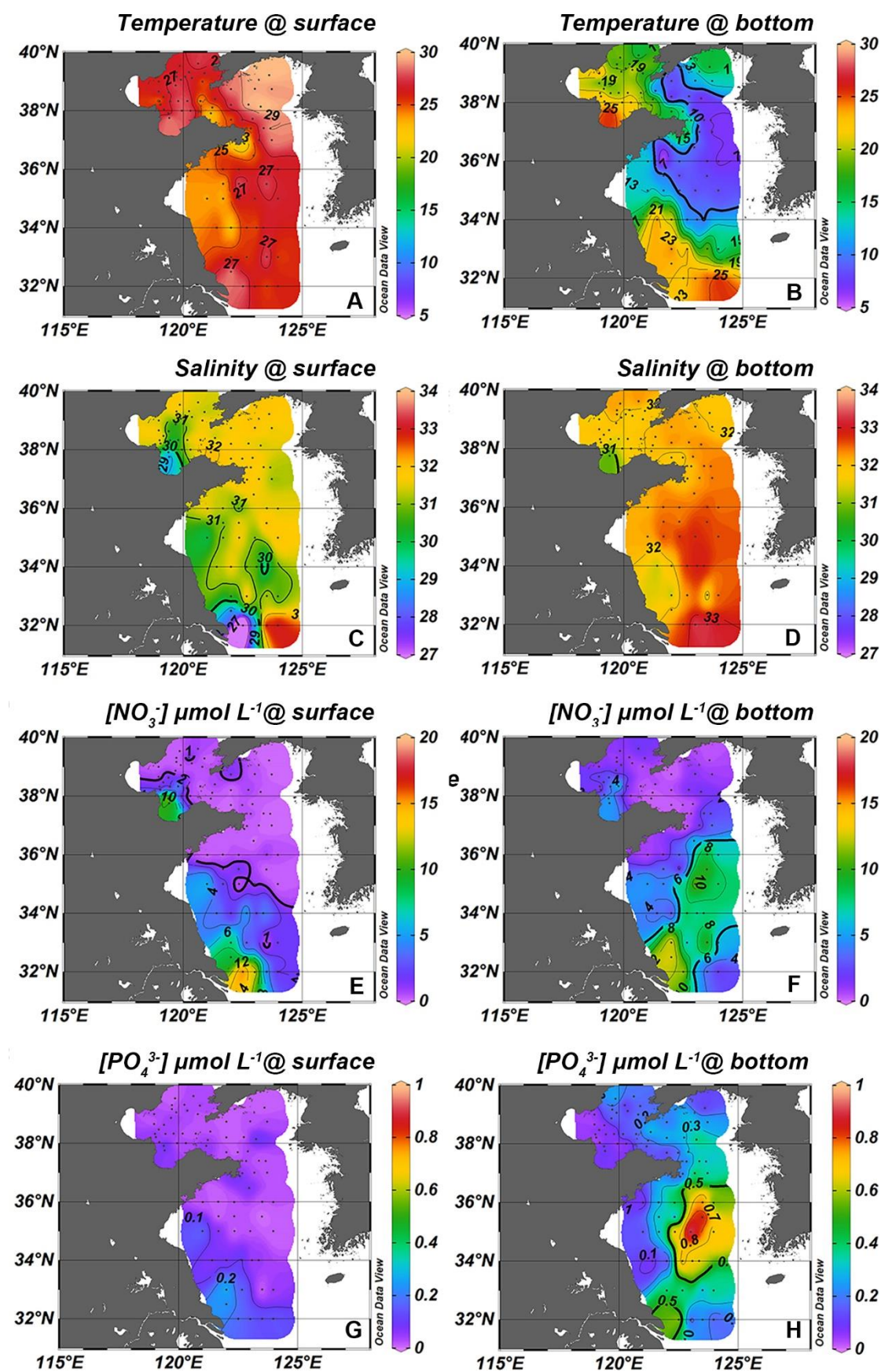
Figure 3.4. Patterns of temperature, salinity, nitrate and phosphate in summer. The left column are surface layers while the right column is the bottom layers

3.3.2. Nitrate and phosphate concentrations

The maxima of nitrate and phosphate in bottom waters ($[NO_3^-] > 6$ μmol L^{-1}, $[PO_4^{3-}] > 0.4$ μmol L^{-1}) in spring match the tongue of YSWC (Figure 3.3d, f, and h). Nitrate and phosphate were enriched ($[NO_3^-] > 6$ μmol L^{-1}, $[PO_4^{3-}] > 0.4$ μmol L^{-1}) along the southmost transect at 32° N. sYS coastal water found further north than 34° N near Jiangsu coast was relatively nutrient depleted ($[NO_3^-] < 4$ μmol L^{-1}, $[PO_4^{3-}] < 0.1$ μmol L^{-1}), probably due to a lack of external replenishment of nutrients in spring. In nYS, nitrate and phosphate concentrations were high in the central area (stations B14 and B23) whereas they were depleted in the northern part (stations B16, B18 and B19) (Figure 3.3e-h).

In summer, nutrients were depleted of the upper layer of the YS, except for the CDW and in the Jiangsu coastal area. CDW had nitrate concentrations > 14 μmol L^{-1} at phosphate concentrations of only around 0.2 μmol L^{-1} in the surface (stations H34 and H35), but nitrate decreased to 12 μmol L^{-1} and phosphate increased to 0.4 μmol L^{-1} in the bottom water. Nitrate and phosphate were enriched in the sCW ($[NO_3^-] > 6$ μmol L^{-1} and $[PO_4^{3-}] > 0.5$ μmol L^{-1}) but remarkably, nitrate was depleted in the nCW ($[NO_3^-] < 1.0$ μmol L^{-1} and $[PO_4^{3-}] > 0.2$ μmol L^{-1}) (Figure 3.4f and h).

3.3.3. Seasonal alteration of DIN in the central YS bottom waters

We divide the YSCWM into nCW and sCW as described in Sect. 3.3.1 for a seasonal comparison of nutrient dynamics. The spring samples were grouped in the same way as summer samples, although the YSCWM had not formed yet in spring. Nitrate concentration of sCW increased from spring to summer, whereas nitrate of nCW decreased (Figure 3.5). Considering that the hydrological properties of nCW and sCW are quite similar, these differing seasonal alterations of nitrate (or DIN) concentrations are remarkable and suggest different modes of operation of these two basins with respect to reactive nitrogen recharge. Ammonium concentration of sCW were relatively low in both seasons (Figure 3.5) and accounted for 6 % and 4 % of DIN in spring and summer, respectively. In the nCW, on the other hand, ammonium accounted for 15 % to 57 % of DIN in spring and summer, respectively. Nitrite concentrations were low with average concentrations < 0.30 μmol L^{-1} accounting for less than 6 % of DIN (Figure 3.5) in both seasons. Phosphate average concentrations were almost uniform in the bottom waters in both seasons except slight increases in the sCW (Table 3.1). The phosphate concentration of sCW was significantly higher than that of the nCW ($p < 0.05$, ANOVA). The average values of DIN/P ratio were relatively high in the sCW (Table 3.1).
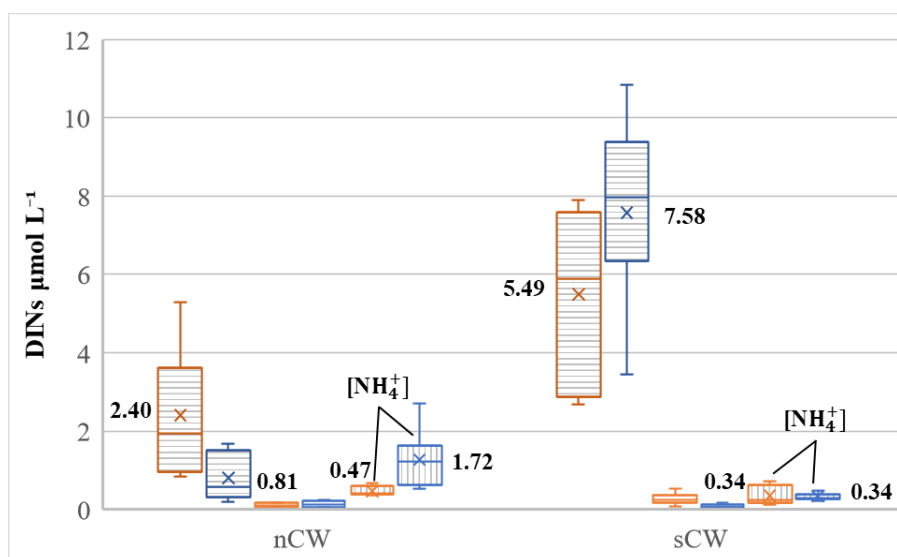
Figure 3.5. Box and whisker plots of DIN variations in different water masses in the central Yellow Sea bottom water. [NO3-] and [NH4+] are marked by horizontal and vertical stripes, respectively. DINs concentrations of spring and summer are in orange and blue, respectively. The crosses and numbers represent the average values of each compound, averages of nitrite were not marked due to space restriction. The lines in the boxes are the medians, the upper and lower boxes denote the corresponding quartiles, whiskers denote the maxima and minima.

The variable and water-mass specific patterns of N/P suggest different mechanisms of N-cycling for the two branches of the deep water mass. N* is a tracer that reflects the combined effects of denitrification and nitrogen fixation, atmospheric deposition and river inflow on the ratio of N to P (Gruber and Sarmiento, 1997). The simplest expression of $N^* = [NO_3^-] - 16[PO_4^-]$ (Deutsch and Weber, 2012) represents the excess of $[NO_3^-]$ over $16[PO_4^-]$, the most commonly used stoichiometric ratio of these two essential nutrients for phytoplankton assimilation. This tracer was first used in studies of the open ocean where nitrate is predominant, whereas nitrite and ammonium have to be accounted for as well in our study area (Zheng and Zhai, 2021), so that here $N^* = [DIN] - 16[PO_4^-]$. N* decreased from spring to summer in the nCW and sCW from -1.4 ± 0.3 to -2.5 ± 1.1 and from -1.6 ± 0.5 to -2.7 ± 0.7, respectively. The decrease in N* suggests that DIN is lost in both nCW and sCW between the spring and summer sampling campaigns by mechanisms different from phytoplankton assimilation.

Nutrient distribution was affected by vertical mixing in spring and by stratification of the water column in summer. Water column integration for nutrients can help us to compare the seasonal variations of inventories by eliminating the effect of stratification. In our study, nCW and sCW areas are 7.9×10³ km² and 37.5×10³ km² respectively, in

the proportions of 2 % and 10 % of the whole YS. Water column integration for total DIN, nitrate, ammonium and phosphate were carried out for every individual station, following interpolation by a gridding method (by ArcGIS). The amount of DIN, nitrate, ammonium and phosphate are shown in Table 1. DIN, nitrate and phosphate decreased by 52 %, 69 % and 82 %, respectively, in summer in the nCW and ammonium increased by 69 %, reflecting loss of DIN and phosphate to biomass and sediment from spring to summer, and their partial recycling. In the sCW, DIN, nitrate and phosphate in summer decreased by 5 %, 11 % and 18 %, respectively, whereas ammonium increased by 137 %. These estimates indicate that although DIN is lost in the whole water column, this loss was compensated by production of DIN in the sCW. Less relative loss of nitrate in sCW than in the nCW points to nutrient replenishment from external sources (see Sect. 3.4.4).

Table 3.1. Important parameters in central bottom waters in the Yellow Sea

Parameters	nCW		sCW	
	Spring	Summer	Spring	Summer
Water column				
$[NO_3^-]$ µmol L^{-1}	2.41 ± 1.58	0.81 ± 0.61	5.49 ± 2.24	7.58 ± 2.2
$[NH_4^+]$ µmol L^{-1}	0.47 ± 0.12	1.27 ± 0.77	0.34 ± 0.24	0.34 ± 0.11
$[NO_2^-]$ µmol L^{-1}	0.16 ± 0.18	0.13 ± 0.08	0.27 ± 0.15	0.09 ± 0.08
$[PO_4^{3-}]$ µmol L^{-1}	0.28 ± 0.10	0.30 ± 0.06	0.48 ± 0.16	0.67 ± 0.16
DIN/P	10.2 ± 2.1	7.5 ± 3.0	12.6 ± 0.8	11.8 ± 1.1
N*	-1.4 ± 0.3	-2.5 ± 1.1	-1.6 ± 0.5	-2.7 ± 0.7
[DIN] mol	1.38×10^6	0.67×10^6	12.6×10^6	12.0×10^6
$[NO_3^-]$ mol	1.09×10^6	0.34×10^6	11.6×10^6	10.3×10^6
$[NH_4^+]$ mol	0.17×10^6	0.29×10^6	0.62×10^6	1.46×10^6
$[PO_4^{3-}]$ mol	0.44×10^6	0.08×10^6	1.05×10^6	0.86×10^6
δ^{15}N-NO$_3^-$ ‰	9.6 ± 1.5	no data	8.6 ± 2.2	5.7 ± 0.2
δ^{18}O-NO$_3^-$ ‰	13.4 ± 1.4	no data	12.1 ± 4.0	4.8 ± 0.9
δ^{15}N-PN ‰	3.7 ± 1.4	5.6 ± 0.7	no data	5.2*
N%-SPM %	0.88 ± 0.46	0.40 ± 0.12	0.76 ± 0.71	0.16 ± 0.03
Sediment				
Water content %	48.4 ± 3.6		53.5 ± 7.2	
N %	0.10 ± 0.02		0.11 ± 0.03	
C$_{org}$ %	0.7 ± 0.2		0.8 ± 0.3	
δ^{15}N-sed ‰	5.3 ± 0.2		5.2 ± 0.2	
C/N	6.7 ± 1.0		7.2 ± 0.5	

*only one valid data point.

3.3.4. Isotopic composition of nitrate and particulate nitrogen

The $\delta^{15}N$ of nitrate ($\delta^{15}N\text{-}NO_3^-$) in spring was on average 8.3 ‰ ± 2.2 ‰ and ranged from 3.6 ‰ to 14.2 ‰, and the corresponding $\delta^{18}O$ of nitrate ($\delta^{18}O\text{-}NO_3^-$) averaged 12.3 ‰ ± 3.5 ‰ and ranged from 7.1 ‰ to 20.6 ‰. High values of $\delta^{15}N\text{-}NO_3^-$ and $\delta^{18}O\text{-}NO_3^-$ ($\delta^{15}N\text{-}NO_3^- > 10.0$ ‰, $\delta^{18}O\text{-}NO_3^- > 15.0$ ‰) were observed in the surface layer of the YSWC, but $\delta^{15}N\text{-}NO_3^-$ and $\delta^{18}O\text{-}NO_3^-$ were relatively low ($\delta^{15}N\text{-}NO_3^- = 7.0$ ‰-8.5 ‰, $\delta^{18}O\text{-}NO_3^- = 9.0$ ‰) in bottom water. Southern coastal water had the lowest $\delta^{15}N\text{-}NO_3^-$ values ($\delta^{15}N\text{-}NO_3^- < 7.5$ ‰). In summer, $\delta^{15}N\text{-}NO_3^-$ was on average 7.9 ‰ ± 3.3 ‰ (range of 1.1 ‰ to 18.1 ‰) and $\delta^{18}O\text{-}NO_3^-$ was on average 8.7 ‰ ± 4.7 ‰ (range of 2.2 ‰ to 22.8 ‰). Low values of $\delta^{15}N\text{-}NO_3^-$ and $\delta^{18}O\text{-}NO_3^-$ characterized the sCW ($\delta^{15}N\text{-}NO_3^- = 5.7 \pm 0.2$ ‰, $\delta^{18}O\text{-}NO_3^- = 4.8 \pm 0.9$ ‰), whereas coastal water masses typically had high values (Table 3.1).

N % of SPM in spring was on average 1.15 % ± 1.03 % and YSWC surface water and nYS surface water had the highest N % (N % > 2.0 %), whereas suspended particulate matter in southern coastal water had the lowest N-concentrations (N % < 0.5 %). N % of SPM in summer was on average 0.40 % ± 0.21 % with N % in surface layer higher than those in the bottom layer. In summer the CDW area had highest values (N % > 0.8 %). The N % of bottom waters in summer were lower than in spring, indicating stronger decomposition of organic particles, resuspension is less likely the major reason because the weaker water mixing in summer. Average N % of sCW (N % = 0.16 % ± 0.03 %) was significantly lower than nCW ($p < 0.05$) (Table 3.1), probably indicating strong remineralization of particles in the sCW.

$\delta^{15}N$ of particulate nitrogen ($\delta^{15}N\text{-}PN$) in spring was on average 4.3 ‰ ± 1.8 ‰. YSWC water had the lowest values ($\delta^{15}N\text{-}PN < 3.0$ ‰) whereas nYS had the highest values ($\delta^{15}N\text{-}PN > 5.0$ ‰). The corresponding high N %, high values of nitrate dual isotopes and low $\delta^{15}N\text{-}PN$ suggest phytoplankton assimilation of nitrate and its conversion to biomass in the surface of YSWC. In summer, $\delta^{15}N\text{-}PN$ was on average 4.7 ‰ ± 1.5 ‰, but the range of values of $\delta^{15}N\text{-}PN$ in the surface was quite wide due to co-occurrence of diverse processes, such as phytoplankton assimilation and nitrification. The values converged to between 4 ‰ and 6 ‰ with increasing water depth and at > 40 m water depth approached the $\delta^{15}N$ of nitrate and sediment (Table 3.1).

3.3.5. Characteristics of sediments

The sediment under different water masses are characterized by similar water content, nitrogen content (N %), organic carbon content (C_{org} %) and $\delta^{15}N$ ($\delta^{15}N\text{-}sed$) of sediment under nCW and sCW. There are no statistically significant differences

between other groups of sediments due to low sample numbers, but the distribution (Figure A6.1) and average values suggest that the sediment under coastal water masses had relative low water content, N %, C_{org} %, and δ^{15}N-sed, whereas they had relatively high C/N ratio.

3.4. Discussion

The inter-seasonal variations of nitrate and ammonium are different for the two branches of deep water in the Yellow Sea (nCW and sCW), although DIN and nitrate loss occurred in both water masses. Nitrate concentration decreased in the nCW in summer, whereas it increased in the sCW. In contrast, ammonium concentrations increased in the nCW, but decreased in the sCW. In the following, we aim to explain and quantify DIN and nitrate loss in the central YS bottom water and shed light on different seasonal dynamics of nitrate and ammonium cycling in nCW and sCW. The key processes, namely denitrification and nitrification, are discussed and the proportion of regenerated nitrate in summer is quantified by an isotope mass balance approach in the sCW. The excess nitrate in sCW compared to the nCW is analyzed as well to elucidate its sources.

3.4.1. Nitrate loss in central Yellow Sea bottom water

The decrease of DIN in the water columns of both nCW and sCW areas from spring to summer (Table 3.1) requires an N loss process such as denitrification or sedimentation of organic matter and associated reactive N.

The YSCWM with its two offshore water masses considered here (nCW and sCW) is isolated from any euphotic assimilation by summer stratification. As these cold water masses are located below the thermocline there is no air-sea exchange of oxygen, and DO is continuously consumed once the thermocline is formed. Thus, Apparent Oxygen Utilization (AOU) represents the net change due to respiration (Xiong et al., 2020). In the YS, approximately 90 % of the organic carbon derived from primary productivity is decomposed in the water column (Song et al., 2016a; Zheng and Zhai, 2021) and the positive AOU values in summer indeed suggest that respiration is the dominant process.

A remineralization stoichiometry of 150 O2 : 1 $[PO_4^{3-}]$: 16 $[NO_3^-]$ (Anderson, 1995) is used to estimate the regenerated nutrients (Rafter et al., 2013; Wu et al., 2019). The regenerated nitrate ($[NO_3^-]_r$) can be calculated following Eq. 3.1 and Eq. 3.2, AOU and $[NO_3^-]$ in these equations with subscript sp and sm stand for data of spring and summer, respectively. The seasonal variation of nitrate ($\Delta[NO_3^-]$) is calculated by Eq. 3.3. The $[NO_3^-]_r$ expected in nCW and sCW from AOU is higher than the actually measured $\Delta[NO_3^-]$ between summer and spring sampling (Table 3.2), implying that regenerated nitrate was removed from the water masses.

$$[NO_3^-]_r = \Delta AOU \times 150 \times 16 \quad (3.1)$$

$$\Delta AOU = AOU_{sm} - AOU_{sp} \quad (3.2)$$

$$\Delta[NO_3^-]_r = [NO_3^-]_{sm} - [NO_3^-]_{sp} \quad (3.3)$$

Table 3.2. Comparison of regenerated $[NO_3^-]_r$ and observed nitrate $\Delta[NO_3^-]$ in nCW and sCW.

Water masses	$[NO_3^-]_{sp}$ μmol L^{-1}	$[NO_3^-]_{sm}$ μmol L^{-1}	$[NO_3^-]_r$ μmol L^{-1}	$\Delta[NO_3^-]$ μmol L^{-1}
nCW	2.41 ± 1.58	0.81 ± 0.61	2.38 ± 1.31	-1.86 ± 1.20
sCW	5.49 ± 2.24	7.58 ± 2.27	6.83 ± 1.22	1.83 ± 1.66

A likely reason for nitrate loss in both the nCW and sCW is denitrification. Water column denitrification can be ruled out, because the lowest value of DO in nCW and sCW was 218.3 μmol L^{-1} (station HS1, at 73 m) in summer, which is much too high to allow denitrification in the water column that can only proceed when DO is below 5 μmol L^{-1} (Altabet, 2006). In addition, the dual isotope values of residual nitrate in that case must show the fractionation effect that enriches ^{15}N and ^{18}O during water column denitrification (Wankel et al., 2006), which is not observed in our data. Instead, the dual nitrate isotope ratios were lower in summer than in spring (Table 3.1).

Sedimentary denitrification is a strong candidate for the observed nitrate loss in the nCW and sCW. Continental shelf sediment are reported to account for > 50 % of global nitrate and DIN loss (Bohlen et al., 2012), and sediment denitrification normally is associated with little or no isotope fractionation due to the limitation of nitrate supply to the reactive sediment zones (Brandes and Devol, 1997; Lehmann et al., 2004; Devol, 2015). In the sediments of YS, nitrate is transported from the sediments to the overlying water at most sampling stations, whereas transport into the sediments was observed in the YSCWM area (Liu et al., 2017c; Wu et al., 2019). The assimilation of nitrate by benthic foraminifera and subsequent intercellular denitrification has been proposed as one reason for N loss in the sCW in summer (Xu et al., 2017; Wu et al., 2019). The distribution of benthic foraminifera was corelated to the median grain size of the sediment and it was abundant in the mud area in the central YS trough (Sun et al., 2009). Sediment denitrification is thus the most plausible reason for the observed nitrate loss in the sCW. The conversion of ammonia and nitrite to N$_2$ by the anammox process cannot be excluded based on our data in hand, but denitrification likely is predominant (Zhang et al., 2018).

Another possible reason of nitrate loss is nitrate vertical diffusion. Upwelling at the boundaries of the YSCWM (Wei et al., 2016) and vertical diffusion can both supply nutrients from deep water to the euphotic layer (Su et al., 2013). Vertical diffusion from the near bottom water in summer has been estimated to supply 4945 μmol m^{-2} d^{-1} of DIN and 236 μmol m^{-2} d^{-1} of P to the thermocline in the sCW (Su et al., 2013).

In summary, the nutrients were regenerated from sinking organic matter or sediments in summer in both the nCW and sCW. However, nitrate concentrations in summer were much lower than the AOU-based estimate of regenerated $[NO_3^-]_r$ in both nCW and sCW. Nitrate diffusion to the surface layer and sedimentary denitrification are the main factors resulting in nitrate loss in the nCW and sCW, and stronger N depletion in the nCW compared to the sCW was observed.

3.4.2. Quantification of regenerated nitrate in sCW

The regenerated nitrate is an important source of YSCWM in summer, the proportion can be estimate by its distinctive δ^{18}O value. δ^{15}N of newly nitrified nitrate bears the signal of the PN source and the fractionation effect nitrate cycling to PN and back to nitrate. Differing from this, δ^{18}O-NO_3^- is a good tracer of nitrification because δ^{18}O of newly nitrified nitrate bears the signal of ambient water and dissolved oxygen without contribution of preformed nitrate. For quantification of the portions of preformed and regenerated nitrate in summer, a simple mixing model can be set up between newly nitrified and preformed nitrate with distinctive δ^{18}O values of each source. The portion of preformed nitrate in spring and newly nitrified nitrate in summer can be calculated following Eq. 3.4 and Eq. 3.5. The calculations below are only based on the sCW due to the fact that nitrate dual isotopes in the nCW were near the detection limit.

$$[NO_3^-]_{sp\_res} + [NO_3^-]_{ntr\_res} = [NO_3^-]_{sm} \quad (3.4)$$

$$\delta^{18}O_{sp}[NO_3^-]_{sp\_res} + \delta^{18}O_{ntr}[NO_3^-]_{ntr\_res} = \delta^{18}O_{sm}[NO_3^-]_{sm} \quad (3.5)$$

where $[NO_3^-]_{sp\_res}$ and $[NO_3^-]_{ntr\_res}$ denote the concentrations of the residual portion of the preformed nitrate in spring and of the residual portion of regenerated nitrate in summer, respectively. $[NO_3^-]_{sm}$ denotes the nitrate concentration of sCW. $\delta^{18}O_{ntr}$ denotes the delta-value of newly nitrified nitrate. If $\delta^{18}O_{ntr}$ is given, $[NO_3^-]_{sp\_res}$ and $[NO_3^-]_{ntr\_res}$ can be quantified.

The values of $\delta^{18}O_{ntr}$ was not documented for the YS before, but its range can be constrained: (1) The average value of δ^{18}O-H$_2$O of YS is -0.7 ± 0.3 ‰ (n = 9) (Schimidt et al., 1999), this must be the lower limit of δ^{18}O-H$_2$O for newly nitrified

nitrate. (2) Assuming that 5/6 of oxygen atoms are from water (Mayer et al., 2001) and the remaining 1/6 has a δ^{18}O-O$_2$ of 23.5 ‰ (Kroopnick and Craig, 1972) the $\delta^{18}O_{ntr}$ can be expected to be 3.3 ± 0.2 ‰. (3) In the open ocean, $\delta^{18}O_{ntr}$ is around 1.1 ‰ higher than in the ambient water (Sigman et al., 2009). Assuming the same systematic difference would result in $\delta^{18}O_{ntr}$ of 0.4 ‰ in the YS. In summary, the $\delta^{18}O_{ntr}$ is theoretically in the range of -0.7 ‰ to 3.3 ‰ in the YS.

To further constrain the value of $\delta^{18}O_{ntr}$, an iterative mixing simulation is employed based on our observed data. This mixing model can be simplified by several assumptions: (1) Reaction rates of nitrification and denitrification in sCW are stable during the study period. (2) Nitrate concentration in sCW is the function of time (in days). As our spring and summer cruises were in April and August, the whole simulation period is about 120 days. (3) Nitrification, mixing and removal of nitrate proceed simultaneously. Because decomposition of organic particulate nitrogen in the water column accounted for around 90 % of total nitrogen loss, the predominant nitrate flux should be directed from water to the sediment so that water column nitrification probably supplies nitrate for sediment denitrification. Thus, the mixing model can be simplified, as nitrate is a mixture of preformed and newly nitrified nitrate, which afterwards is removed by denitrification or diffusion (Eq. 3.6 and Eq. 3.7). $\delta^{18}O_{loss}$ in Eq. 3.7 can be calculated by Eq. 3.8 to Eq. 3.10.

$$[NO_3^-]_n + n[NO_3^-]_{ntr} - n[NO_3^-]_{loss} = [NO_3^-]_{n+1} \quad (3.6)$$

$$\delta^{18}O_n[NO_3^-]_n + \delta^{18}O_{ntr}n[NO_3^-]_{ntr} - \delta^{18}O_{loss}n[NO_3^-]_{loss} = \delta^{18}O_{n+1}[NO_3^-]_{n+1} \quad (3.7)$$

$$[NO_3^-]_{n+1} = [NO_3^-]_n - n[NO_3^-]_{ntr} \quad (3.8)$$

$$\delta^{18}O_{n+1}[NO_3^-]_{n+1} = \delta^{18}O_n[NO_3^-]_n + \delta^{18}O_{ntr}n[NO_3^-]_{ntr} \quad (3.9)$$

$$\delta^{18}O_{loss} = \delta^{18}O_{n+1} \quad (3.10)$$

where n denotes the number of steps (= days) of the simulation (in d, $1 \leq n \leq 120$). $[NO_3^-]_n$ and $\delta^{18}O_n$ denote the nitrate concentration and δ^{18}O in sCW of day n, respectively. When the simulation starts (i.e., n = 1), $[NO_3^-]_n$ and $\delta^{18}O_n$ values are equivalent to the corresponding observed values of spring. When the simulation ends (i.e., n = 120), $[NO_3^-]_n$ and $\delta^{18}O_n$ values are equivalent to the corresponding observed values of summer. $[NO_3^-]_{ntr}$ denotes the reaction rate of nitrification ($[NO_3^-]_{ntr}$ = $[NO_3^-]_r$/120, µmol L^{-1} d^{-1}), $[NO_3^-]_{loss}$ denotes the reaction rate of denitrification and nitrate diffusion together (µmol L^{-1} d^{-1}, $[NO_3^-]_{loss} = [NO_3^-]_{sp}/$

$120 + [NO_3^-]_{ntr} - [NO_3^-]_{sm}/120$, µmol L^{-1} d^{-1}).

The result of the mixing model is shown in Figure 3.6. $\delta^{18}O_{ntr}$ is 0.9 ‰ and in good agreement with our initial assumption. Combining this value with Eq. 3.4 and Eq. 3.5 suggests that nitrate in summer in the sCW consists of 35 % preformed and 65 % regenerated nitrate. Furthermore, the $\delta^{15}N$ of regenerated nitrate ($\delta^{15}N_r$) is 3.3 ‰ that was calculated following Eq. 3.11. Different from the result of $\delta^{18}O_{ntr}$, the value of 3.3 ‰ for $\delta^{15}N_r$ reflects not only the $\delta^{15}N$ of regenerated nitrate, but also the potential fractionation effects on N cycling.

$$\delta^{15}N_{sp}[NO_3^-]_{sp\_res} + \delta^{15}N_r[NO_3^-]_{ntr\_res} = \delta^{15}N_{sm}[NO_3^-]_{sm} \quad (3.11)$$
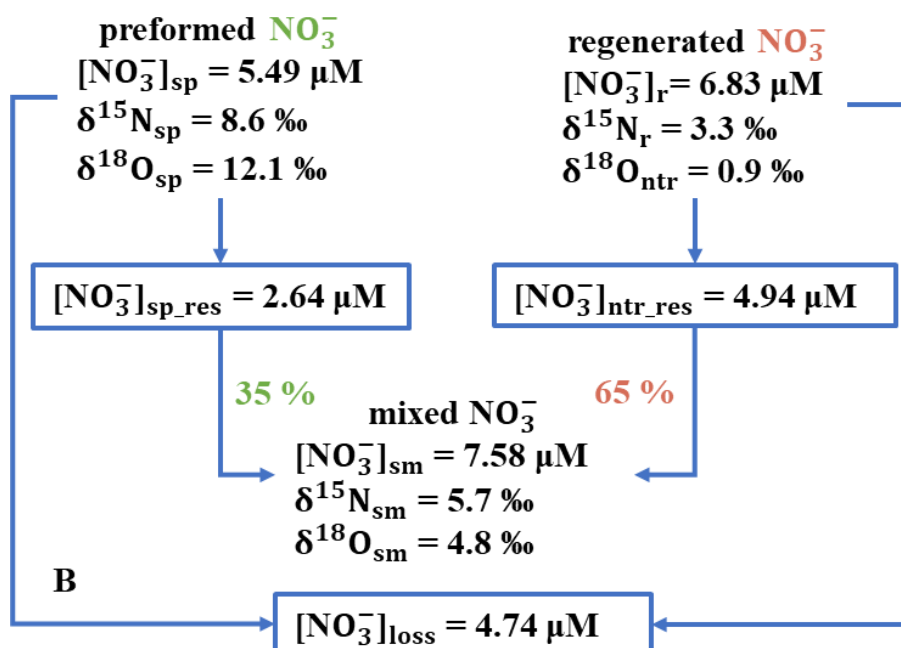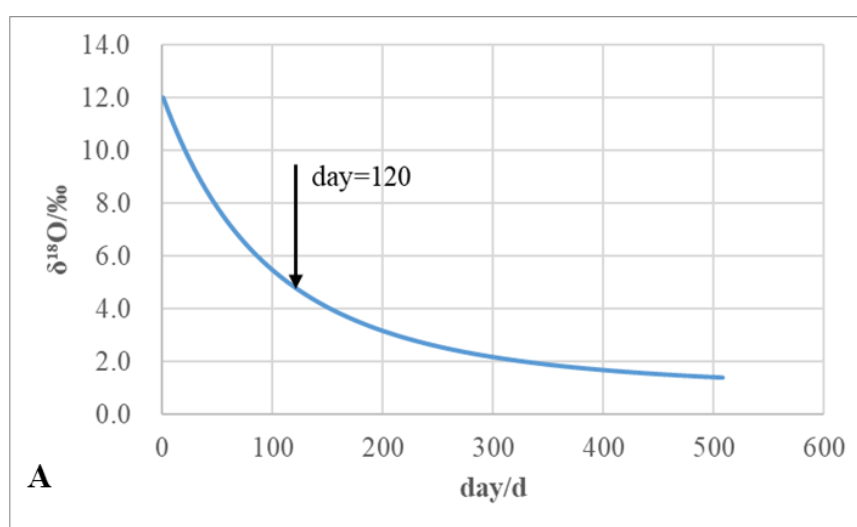
Figure 3.6. Simulation results of the mixing model for the sCW: $\delta^{18}O$-NO$_3^-$ decreases along with simulation time when $\delta^{18}O_{ntr}$ is set to 0.9 ‰ (A). Schematic diagram of the

mixing model, in which the sCW nitrate pool consists of 35 % preformed and 65 % regenerated nitrate in summer (B).

Overall, regenerated nitrate had a $\delta^{15}N_r$ of 3.3 ‰ and an $\delta^{18}O_{ntr}$ of 0.9 ‰ and contributed 65 % to the nitrate pool of sCW. Because nitrate is depleted in the upper layer in summer, 10.3×10^6 mol nitrate of the sCW water column (Table 3.1) can be considered as the inventory of the sCW. This means that 3.6×10^6 mol nitrate were preformed in spring and 6.7×10^6 mol nitrate was regenerated.

3.4.3. Reset of δ¹⁵N in nitrate and PN by remineralization and nitrification

The comparison of inter-seasonal changes in nitrate and ammonium concentrations between nCW and sCW implies that the biogeochemical processes in these two water masses were different. In summer, nitrate was depleted in nCW but ammonium was relatively enriched, whereas nitrate accumulated in sCW while ammonium was consumed. In general, ammonium is produced below the euphotic zone by remineralization and is consumed by nitrification or/and annamox. In the sCW, lower N % and higher AOU than those of nCW suggest that the decomposition of particulate nitrogen was stronger. The low levels of ammonium and accumulation of nitrate imply that nitrification converting ammonium to nitrate is a major process in the sCW.

We introduce the molar ratio of nitrate/DIN ($[NO_3^-]$/[DIN]) for simply representing the degree of nitrification. As nitrification proceeds, ammonium is converted to nitrate, resulting in increased $[NO_3^-]$/[DIN] ratios approaching unity. The $[NO_3^-]$/[DIN] in nCW and sCW was 0.35 ± 0.20 and 0.94 ± 0.24, respectively; it was significantly higher in the sCW ($p < 0.05$) indicating stronger nitrification. δ^{15}N-NO_3^- in bottom layer of the whole sYS has a negative linear relationship with $[NO_3^-]$/[DIN] ($R^2 = 0.80$, Figure 3.7) and converged to 5.7 ‰ in sCW.

According to our discussion above, remineralization of PN was the major original source of nitrate in the bottom waters. δ^{15}N-PN versus $[NO_3^-]$/[DIN] of sYS bottom layer presented a weak positive linear relationship ($R^2 = 0.19$, Figure 3.7). The likely reason for the weak correlation is that the relationship between δ^{15}N-PN and $[NO_3^-]$/[DIN] is indirect and combines PN ammonification and ammonium nitrification. In consequence it is only reliable when $[NO_3^-]$/[DIN] is close to 1 due to decreasing importance of intermediate products (ammonium and nitrite). Setting $[NO_3^-]$/[DIN] = 1 results in similar values of δ^{15}N-PN = 5.1 ‰ and δ^{15}N-NO_3^- = 5.0 ‰, indicating that nitrification forces δ^{15}N-PN and δ^{15}N-NO_3^- to become similar. This finding in the sYS bottom water is in agreement with results in the ocean interior, where nitrate regeneration by nitrification dictates δ^{15}N-NO_3^- to be similar to δ^{15}N-PN (Sigman et al., 2009; Buchwald et al., 2012; Casciotti, 2016). The same is evident in the values of

δ^{15}N-NO_3^- in the sYs of 5.0 ‰ in autumn before winter mixing (Wu et al., 2019). Besides, sediment nitrogen isotope under the sCW was also close to isotope values of particles and nitrate (δ^{15}N-sed = 5.2 ‰), these similar delta-values imply that the fractionation of δ^{15}N of PN, nitrate and sediment nitrogen was almost equilibrium.
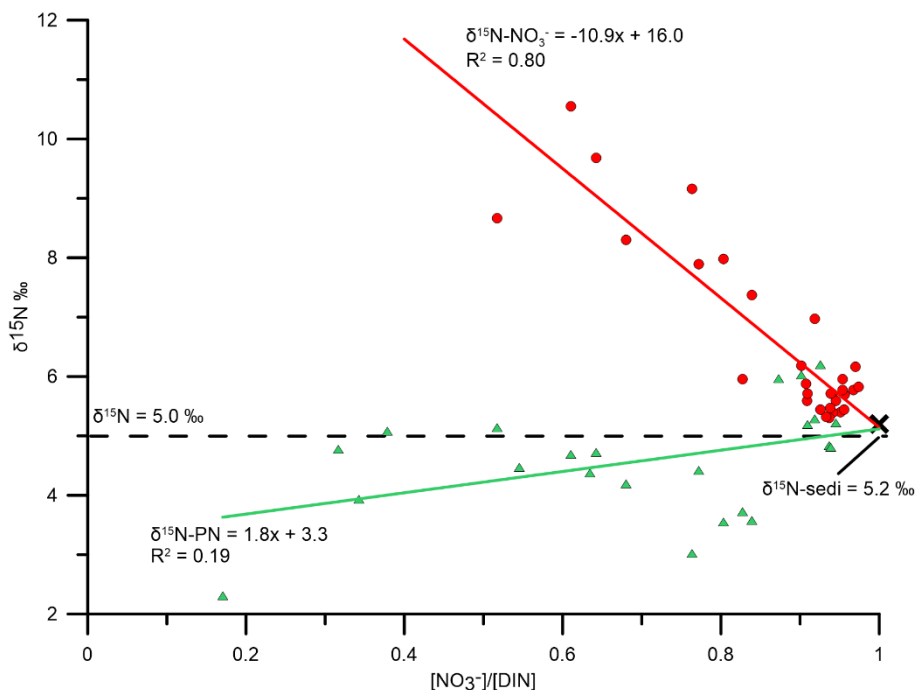
Figure 3.7. [NO_3^-]/[DIN] vs. δ^{15}N- NO_3^- and [NO_3^-]/[DIN] vs. δ^{15}N-PN sampled from south YS. With proceeding nitrification, the values of δ^{15}N- NO_3^-, δ^{15}N-PN and δ^{15}N-sed are converging. δ^{15}N-sedi marked by a black cross is the average value for sediment of the sCW.

3.4.4. Sources of excess nitrogen in the southern part of central Yellow Sea bottom water

sCW had higher nitrate concentrations than the nCW in spring and summer even though sediment denitrification occurred in both areas In the following we explore this difference and summarize nitrogen budgets of the sCW and nCW.

In spring, nitrate concentrations in the sCW were higher than those in the nCW. The reason is the strong impact of the YSWC, the sub-branch of Kuroshio Current, on the sCW area, reflected in higher concentrations in the south and low nutrient concentrations near 36° N before reaching the nYS in spring (Figure 3.3). The δ^{15}N-NO_3^- in the water column correspondingly increased northward due to the fractionation effect during nitrate assimilation when YSWC flows northward (Umezawa et al., 2013; Liu et al., 2017c). Specifically, the δ^{15}N-NO_3^- of Kuroshio invasion water was 5.5 ± 2.0 ‰ (Liu et al., 2020), while δ^{15}N-NO_3^- of sCW and nCW was 8.6 ± 2.2 ‰ and 9.6

± 1.5 ‰, respectively.

In summer 2018, Changjiang River discharged 8.0×10^{11} m^3 of fresh water into the YS and ECS (MWR, 2019) and approximately 14–28 % of the waters from Changjiang enter the southern YS during summer by the northward transported CDW which dominated surface circulation (Liu et al., 2003a; Fan and Song, 2014). DIN/P ratios of CDW in the range of 48.3-106.4 (in the salinity range from 24.8-28.4) during our survey were much higher than those of sCW. Formation of the thermocline prevents CDW from being a direct nutrient source to the bottom water. In the northeastward CDW frontal area, nitrate concentration increased with water depth, whereas nitrate isotope values and N % of particles decreased. This indicated a CDW-sourced nitrate supply to the sCW by the production and subsequent decomposition of sinking particles and nitrate regeneration.

δ^{15}N-NO_3^- in the Changjiang and its estuary have δ^{15}N values in range of 2.0 ‰ to 6.6 ‰ (Liu et al., 2009b; Chen et al., 2013; Yu et al., 2015; Wang et al., 2016; Liu et al., 2020; Zhong et al., 2020). Taking 5.8 ± 2.0 ‰ as the end member of the Changjiang River (Liu et al., 2020) the calculated value above from the mixing model of regenerated nitrate of $\delta^{15}N_r$ =3.3 ‰ is lower. Two possible reasons should account for this difference: (1) during decomposition of PN CDW there is a fractionation effect, and (2) there are other external sources with lower δ^{15}N-NO_3^- values.

In the nCW the river influence on the N-pool was low. Yalu River has an annual average water discharge of 3.20×10^8 m^3 (Li et al., 2017a) which is about 89 % of river input from the Liaodong Peninsula (Chen et al., 2012). It was restricted to the coastal area northwest of the nYS (Duan et al., 2016; Yang et al., 2018a). Although 70 % to 80 % of this input occurs during the flood season (July and August) (Li et al., 2017a), resulting in a negative correlation between DIN and salinity in coastal area of nYS (Duan et al., 2016), there was no low salinity water during our survey, so that the influence of rivers to central nYS must have been quite limited. The difference of river impacts to nYS and sYS in summer is the reason for higher nitrate concentration in sCW.

Atmospheric deposition is probably responsible for the increase of nitrate concentrations in the YS and in the northwest Pacific Ocean in recent decades (Kim et al., 2011; Moon et al., 2021). This input contributed more than 2 times of the nitrate flux of rivers to the YS (Liu et al., 2017c). Accidental events like dust storm accompanied by precipitation can also stimulate the phytoplankton bloom in the YS (Shi et al., 2012).

There are no directly measured data of atmospheric deposited of nitrate in the YS.

δ^{15}N-NO_3^- of precipitation in northern China and the Japan Sea ranged from -2.5 to +0.9 ‰ (Zhang et al., 2008b; Chang et al., 2019; Kim et al., 2019; Li et al., 2019b), whereas δ^{15}N-NO_3^- values of PM2.5 (fine particulate matter suspended in the air) ranged from 3.5-17.8 ‰ in northern China (Zong et al., 2017; Fan et al., 2019; Zhang et al., 2019; Song et al., 2020). The ratio of wet to dry nitrogen deposition is close to 1:1 in China on land (Yu et al., 2019) and 1.9:1 in the eastern YS (Kim et al., 2010). Taking the δ^{15}N value of 8.2 ‰ reported from in Bohai Strait for dry deposition (Zong et al., 2017), and the δ^{15}N value of -2.35 ‰ for precipitation (Chang et al., 2019), results in the δ^{15}N-NO_3^- of atmospheric deposited nitrate of 1.3 ‰ to 2.9 ‰. These values are slightly lower but similar to the 3.3 ‰ of $\delta^{15}N_r$, implying that atmospheric deposition is an important external nitrate source to the sCW from the perspective of nitrate isotope.

However, most of the studies considered the difference of the atmospheric deposition between the nYS and sYS as not significant (Zhang et al., 2007; Zhang et al., 2010; Shi et al., 2012; Han et al., 2013; Qi et al., 2013). We surmise that atmospheric deposition is an important external nitrate source to the YS, but less likely to be the reason for the higher nitrate concentration in the sCW.

In addition, the organic carbon content, nitrogen content and δ^{15}N of sediments in central areas of both the nYS and sYS are very similar (Table 3.1), sediments in both nYS and sYS are mostly clayey silt (Qiao et al., 2017). This implies that reflux from sediment probably did not account for the different nitrate concentration in nCW and sCW, specifically as 90 % of organic particles are decomposed in the water column.

Overall, the higher nitrate concentration in the sCW compared to the nCW is due to the stronger inflow of nitrate via YSWC to the sYS in spring, and more river input via the Changjiang River in summer (Figure 3.8). Atmospheric deposition is an important source of the YS, but it is not the reason for higher nitrate concentrations in the sCW. The δ^{15}N value of newly regenerated nitrate to the sCW of 3.3 ‰ combines the isotope fingerprints of nitrate from Changjiang River and atmospheric deposition.
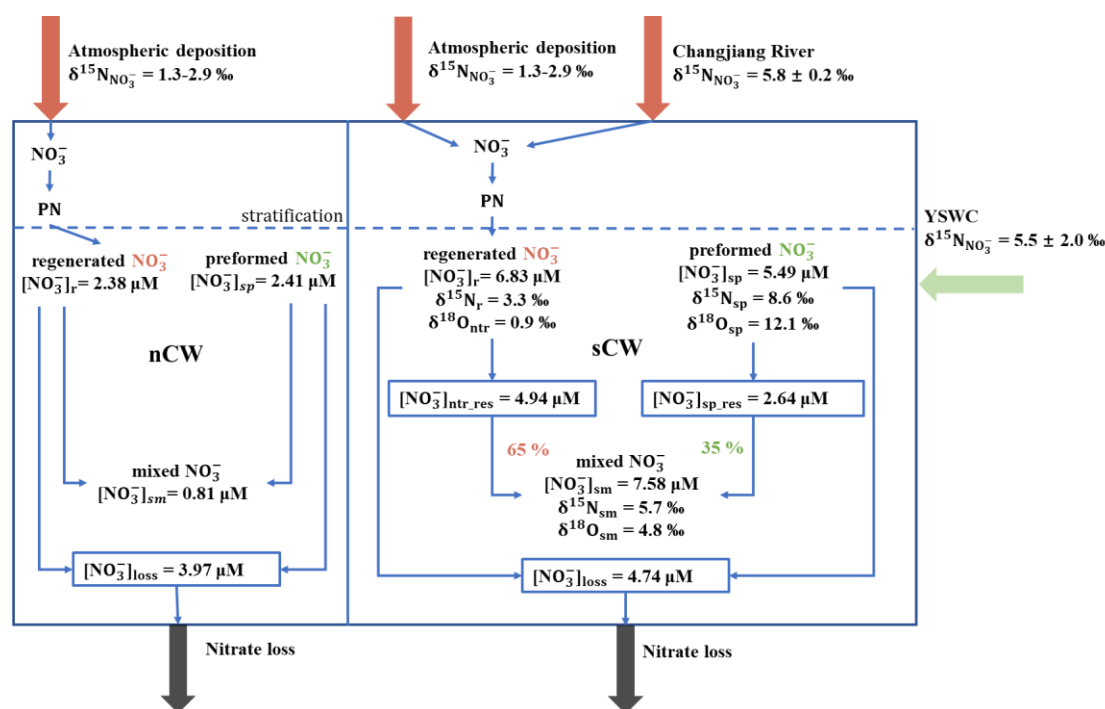
Figure 3.8. Different nitrate budgets in the nCW and sCW. In both water masses, nitrate consists of the preformed nitrate and regenerated nitrate. The sCW is impacted by the inflow of Yellow Sea Warm Current (YSWC) in spring, the input from atmospheric deposition and inflow of the Changjiang River in summer, while nitrate is lost mainly to benthic denitrification. The nCW is impacted by the input of nitrate by atmospheric deposition only and nitrate loss mainly to benthic denitrification, the prevalence of which makes the area filled by nCW a net sink for nitrate in summer. Proportions for regenerated and preformed nitrate are estimated by the isotopic mixing only for the sCW because of a lack of isotope values in the nCW. $[NO_3^-]$, $\delta^{15}N$ and $\delta^{18}O$ are labeled by different subscript, "sp", "sm" denotes the corresponding average values observed in spring and summer, respectively, "r/ntr" and "loss" denotes regeneration and loss, respectively, "ntr_res" and "sp_res" denotes the residual portion of the preformed nitrate in spring and of the residual portion of regenerated nitrate in summer, respectively.

3.5. Conclusion

Based on analyses of nutrient concentrations and nitrate isotope composition in water, particulate matter and sediments in spring and summer, we distinguish differences in nitrogen cycling in two prominent sub-thermocline water masses in the Yellow Sea. Although the hydrographic conditions were quite similar in the northern part (nCW) and southern part (sCW) of the YSCWM, nitrate concentrations of nCW were much lower than those in the sCW in both spring and summer. In spring, nitrate concentrations of nCW were lower than in sCW due to weakening northward transport of YSWC that is expressed as a nutrient gradient between the nYS and the sYS. In

summer, the influx of nitrate with Changjiang Diluted Water (CDW), its assimilation into biomass and subsequent nitrification enhanced the nitrate in sCW, but the central area of nYS was hardly impacted by terrestrial influx. DIN pool decreased by 52 % and 5 % in nCW and sCW, respectively, sediment denitrification and vertical diffusion accounted for DIN loss in the central YS bottom water. However, substantial nitrification in sCW was revealed by dual nitrate isotopes, resulted in DIN in sCW increased in summer opposite to the nCW, A simple mixing model based on $\delta^{18}O\text{-}NO_3^-$ suggested that nitrate of sCW in summer is the mixture of nitrate preformed in spring and regenerated nitrate in summer, co-occurring with DIN loss. Preformed and regenerated nitrate was estimated to amount to 35 % and 65 % of the total nitrate in the sCW, respectively. Sedimentary denitrification proceeded beneath both water masses gradually reduced the pool of DIN in nCW, whereas higher rates of nitrate regeneration than of denitrification increased the sub-thermocline nitrate pool in sCW. These diverging trends suggest that the sYS is more sensitive to deoxygenation than the nYS. Although the bottom water is still oxic in the south-central YS, the ecological risk of continued and rising excess nitrogen from Changjiang River should not be ignored.

4. Chapter 4 – Conclusions and outlook

4.1. Conclusions

Our study investigated the physical and biogeochemical parameters of the BHS and YS in spring and summer (i.e., in biologically inactive and active periods); the dual isotopes of nitrate, nitrogen isotopes of particulate matter and surface sediments are the key parameters. The study region is a hotspot to explore how anthropogenic activities interact with the ocean and oceanic processes. N-containing substances are carried by the largest rivers, YR and CJR, which are nutrient enriched by numerous big cities in their drainage basins; they are further supplied to the sea by aeolian transport from agriculture and combustion on land. These N loads mix with those transported by a sub-branch of the Kuroshio Current into the BHS and YS.

For the BHS, we propose a nitrate budget of nitrate with each mass fluxes of inputs and outputs constrained by the corresponding dual isotope values. We used a box model to mimic the nitrogen budget and in particular the internal sources and sinks of nitrate and constrained import, export and internal cycling processes by using a mass-based and dual stable-isotope approach based on $\delta^{15}N$ and $\delta^{18}O$ of nitrate. Compared to previous estimates, this budget is more complete and includes the impact of internal cycling (nitrification) on the nitrate pool. The main nitrate sources are rivers contributing 19.2–25.6 % and the combined terrestrial runoff (including submarine fresh groundwater discharge of nitrate) accounts for 27.8–37.1 % of the nitrate input to the BHS while atmospheric input contributes 6.9–22.2 % to total nitrate. An unusually active interior nitrogen cycling contributes 40.7–65.3 % to total nitrate via nitrification. Nitrogen is mainly trapped in the BHS and mainly removed by sedimentation (70.4–77.8 %) and only very little is exported to the Yellow Sea (YS) (only 1.8–2.4 %). At present denitrification is active in the sediments and removes 20.4–27.2 % of nitrate from the pool.

In the YS, we revealed the differences in nitrate cycling in the two parts of the central YS bottom water. We found that the nitrate concentration decreased from 2.41 ± 1.58 μmol L^{-1} in spring to 0.81 ± 0.61 μmol L^{-1} in summer in the northern part of the YSCWM. In contrast, nitrate increased from 5.49 ± 2.24 μmol L^{-1} to 7.58 ± 2.20 μmol L^{-1} in the southern part, accompanied by a decrease in $\delta^{15}N\text{-}NO_3^-$ and $\delta^{18}O\text{-}NO_3^-$ by ~5.0 ‰ from values near 10.0 ‰ in the southern deep water mass. The increasing nitrate concentration and decreasing $\delta^{15}N\text{-}NO_3^-$ and $\delta^{18}O\text{-}NO_3^-$ values of nitrate are indicative of nitrification that was a significant source of recycled nitrate in the southern part of YSCWM.

We propose a mixing model with end members of preformed nitrate in spring and regenerated nitrate in summer both with their distinct dual isotope values. The values

of $\delta^{15}N$ and $\delta^{18}O$ for regenerated nitrate were first constrained as 3.3 ‰ and 0.9 ‰, respectively. The results of the combined mass and isotope balance model suggest that in summer 65 % of the nitrate in the southern branch of YSCWM was regenerated and only 35 % of nitrate was a residual of nitrate preformed in spring. Our findings indicate that the northern part of YSCWM is a sink of reactive nitrogen in the sub-thermocline water column, mainly because of denitrification in sediments. In contrast, the southern pool of YSCWM is a growing reservoir of regenerated terrestrial reactive nitrogen, the addition of which compensates the removal by co-occurring sediment denitrification.

Our results above provide a comprehensive picture of N cycling in the BHS and YS: terrestrial sources are mainly the YR and CJR but their impacts were restricted to the BHS and the southern YS. Atmospheric deposition is approximately equivalent to the terrestrial input, while the outer shelf water supplies nutrients to the YS with a northward weakening gradient in wintertime. River discharge into the BHS and YS has higher $\delta^{15}N$-NO_3^- than the ocean nitrate pool. However, these high $\delta^{15}N$ values are either masked by low $\delta^{15}N$ of the atmospheric deposition or removed by sediment denitrification. Active nitrification in the BHS and YS supply high amounts of regenerated nitrate. This process forces the $\delta^{15}N$ of nitrate, particles and surface sediment to converge to about 5 ‰, similar to the $\delta^{15}N$-NO_3^- of the invading outer shelf water. Small exchange between BHS and YS restricts the impact some of the largest cities to the BHS, the BHS and YS have played the role as a buffer of the increasing anthropogenic N by sedimentary denitrification, however, seasonal low oxygen areas have already been observed in the YR and CJR estuaries (Zhai et al., 2019; Guo et al., 2020b; Song et al., 2021).

4.2. Outlook

The measurement of dual nitrate isotopes in seasons or regions of low nitrate concentration (< 1.7 μmol L^{-1} for our method) is difficult to carry out and there are data gaps. In some regions of the central BHS and YS, and in the surface waters with low nitrate concentrations dual isotope values areas are lacking. The detection of these data will fill the missing knowledge of nitrate cycling, for instance, the regeneration nitrate of the north YS could be quantified. Besides, the direct measurement of nitrification rates in the water column will help us to quantify the regenerated nitrate in order to verify our model results.

Our study covered the two typical seasons in the system which are basic to explain the N cycling. However, to complete the understanding of the annual fluctuation of the N isotopic values in the BHS and YS, data of autumn and winter will be helpful. These data probably can further help us to build on the hypothesis of N cycling in the BHS and YS and better understand how and when the decreased dual isotopes of nitrate in the central YS become enhanced in the next spring. Furthermore, long time monitoring

will give us the opportunity to reveal how the anthropogenic N supply changes the N pool and cycling processes in the marginal seas. Because the research of nitrate dual isotopes is a new topic in our study area, we don't have sufficient data on the long-term trend of nitrate isotopes. As the excess N has already exhausted the attenuation capacity for N_r of the BHS and southern YS, whether this will invigorate water-column denitrification to balance the additional inputs is an open question, as is the capacity of BHS and south YS as a nitrate buffer between the growing source of N_r on land and the open ocean. The role of north YS could be more and more important as a sink of N transported from the BHS and southern YS.

Abbreviations

BHS	Bohai Sea
YS	Yellow Sea
ECS	East China Sea
YR	Yellow River
CJR	Changjiang River
YSWC	Yellow Sea Warm Current
YSCWM	Yellow Sea Cold Water Mass
nCW	north Cold Water
sCW	south Cold Water
N_r	reactive nitrogen
DIN	dissolved inorganic nitrogen
DO	dissolved oxygen
AOU	Apparent Oxygen Utilization
$N*$	nitrate concentration anomaly
Tg	Teragram (10^{12})
‰	per mil
δ	"delta" convention for expressing natural variation in isotopic ratio
ε	isotope fractionation factor
f	fraction of remaining substrate
$\delta^{15}N\text{-}NO_3^-$	$\delta^{15}N$ of nitrate
$\delta^{18}O\text{-}NO_3^-$	$\delta^{18}O$ of nitrate
T	Temperature
S	Salinity
HABs	Harmful algal blooms
LCC	Lubei Coastal Current
SCC	Subei Coastal Current
KCC	Korean Coastal Current
YSCC	Yellow Sea Coastal Current
TWC	Taiwan Warm Current
KC	Kuroshio Current
CDW	Changjiang Diluted Water

References

Altabet, M.A. (2006). "Isotopic tracers of the marine nitrogen cycle: present and past," in *Marine organic matter: biomarkers, isotopes and DNA*. Springer), 251-293.

Altabet, M.A., and Francois, R. (1994). Sedimentary nitrogen isotopic ratio as a recorder for surface ocean nitrate utilization. *Global biogeochemical cycles* 8(1), 103-116.

Anderson, L.A. (1995). On the hydrogen and oxygen content of marine phytoplankton. *Deep Sea Research Part I: Oceanographic Research Papers* 42(9), 1675-1680. doi: https://doi.org/10.1016/0967-0637(95)00072-E.

Aravena, R., Evans, M., and Cherry, J.A. (1993). Stable isotopes of oxygen and nitrogen in source identification of nitrate from septic systems. *Groundwater* 31(2), 180-186.

Arrigo, K.R. (2005). Marine microorganisms and global nutrient cycles. *Nature* 437(7057), 349-355. doi: 10.1038/nature04159.

Backhaus, J.O. (1985). A three-dimensional model for the simulation of shelf sea dynamics. *Deutsche Hydrografische Zeitschrift* 38(4), 165-187. doi: https://doi.org/10.1007/BF02328975.

Benson, B.B., and Krause Jr, D. (1984). The concentration and isotopic fractionation of oxygen dissolved in freshwater and seawater in equilibrium with the atmosphere 1. *Limnology and oceanography* 29(3), 620-632. doi: https://doi.org/10.4319/lo.1984.29.3.0620.

Bohlen, L., Dale, A.W., and Wallmann, K. (2012). Simple transfer functions for calculating benthic fixed nitrogen losses and C:N:P regeneration ratios in global biogeochemical models. *Global Biogeochemical Cycles* 26(3). doi: https://doi.org/10.1029/2011GB004198.

Brandes, J.A., and Devol, A.H. (1997). Isotopic fractionation of oxygen and nitrogen in coastal marine sediments. *Geochimica et Cosmochimica Acta* 61(9), 1793-1801.

Brandes, J.A., and Devol, A.H. (2002). A global marine-fixed nitrogen isotopic budget: Implications for Holocene nitrogen cycling. *Global Biogeochemical Cycles* 16(4).

Brandes, J.A., Devol, A.H., Yoshinari, T., Jayakumar, D., and Naqvi, S. (1998). Isotopic composition of nitrate in the central Arabian Sea and eastern tropical North Pacific: A tracer for mixing and nitrogen cycles. *Limnology and Oceanography* 43(7), 1680-1689.

Buchwald, C., Santoro, A.E., McIlvin, M.R., and Casciotti, K.L. (2012). Oxygen isotopic composition of nitrate and nitrite produced by nitrifying cocultures and natural marine assemblages. *Limnology and Oceanography* 57(5), 1361-1375. doi: 10.4319/lo.2012.57.5.1361.

Carpenter, E.J., Harvey, H.R., Fry, B., and Capone, D.G. (1997). Biogeochemical tracers of the marine cyanobacterium Trichodesmium. *Deep Sea Research Part I: Oceanographic Research Papers* 44(1), 27-38. doi: https://doi.org/10.1016/S0967-0637(96)00091-X.

Casciotti, K., Trull, T., Glover, D., and Davies, D. (2008a). Constraints on nitrogen cycling at the subtropical North Pacific Station ALOHA from isotopic measurements of nitrate and particulate nitrogen. *Deep Sea Research Part II: Topical Studies in Oceanography* 55(14-15), 1661-1672.

Casciotti, K.L. (2009). Inverse kinetic isotope fractionation during bacterial nitrite oxidation. *Geochimica et Cosmochimica Acta* 73(7), 2061-2076.

Casciotti, K.L. (2016). Nitrogen and Oxygen Isotopic Studies of the Marine Nitrogen Cycle. *Ann Rev Mar Sci* 8, 379-407. doi: 10.1146/annurev-marine-010213-135052.

Casciotti, K.L., Böhlke, J.K., McIlvin, M.R., Mroczkowski, S.J., and Hannon, J.E. (2007). Oxygen isotopes in nitrite: Analysis, calibration, and equilibration. *Analytical Chemistry* 79(6)**,** 2427-2436. doi: https://doi.org/10.1021/ac061598h.

Casciotti, K.L., McIlvin, M., and Buchwald, C. (2010). Oxygen isotopic exchange and fractionation during bacterial ammonia oxidation. *Limnology and Oceanography* 55(2)**,** 753-762.

Casciotti, K.L., Sigman, D.M., Hastings, M.G., Böhlke, J., and Hilkert, A. (2002). Measurement of the oxygen isotopic composition of nitrate in seawater and freshwater using the denitrifier method. *Analytical Chemistry* 74(19)**,** 4905-4912. doi: https://doi.org/10.1021/ac020113w.

Casciotti, K.L., Sigman, D.M., and Ward, B.B. (2003). Linking Diversity and Stable Isotope Fractionation in Ammonia-Oxidizing Bacteria. *Geomicrobiology Journal* 20(4)**,** 335-353. doi: 10.1080/01490450303895.

Casciotti, K.L., Trull, T.W., Glover, D.M., and Davies, D. (2008b). Constraints on nitrogen cycling at the subtropical North Pacific Station ALOHA from isotopic measurements of nitrate and particulate nitrogen. *Deep Sea Research Part II: Topical Studies in Oceanography* 55(14)**,** 1661-1672. doi: https://doi.org/10.1016/j.dsr2.2008.04.017.

[Dataset] CCCS (2017). *ERA5: Fifth generation of ECMWF atmospheric reanalyses of the global climate*. doi: doi.org/10.1002/qj.3803.

Chang, Y., Zhang, Y.L., Li, J., Tian, C., Song, L., Zhai, X., et al. (2019). Isotopic constraints on the atmospheric sources and formation of nitrogenous species in clouds influenced by biomass burning. *Atmospheric Chemistry and Physics* 19(19)**,** 12221-12234. doi: https://doi.org/10.5194/acp-19-12221-2019.

Chen, C.-T.A. (2009). Chemical and physical fronts in the Bohai, Yellow and East China seas. *Journal of Marine Systems* 78(3)**,** 394-410. doi: https://doi.org/10.1016/j.jmarsys.2008.11.016.

Chen, F., Chen, J., Jia, G., Jin, H., Xu, J., Yang, Z., et al. (2013). Nitrate δ 15 N and δ 18 O evidence for active biological transformation in the Changjiang Estuary and the adjacent East China Sea. *Acta Oceanologica Sinica* 32(4)**,** 11-17. doi: DOI: 10.1007/s13131-013-0294-4.

Chen, F., Lao, Q., Zhang, S., Bian, P., Jin, G., Zhu, Q., et al. (2020). Nitrate sources and biogeochemical processes identified using nitrogen and oxygen isotopes on the eastern coast of Hainan Island. *Continental Shelf Research***,** 104209. doi: https://doi.org/10.1016/j.csr.2020.104209.

Chen, J., Taniguchi, M., Liu, G., Miyaoka, K., Onodera, S.-i., Tokunaga, T., et al. (2007). Nitrate pollution of groundwater in the Yellow River delta, China. *Hydrogeology Journal* 15(8)**,** 1605-1614. doi: 10.1007/s10040-007-0196-7.

Chen, J., Wang, F., Meybeck, M., He, D., Xia, X., and Zhang, L. (2005). Spatial and temporal analysis of water chemistry records (1958-2000) in the Huanghe (Yellow River) basin. *Global Biogeochemical Cycles* 19(3). doi: 10.1029/2004gb002325.

Chen, P., Lu, Z., Shi, X.Y., and Zhang, C.S. (2012). Estimated Nutrients Contribution of the North Yellow Sea Cold Water(Yc) Mass in Summer. *Periodical of Ocean University of China*.

China, M.o.W.R.o. (2015-2018). *China Water Resources Bulletin*. Beijing: China Water & Power Press.

Dähnke, K., Bahlmann, E., and Emeis, K. (2008). A nitrate sink in estuaries? An assessment by means of stable nitrate isotopes in the Elbe estuary. *Limnology and Oceanography* 53(4)**,** 1504-1511. doi: https://doi.org/10.4319/lo.2008.53.4.1504.

Dejwakh, N.R., Meixner, T., Michalski, G., and McIntosh, J. (2012). Using 17O to Investigate Nitrate

Sources and Sinks in a Semi-Arid Groundwater System. *Environmental Science & Technology* 46(2), 745-751. doi: 10.1021/es203450z.

Deutsch, C., and Weber, T. (2012). Nutrient Ratios as a Tracer and Driver of Ocean Biogeochemistry. *Annual Review of Marine Science* 4(1), 113-141. doi: 10.1146/annurev-marine-120709-142821.

Devol, A.H. (2015). Denitrification, Anammox, and N2 Production in Marine Sediments. *Annual Review of Marine Science* 7(1), 403-423. doi: 10.1146/annurev-marine-010213-135040.

DiFiore, P.J., Sigman, D.M., and Dunbar, R.B. (2009). Upper ocean nitrogen fluxes in the Polar Antarctic Zone: Constraints from the nitrogen and oxygen isotopes of nitrate. *Geochemistry, Geophysics, Geosystems* 10(11). doi: https://doi.org/10.1029/2009GC002468.

DiFiore, P.J., Sigman, D.M., Trull, T.W., Lourey, M.J., Karsh, K., Cane, G., et al. (2006). Nitrogen isotope constraints on subantarctic biogeochemistry. *Journal of Geophysical Research: Oceans* 111(C8). doi: https://doi.org/10.1029/2005JC003216.

Ding, X., Guo, X., Gao, H., Gao, J., Shi, J., Yu, X., et al. (2021). Seasonal variations of nutrient concentrations and their ratios in the central Bohai Sea. *Science of The Total Environment* 799, 149416. doi: https://doi.org/10.1016/j.scitotenv.2021.149416.

Duan, L.-Q., Song, J.-M., Yuan, H.-M., Li, X.-G., and Li, N. (2016). Distribution, partitioning and sources of dissolved and particulate nitrogen and phosphorus in the north Yellow Sea. *Estuarine, Coastal and Shelf Science* 181, 182-195. doi: https://doi.org/10.1016/j.ecss.2016.08.044.

Egbert, G.D., and Erofeeva, S.Y. (2002). Efficient inverse modeling of barotropic ocean tides. *Journal of Atmospheric and Oceanic Technology* 19(2), 183-204. doi: https://doi.org/10.1175/1520-0426(2002)019<0183:EIMOBO>2.0.CO;2.

Emeis, K.C., Mara, P., Schlarbaum, T., Möbius, J., Dähnke, K., Struck, U., et al. (2010). External N inputs and internal N cycling traced by isotope ratios of nitrate, dissolved reduced nitrogen, and particulate nitrogen in the eastern Mediterranean Sea. *Journal of Geophysical Research: Biogeosciences* 115(G4). doi: https://doi.org/10.1029/2009JG001214.

Erisman, J.W., Sutton, M.A., Galloway, J., Klimont, Z., and Winiwarter, W.J.N.G. (2008). How a century of ammonia synthesis changed the world. 1(10), 636.

Fan, M.-Y., Zhang, Y.-L., Lin, Y.-C., Chang, Y.-H., Cao, F., Zhang, W.-Q., et al. (2019). Isotope-based source apportionment of nitrogen-containing aerosols: A case study in an industrial city in China. *Atmospheric Environment* 212, 96-105. doi: https://doi.org/10.1016/j.atmosenv.2019.05.020.

Fan, W., and Song, J. (2014). A numerical study of the seasonal variations of nutrients in the Changjiang River estuary and its adjacent sea area. *Ecological modelling* 291, 69-81.

Fowler, D., Coyle, M., Skiba, U., Sutton, M.A., Cape, J.N., Reis, S., et al. (2013). The global nitrogen cycle in the twenty-first century. 368(1621), 20130164. doi: https://doi.org/10.1098/rstb.2013.0164.

Fu, M., Wang, Z., Pu, X., Xu, Z., and Zhu, M. (2012). Changes of nutrient concentrations and N: P: Si ratios and their possible impacts on the Huanghai Sea ecosystem. *Acta Oceanologica Sinica* 31(4), 101-112.

Fu, Y., Xu, S., and Liu, J. (2016). Temporal-spatial variations and developing trends of Chlorophyll-

a in the Bohai Sea, China. *Estuarine, Coastal and Shelf Science* 173**,** 49-56. doi: https://doi.org/10.1016/j.ecss.2016.02.016.

Galloway, J.N., Leach, A.M., Bleeker, A., and Erisman, J.W.J.P.T.o.t.R.S.B.B.S. (2013). A chronology of human understanding of the nitrogen cycle. 368(1621)**,** 20130120.

Gao, X., Yang, Y., and Wang, C. (2012). Geochemistry of organic carbon and nitrogen in surface sediments of coastal Bohai Bay inferred from their ratios and stable isotopic signatures. *Marine Pollution Bulletin* 64(6)**,** 1148-1155. doi: https://doi.org/10.1016/j.marpolbul.2012.03.028.

Gaye, B., Wiesner, M.G., and Lahajnar, N. (2009). Nitrogen sources in the South China Sea, as discerned from stable nitrogen isotopic ratios in rivers, sinking particles, and sediments. *Marine Chemistry* 114(3-4)**,** 72-85. doi: 10.1016/j.marchem.2009.04.003.

Glibert, P.M., Wilkerson, F.P., Dugdale, R.C., Raven, J.A., Dupont, C.L., Leavitt, P.R., et al. (2016). Pluses and minuses of ammonium and nitrate uptake and assimilation by phytoplankton and implications for productivity and community composition, with emphasis on nitrogen - enriched conditions. *Limnology and Oceanography* 61(1)**,** 165-197. doi: https://doi.org/10.1002/lno.10203.

Granger, J., Sigman, D., Lehmann, M., and Tortell, P. (Year). "Nitrogen and oxygen isotope effects associated with nitrate assimilation and denitrification by laboratory cultures of marine plankton", in: *AGU Fall Meeting Abstracts*).

Granger, J., and Sigman, D.M. (2009). Removal of nitrite with sulfamic acid for nitrate N and O isotope analysis with the denitrifier method. *Rapid Communications in Mass Spectrometry* 23(23)**,** 3753-3762. doi: https://doi.org/10.1002/rcm.4307.

Granger, J., Sigman, D.M., Lehmann, M.F., and Tortell, P.D. (2008). Nitrogen and oxygen isotope fractionation during dissimilatory nitrate reduction by denitrifying bacteria. *Limnology and Oceanography* 53(6)**,** 2533-2545.

Granger, J., Sigman, D.M., Rohde, M., Maldonado, M., and Tortell, P. (2010). N and O isotope effects during nitrate assimilation by unicellular prokaryotic and eukaryotic plankton cultures. *Geochimica et Cosmochimica Acta* 74(3)**,** 1030-1040. doi: https://doi.org/10.1016/j.gca.2009.10.044.

Grasshoff, K., Kremling, K., and Ehrhardt, M. (2009). *Methods of seawater analysis.* John Wiley & Sons.

Grischek, T., Hiscock, K., Metschies, T., Dennis, P., and Nestler, W. (1998). Factors affecting denitrification during infiltration of river water into a sand and gravel aquifer in Saxony, Germany. *Water Research* 32(2)**,** 450-460.

Gruber, N. (Year). "The Dynamics of the Marine Nitrogen Cycle and its Influence on Atmospheric CO2 Variations": Springer Netherlands), 97-148.

Gruber, N. (2008a). "Chapter 1 - The Marine Nitrogen Cycle: Overview and Challenges," in *Nitrogen in the Marine Environment (Second Edition),* eds. D.G. Capone, D.A. Bronk, M.R. Mulholland & E.J. Carpenter.   (San Diego: Academic Press), 1-50.

Gruber, N. (2008b). The marine nitrogen cycle: overview and challenges. *Nitrogen in the marine environment* 2**,** 1-50.

Gruber, N., and Sarmiento, J.L. (1997). Global patterns of marine nitrogen fixation and denitrification. *Global Biogeochemical Cycles* 11(2)**,** 235-266. doi: https://doi.org/10.1029/97GB00077.

Gu, B., Ju, X., Chang, J., Ge, Y., and Vitousek, P.M. (2015). Integrated reactive nitrogen budgets and future trends in China. *Proceedings of the National Academy of Sciences, USA* 112(28), 8792. doi: https://doi.org/10.1073/pnas.1510211112.

Guo, C., Zhang, G., Sun, J., Leng, X., Xu, W., Wu, C., et al. (2020a). Seasonal responses of nutrient to hydrology and biology in the southern Yellow Sea. *Continental Shelf Research*, 104207.

Guo, J., Yuan, H., Song, J., Li, X., and Duan, L. (2020b). Hypoxia, acidification and nutrient accumulation in the Yellow Sea Cold Water of the South Yellow Sea. *Science of The Total Environment* 745, 141050. doi: https://doi.org/10.1016/j.scitotenv.2020.141050.

Hainbucher, D., Hao, W., Pohlmann, T., Sündermann, J., and Feng, S. (2004). Variability of the Bohai Sea circulation based on model calculations. *Journal of Marine Systems* 44(3), 153-174. doi: https://doi.org/10.1016/j.jmarsys.2003.09.008.

Han, L., Zhu, Y., Liu, S., Zhang, J., and Li, R. (2013). Nutrients of atmospheric wet deposition from the Qianliyan Island of the Yellow Sea. *China Environmental Science* 33(7), 1174-1184.

Heaton, T.H. (1986). Isotopic studies of nitrogen pollution in the hydrosphere and atmosphere: a review. *Chemical Geology: Isotope Geoscience Section* 59, 87-102.

Hoch, M.P., Fogel, M.L., and Kirchman, D.L. (1992). Isotope fractionation associated with ammonium uptake by a marine bacterium. *Limnology and Oceanography* 37(7), 1447-1459. doi: https://doi.org/10.4319/lo.1992.37.7.1447.

Huang, D., Su, J., and Backhaus, J.O. (1999). Modelling the seasonal thermal stratification and baroclinic circulation in the Bohai Sea. *Continental Shelf Research* 19(11), 1485-1505. doi: https://doi.org/10.1016/S0278-4343(99)00026-6.

Hyun, J.-H., and Kim, K.-H. (2003). Bacterial abundance and production during the unique spring phytoplankton bloom in the central Yellow Sea. *Marine Ecology Progress Series* 252, 77-88.

IFA (2019). "Short-Term Fertilizer Outlook 2019 – 2020". (Versailles).

Jahnke, R.A. (2010). "Global Synthesis1," in *Carbon and Nutrient Fluxes in Continental Margins: A Global Synthesis,* eds. K.-K. Liu, L. Atkinson, R. Quiñones & L. Talaue-McManus. (Berlin, Heidelberg: Springer Berlin Heidelberg), 597-615.

Jia, B., and Chen, X.e. (2021). Application of an ice-ocean coupled model to Bohai Sea ice simulation. *Journal of Oceanology and Limnology* 39(1), 1-13. doi: 10.1007/s00343-020-9168-8.

Jia, G., and Chen, F. (2010). Monthly variations in nitrogen isotopes of ammonium and nitrate in wet deposition at Guangzhou, south China. *Atmospheric Environment* 44(19), 2309-2315. doi: https://doi.org/10.1016/j.atmosenv.2010.03.041.

Jin, J., Liu, S.M., Ren, J.L., Liu, C.G., Zhang, J., Zhang, G.L., et al. (2013). Nutrient dynamics and coupling with phytoplankton species composition during the spring blooms in the Yellow Sea. *Deep Sea Research Part II: Topical Studies in Oceanography* 97, 16-32.

Johannsen, A., Dähnke, K., and Emeis, K. (2008). Isotopic composition of nitrate in five German rivers discharging into the North Sea. *Organic Geochemistry* 39(12), 1678-1689.

Jung, F. (2015). *Nitrogen isotopes in atmospheric deposition in Northern Germany : consequences of emission changes.* Doctor of Science, University of Hamburg.

Kang, D.-J., Chung, C.S., Kim, S.H., Hong, G.H., and Kim, K.-R. (1994). Oxygen isotope characteristics of seawaters in the Yellow Sea. *La mer* 32(4), 279-284.

Karl, D., Michaels, A., Bergman, B., Capone, D., Carpenter, E., Letelier, R., et al. (2002). Dinitrogen

fixation in the world's oceans. *Biogeochemistry* 57(1)**,** 47-98. doi: 10.1023/A:1015798105851.

Karsh, K.L., Granger, J., Kritee, K., and Sigman, D.M. (2012). Eukaryotic Assimilatory Nitrate Reductase Fractionates N and O Isotopes with a Ratio near Unity. *Environmental Science & Technology* 46(11)**,** 5727-5735. doi: 10.1021/es204593q.

Kendall, C., Elliott, E.M., and Wankel, S.D. (2007). "Tracing Anthropogenic Inputs of Nitrogen to Ecosystems," in *Stable Isotopes in Ecology and Environmental Science*.), 375-449.

Kim, H., Park, G.-H., Lee, S.-E., Kim, Y.-i., Lee, K., Kim, Y.-H., et al. (2019). Stable isotope ratio of atmospheric and seawater nitrate in the East Sea in the northwestern Pacific ocean. *Marine Pollution Bulletin* 149**,** 110610. doi: https://doi.org/10.1016/j.marpolbul.2019.110610.

Kim, J., Ghim, Y., Lee, S., Moon, K.-C., Shim, S.-G., Bae, G., et al. (2010). Atmospheric deposition of nitrogen and sulfur in the Yellow Sea region: Significance of long-range transport in East Asia. *Water, air, and soil pollution* 205(1-4)**,** 259.

Kim, T.-W., Lee, K., Najjar, R.G., Jeong, H.-D., and Jeong, H.J. (2011). Increasing N abundance in the northwestern Pacific Ocean due to atmospheric nitrogen deposition. *Science* 334(6055)**,** 505-509.

Kroopnick, P., and Craig, H. (1972). Atmospheric oxygen: isotopic composition and solubility fractionation. *Science* 175(4017)**,** 54-55.

Lehmann, M.F., Sigman, D.M., and Berelson, W.M. (2004). Coupling the 15N/14N and 18O/16O of nitrate as a constraint on benthic nitrogen cycling. *Marine Chemistry* 88(1-2)**,** 1-20. doi: https://doi.org/10.1016/j.marchem.2004.02.001.

[Dataset] Lellouche, J., Legalloudec, O., Regnier, C., Levier, B., Greiner, E., and Drevillon, M. (2019). *Quality information document for global sea physical analysis and forecasting product global analysis forecast phy 001 024(Tech. Rep. Issue: 2.1): EU Copernicus Marine Service.*. doi: http://cmems-resources.cls.fr/documents/QUID/CMEMS-GLO-QUID-001-024.pdf.

Levin, L.A., Liu, K.-K., Emeis, K.-C., Breitburg, D.L., Cloern, J., Deutsch, C., et al. (2015a). Comparative biogeochemistry–ecosystem–human interactions on dynamic continental margins. *Journal of Marine Systems* 141**,** 3-17.

Levin, L.A., Liu, K.-K., Emeis, K.-C., Breitburg, D.L., Cloern, J., Deutsch, C., et al. (2015b). Comparative biogeochemistry–ecosystem–human interactions on dynamic continental margins. *Journal of Marine Systems* 141**,** 3-17. doi: https://doi.org/10.1016/j.jmarsys.2014.04.016.

Li, H.-M., Zhang, C.-S., Han, X.-R., and Shi, X.-Y. (2015a). Changes in concentrations of oxygen, dissolved nitrogen, phosphate, and silicate in the southern Yellow Sea, 1980–2012: sources and seaward gradients. *Estuarine, Coastal and Shelf Science* 163**,** 44-55.

Li, H., Lin, L., Ye, S., Li, H., and Fan, J. (2017a). Assessment of nutrient and heavy metal contamination in the seawater and sediment of Yalujiang Estuary. *Marine Pollution Bulletin* 117(1)**,** 499-506. doi: https://doi.org/10.1016/j.marpolbul.2017.01.069.

Li, H., Zhang, Y., Tang, H., Shi, X., Rivkin, R.B., and Legendre, L. (2017b). Spatiotemporal variations of inorganic nutrients along the Jiangsu coast, China, and the occurrence of macroalgal blooms (green tides) in the southern Yellow Sea. *Harmful Algae* 63**,** 164-172.

Li, S.-L., Liu, C.-Q., Li, J., Liu, X., Chetelat, B., Wang, B., et al. (2010). Assessment of the sources of nitrate in the Changjiang River, China using a nitrogen and oxygen isotopic approach. *Environmental Science & Technology* 44(5)**,** 1573-1578.

Li, Y., Wolanski, E., and Zhang, H. (2015b). What processes control the net currents through shallow

straits? A review with application to the Bohai Strait, China. *Estuarine, Coastal and Shelf Science* 158, 1-11. doi: https://doi.org/10.1016/j.ecss.2015.03.013.

Li, Y., Yan, W., Wang, F., Lv, S., Li, Q., and Yu, Q. (2019a). Nitrogen pollution and sources in an aquatic system at an agricultural coastal area of Eastern China based on a dual-isotope approach. *Environmental Science and Pollution Research* 26(23), 23807-23823. doi: 10.1007/s11356-019-05665-2.

Li, Y., Zhang, H., Tu, C., Fu, C., Xue, Y., and Luo, Y. (2016). Sources and fate of organic carbon and nitrogen from land to ocean: Identified by coupling stable isotopes with C/N ratio. *Estuarine, Coastal and Shelf Science* 181, 114-122. doi: 10.1016/j.ecss.2016.08.024.

Li, Z., Walters, W.W., Hastings, M.G., Zhang, Y., Song, L., Liu, D., et al. (2019b). Nitrate Isotopic Composition in Precipitation at a Chinese Megacity: Seasonal Variations, Atmospheric Processes, and Implications for Sources. *Earth and Space Science*. doi: https://doi.org/10.1029/2019EA000759.

Lin, X., and Yang, J. (2011). An asymmetric upwind flow, Yellow Sea Warm Current: 2. Arrested topographic waves in response to the northwesterly wind. *Journal of Geophysical Research* 116.

Liu, D., Li, X., Emeis, K.-C., Wang, Y., and Richard, P. (2015a). Distribution and sources of organic matter in surface sediments of Bohai Sea near the Yellow River Estuary, China. *Estuarine, Coastal and Shelf Science* 165, 128-136. doi: https://doi.org/10.1016/j.ecss.2015.09.007.

Liu, J., Du, J., and Yi, L. (2017a). Ra Tracer-Based Study of Submarine Groundwater Discharge and Associated Nutrient Fluxes into the Bohai Sea, China: A Highly Human-Affected Marginal Sea. *Journal of Geophysical Research: Oceans* 122(11), 8646-8660. doi: https://doi.org/10.1002/2017JC013095.

Liu, J.a., Su, N., Wang, X., and Du, J. (2017b). Submarine groundwater discharge and associated nutrient fluxes into the Southern Yellow Sea: A case study for semi-enclosed and oligotrophic seas-implication for green tide bloom. *Journal of Geophysical Research: Oceans* 122(1), 139-152. doi: https://doi.org/10.1002/2016JC012282.

Liu, K.-K., and Kaplan, I.R. (1989). The eastern tropical Pacific as a source of 15N enriched nitrate in seawater off southern California. *Limnology and Oceanography* 34, 820-830.

Liu, K.-K., Su, M.J., Hsueh, C.-R., and Gong, G.C. (1996). The nitrogen isotopic composition of nitrate in the Kuroshio Water northeast of Taiwan: evidence for nitrogen fixation as a source of isotopically light nitrate. *Marine Chemistry* 54, 273-292.

Liu, S., Hong, G.-H., Zhang, J., Ye, X., and Jiang, X. (2009a). Nutrient budgets for large Chinese estuaries. *Biogeosciences* 6(10), 2245-2263. doi: https://doi.org/10.5194/bg-6-2245-2009.

Liu, S., Zhang, J., Chen, S.Z., Chen, H., Hong, G., Wei, H., et al. (2003a). Inventory of nutrient compounds in the Yellow Sea. *Continental Shelf Research* 23(11-13), 1161-1174.

Liu, S.M., Altabet, M.A., Zhao, L., Larkum, J., Song, G.D., Zhang, G.L., et al. (2017c). Tracing Nitrogen Biogeochemistry During the Beginning of a Spring Phytoplankton Bloom in the Yellow Sea Using Coupled Nitrate Nitrogen and Oxygen Isotope Ratios. *Journal of Geophysical Research: Biogeosciences* 122(10), 2490-2508. doi: 10.1002/2016jg003752.

Liu, S.M., Li, L.W., and Zhang, Z. (2011). Inventory of nutrients in the Bohai. *Continental Shelf Research* 31(16), 1790-1797. doi: https://doi.org/10.1016/j.csr.2011.08.004.

Liu, S.M., Ning, X., Dong, S., Song, G., Wang, L., Altabet, M.A., et al. (2020). Source Versus Recycling

Influences on the Isotopic Composition of Nitrate and Nitrite in the East China Sea. *Journal of Geophysical Research: Oceans* 125(8), e2020JC016061. doi: https://doi.org/10.1029/2020JC016061.

Liu, S.M., Zhang, J., and Jiang, W.S. (2003b). Pore water nutrient regeneration in shallow coastal Bohai Sea, China. *Journal of oceanography* 59(3), 377-385. doi: https://doi.org/10.1023/A:1025576212927.

Liu, T., Wang, F., Michalski, G., Xia, X., and Liu, S. (2013). Using 15N, 17O, and 18O to determine nitrate sources in the Yellow River, China. *Environmental science & technology* 47(23), 13412-13421.

Liu, X., Beusen, A.H., Van Beek, L.P., Mogollón, J.M., Ran, X., and Bouwman, A.F. (2018). Exploring spatiotemporal changes of the Yangtze River (Changjiang) nitrogen and phosphorus sources, retention and export to the East China Sea and Yellow Sea. *Water research* 142, 246-255.

Liu, X., Chiang, K.-P., Liu, S.-M., Wei, H., Zhao, Y., and Huang, B.-Q. (2015b). Influence of the Yellow Sea Warm Current on phytoplankton community in the central Yellow Sea. *Deep Sea Research Part I: Oceanographic Research Papers* 106, 17-29.

Liu, X., Huang, B., Huang, Q., Wang, L., Ni, X., Tang, Q., et al. (2015c). Seasonal phytoplankton response to physical processes in the southern Yellow Sea. *Journal of Sea Research* 95, 45-55. doi: https://doi.org/10.1016/j.seares.2014.10.017.

Liu, X., Yu, Z., Song, X., and Cao, X. (2009b). The nitrogen isotopic composition of dissolved nitrate in the Yangtze River (Changjiang) estuary, China. *Estuarine, Coastal and Shelf Science* 85(4), 641-650. doi: https://doi.org/10.1016/j.ecss.2009.09.017.

Lu, C.C., and Tian, H. (2017). Global nitrogen and phosphorus fertilizer use for agriculture production in the past half century: shifted hot spots and nutrient imbalance. *Earth System Science Data* 9, 181. doi: 10.5194/essd-9-181-2017.

Luo, X., and Jiao, J.J. (2016). Submarine groundwater discharge and nutrient loadings in Tolo Harbor, Hong Kong using multiple geotracer-based models, and their implications of red tide outbreaks. *Water research* 102, 11-31. doi: https://doi.org/10.1016/j.watres.2016.06.017.

Ma, S., Xin, F., Cui, Y., and Qiao, X. (2004). Assessment of Main Pollution Matter Volume into the Sea from Yellow River and Xiaoqing Rive. *Progress in Fishery Sciences (in Chinese)* 25(5), 47-51. doi: 10.3969/j.issn.1000-7075.2004.05.009.

Mariotti, A., Germon, J., Hubert, P., Kaiser, P., Letolle, R., Tardieux, A., et al. (1981). Experimental determination of nitrogen kinetic isotope fractionation: some principles; illustration for the denitrification and nitrification processes. *Plant and soil* 62(3), 413-430.

Mariotti, A., Germon, J.C., Hubert, P., Kaiser, P.M., Létolle, R.R., Tardieux, A., et al. (2006). Experimental determination of nitrogen kinetic isotope fractionation: Some principles; illustration for the denitrification and nitrification processes. *Plant and Soil* 62, 413-430.

Mayer, B., Bollwerk, S.M., Mansfeldt, T., Hütter, B., and Veizer, J. (2001). The oxygen isotope composition of nitrate generated by nitrification in acid forest floors. *Geochimica et Cosmochimica Acta* 65(16), 2743-2756.

MEE, C. (2019). "Bulletin of Marine Ecology and Environment Status of China in 2018".).

Minagawa, M., and Wada, E. (1986). Nitrogen isotope ratios of red tide organisms in the East China Sea: A characterization of biological nitrogen fixation. *Marine Chemistry* 19, 245-259.

Möbius, J. (2013). Isotope fractionation during nitrogen remineralization (ammonification): Implications for nitrogen isotope biogeochemistry. *Geochimica et Cosmochimica Acta* 105**,** 422-432. doi: https://doi.org/10.1016/j.gca.2012.11.048.

Möbius, J., and Dähnke, K. (2015). Nitrate drawdown and its unexpected isotope effect in the D anube estuarine transition zone. *Limnology and Oceanography* 60(3)**,** 1008-1019.

Montoya, J.P., Carpenter, E.J., and Capone, D.G. (2002). Nitrogen fixation and nitrogen isotope abundances in zooplankton of the oligotrophic North Atlantic. *Limnology and Oceanography* 47(6)**,** 1617-1628. doi: https://doi.org/10.4319/lo.2002.47.6.1617.

Montoya, J.P., and McCarthy, J.J. (1995). Isotopic fractionation during nitrate uptake by phytoplankton grown in continuous culture. *Journal of Plankton Research* 17(3)**,** 439-464. doi: 10.1093/plankt/17.3.439.

Moon, J.-Y., Lee, K., Lim, W.-A., Lee, E., Dai, M., Choi, Y.-H., et al. (2021). Anthropogenic nitrogen is changing the East China and Yellow seas from being N deficient to being P deficient. *Limnology and Oceanography* 66(3)**,** 914-924. doi: https://doi.org/10.1002/lno.11651.

Muller-Karger, F.E., Varela, R., Thunell, R., Luerssen, R., Hu, C., and Walsh, J.J. (2005). The importance of continental margins in the global carbon cycle. *Geophysical Research Letters* 32(1). doi: https://doi.org/10.1029/2004GL021346.

Müller Schmied, H., Eisner, S., Franz, D., Wattenbach, M., Portmann, F.T., Flörke, M., et al. (2014). Sensitivity of simulated global-scale freshwater fluxes and storages to input data, hydrological model structure, human water use and calibration. *Hydrology and Earth System Sciences* 18(9)**,** 3511-3538. doi: 10.5194/hess-18-3511-2014.

MWR, C. (2019). "China River Sediment Bulletin 2018 (in Chinese)", (ed.) Z. Wang. (Beijing).

Ning, X., Lin, C., Su, J., Liu, C., Hao, Q., Le, F., et al. (2010). Long-term environmental changes and the responses of the ecosystems in the Bohai Sea during 1960–1996. *Deep Sea Research Part II: Topical Studies in Oceanography* 57(11-12)**,** 1079-1091. doi: https://doi.org/10.1016/j.dsr2.2010.02.010.

Pätsch, J., Serna, A., Dähnke, K., Schlarbaum, T., Johannsen, A., and Emeis, K.-C. (2010). Nitrogen cycling in the German Bight (SE North Sea)—Clues from modelling stable nitrogen isotopes. *Continental Shelf Research* 30(2)**,** 203-213. doi: https://doi.org/10.1016/j.csr.2009.11.003.

Peterson, R.N., Burnett, W.C., Taniguchi, M., Chen, J., Santos, I.R., and Ishitobi, T. (2008). Radon and radium isotope assessment of submarine groundwater discharge in the Yellow River delta, China. *Journal of Geophysical Research: Oceans* 113(C9). doi: https://doi.org/10.1029/2008JC004776.

Qi, J., Yu, Y., Yao, X., Gang, Y., and Gao, H. (2020). Dry deposition fluxes of inorganic nitrogen and phosphorus in atmospheric aerosols over the Marginal Seas and Northwest Pacific. *Atmospheric Research* 245**,** 105076. doi: https://doi.org/10.1016/j.atmosres.2020.105076.

Qi, J.H., Shi, J.H., Gao, H.W., and Sun, Z. (2013). Atmospheric dry and wet deposition of nitrogen species and its implication for primary productivity in coastal region of the Yellow Sea, China. *Atmospheric Environment* 81**,** 600-608. doi: https://doi.org/10.1016/j.atmosenv.2013.08.022.

Qiao, S., Shi, X., Wang, G., Zhou, L., Hu, B., Hu, L., et al. (2017). Sediment accumulation and budget in the Bohai Sea, Yellow Sea and East China Sea. *Marine Geology* 390**,** 270-281.

Rafter, P.A., DiFiore, P.J., and Sigman, D.M. (2013). Coupled nitrate nitrogen and oxygen isotopes

and organic matter remineralization in the Southern and Pacific Oceans. *Journal of Geophysical Research: Oceans* 118(10)**,** 4781-4794.

[Dataset] Schmidt, G.A., Bigg, G.R., and Rohling, E.J. (1999). *Global Seawater Oxygen-18 Database.* 1.22. Available: https://data.giss.nasa.gov/o18data/.

Seitzinger, S., Harrison, J., Dumont, E., Beusen, A.H., and Bouwman, A. (2005). Sources and delivery of carbon, nitrogen, and phosphorus to the coastal zone: An overview of Global Nutrient Export from Watersheds (NEWS) models and their application. *Global Biogeochemical Cycles* 19(4).

Serna, A., Pätsch, J., Dähnke, K., Wiesner, M.G., Hass, H.C., Zeiler, M., et al. (2010). History of anthropogenic nitrogen input to the German Bight/SE North Sea as reflected by nitrogen isotopes in surface sediments, sediment cores and hindcast models. *Continental Shelf Research* 30(15)**,** 1626-1638. doi: https://doi.org/10.1016/j.csr.2010.06.010.

Shi, J.H., Gao, H.W., Zhang, J., Tan, S.C., Ren, J.L., Liu, C.G., et al. (2012). Examination of causative link between a spring bloom and dry/wet deposition of Asian dust in the Yellow Sea, China. *Journal of Geophysical Research: Atmospheres* 117(D17).

Sigman, D., Robinson, R., Knapp, A., Van Geen, A., McCorkle, D., Brandes, J., et al. (2003). Distinguishing between water column and sedimentary denitrification in the Santa Barbara Basin using the stable isotopes of nitrate. *Geochemistry, Geophysics, Geosystems* 4(5).

Sigman, D.M., Altabet, M.A., Michener, R., McCorkle, D.C., Fry, B., and Holmes, R.M. (1997). Natural abundance-level measurement of the nitrogen isotopic composition of oceanic nitrate: an adaptation of the ammonia diffusion method. *Marine Chemistry* 57(3)**,** 227-242. doi: https://doi.org/10.1016/S0304-4203(97)00009-1.

Sigman, D.M., and Boyle, E.A. (2000). Glacial/interglacial variations in atmospheric carbon dioxide. *Nature* 407(6806)**,** 859-869. doi: 10.1038/35038000.

Sigman, D.M., Casciotti, K.L., Andreani, M., Barford, C., Galanter, M., and Böhlke, J. (2001). A bacterial method for the nitrogen isotopic analysis of nitrate in seawater and freshwater. *Analytical chemistry* 73(17)**,** 4145-4153. doi: https://doi.org/10.1021/ac010088e.

Sigman, D.M., DiFiore, P.J., Hain, M.P., Deutsch, C., Wang, Y., Karl, D.M., et al. (2009). The dual isotopes of deep nitrate as a constraint on the cycle and budget of oceanic fixed nitrogen. *Deep Sea Research Part I: Oceanographic Research Papers* 56(9)**,** 1419-1439. doi: https://doi.org/10.1016/j.dsr.2009.04.007.

Sigman, D.M., and Fripiat, F. (2019). "Nitrogen Isotopes in the Ocean," in *Encyclopedia of Ocean Sciences (Third Edition),* eds. J.K. Cochran, H.J. Bokuniewicz & P.L. Yager. (Oxford: Academic Press), 263-278.

Sigman, D.M., Granger, J., DiFiore, P.J., Lehmann, M.M., Ho, R., Cane, G., et al. (2005). Coupled nitrogen and oxygen isotope measurements of nitrate along the eastern North Pacific margin. *Global Biogeochemical Cycles* 19(4). doi: https://doi.org/10.1029/2005GB002458.

Smith, S.V., Swaney, D.P., Talaue-Mcmanus, L., Bartley, J.D., Sandhei, P.T., McLAUGHLIN, C.J., et al. (2003). Humans, hydrology, and the distribution of inorganic nutrient loading to the ocean. *BioScience* 53(3)**,** 235-245. doi: https://doi.org/10.1641/0006-3568(2003)053[0235:HHATDO]2.0.CO;2.

Soares, M. (2000). Biological denitrification of groundwater. *Water, Air, and Soil Pollution* 123(1-4)**,** 183-193.

Song, G., Liu, S., Zhang, J., Zhu, Z., Zhang, G., Marchant, H.K., et al. (2021). Response of benthic nitrogen cycling to estuarine hypoxia. *Limnology and Oceanography* 66(3), 652-666. doi: https://doi.org/10.1002/lno.11630.

Song, G., Liu, S., Zhu, Z., Zhai, W., Zhu, C., and Zhang, J. (2016a). Sediment oxygen consumption and benthic organic carbon mineralization on the continental shelves of the East China Sea and the Yellow Sea. *Deep Sea Research Part II: Topical Studies in Oceanography* 124, 53-63.

Song, N.-q., Wang, N., Lu, Y., and Zhang, J.-r. (2016b). Temporal and spatial characteristics of harmful algal blooms in the Bohai Sea during 1952–2014. *Continental Shelf Research* 122, 77-84. doi: https://doi.org/10.1016/j.csr.2016.04.006.

Song, W., Liu, X.-Y., Wang, Y.-L., Tong, Y.-D., Bai, Z.-P., and Liu, C.-Q. (2020). Nitrogen isotope differences between atmospheric nitrate and corresponding nitrogen oxides: A new constraint using oxygen isotopes. *Science of The Total Environment* 701, 134515. doi: https://doi.org/10.1016/j.scitotenv.2019.134515.

Su, J. (2001). A review of circulation dynamics of the coastal oceans near China (in Chinese). *Acta Oceanologica Sinica* 23(4), 1-16. doi: 10.3321/j.issn:0253-4193.2001.04.001.

Su, N., Du, J., Liu, S., and Zhang, J. (2013). Nutrient fluxes via radium isotopes from the coast to offshore and from the seafloor to upper waters after the 2009 spring bloom in the Yellow Sea. *Deep Sea Research Part II: Topical Studies in Oceanography* 97, 33-42.

Sugimoto, R., Kasai, A., Miyajima, T., and Fujita, K. (2009). Transport of oceanic nitrate from the continental shelf to the coastal basin in relation to the path of the Kuroshio. *Continental Shelf Research* 29(14), 1678-1688. doi: https://doi.org/10.1016/j.csr.2009.05.013.

Sun, J., Feng, Y., Wang, D., Song, S., Jiang, Y., Ding, C., et al. (2013). Bottom-up control of phytoplankton growth in spring blooms in Central Yellow Sea, China. *Deep Sea Research Part II: Topical Studies in Oceanography* 97, 61-71.

Sun, R., Li, T., and Chang, F. (2009). Distribution of benthic foraminifera and its bearing on marine environmental factors in the north Yellow Sea serface sediments. *Marine Geology & Quaternary Geology (in Chineses)* 29(4), 21-28. doi: 10.3724/sp.J.1140.2009.04021.

Umezawa, Y., Yamaguchi, A., Ishizaka, J., Hasegawa, T., Yoshimizu, C., Tayasu, I., et al. (2013). Seasonal shifts in the contributions of the Changjiang River and the Kuroshio Current to nitrate dynamics at the continental shelf of the northern East China Sea based on a nitrate dual isotopic composition approach. *Biogeosciences Discussions* 10, 10143-10188. doi: https://doi.org/10.5194/bg-11-1297-2014.

Voss, M., Bange, H.W., Dippner, J.W., Middelburg, J.J., Montoya, J.P., and Ward, B.J.P.T.R.S.B. (2013). The marine nitrogen cycle: recent discoveries, uncertainties and the potential relevance of climate change. 368(1621), 20130121.

Voss, M., Dippner, J.W., and Montoya, J.P. (2001). Nitrogen isotope patterns in the oxygen-deficient waters of the Eastern Tropical North Pacific Ocean. *Deep Sea Research Part I: Oceanographic Research Papers* 48(8), 1905-1921. doi: https://doi.org/10.1016/S0967-0637(00)00110-2.

Wang, B., Xin, M., Wei, Q., and Xie, L. (2018). A historical overview of coastal eutrophication in the China Seas. *Mar Pollut Bull* 136, 394-400. doi: 10.1016/j.marpolbul.2018.09.044.

Wang, J., Beusen, A.H.W., Liu, X., and Bouwman, A.F. (2020a). Aquaculture Production is a Large, Spatially Concentrated Source of Nutrients in Chinese Freshwater and Coastal Seas.

Environmental Science & Technology 54(3), 1464-1474. doi: 10.1021/acs.est.9b03340.

Wang, J., Beusen, A.H.W., Liu, X., Van Dingenen, R., Dentener, F., Yao, Q., et al. (2020b). Spatially Explicit Inventory of Sources of Nitrogen Inputs to the Yellow Sea, East China Sea, and South China Sea for the Period 1970–2010. *Earth's Future* 8(10), e2020EF001516. doi: https://doi.org/10.1029/2020EF001516.

Wang, J., Bouwman, A.F., Liu, X., Beusen, A.H.W., Van Dingenen, R., Dentener, F., et al. (2021). Harmful Algal Blooms in Chinese Coastal Waters Will Persist Due to Perturbed Nutrient Ratios. *Environmental Science & Technology Letters* 8(3), 276-284. doi: 10.1021/acs.estlett.1c00012.

Wang, J., Yu, Z., Wei, Q., Yang, F., Dong, M., Li, D., et al. (2020c). Intra-and inter-seasonal variations in the hydrological characteristics and nutrient conditions in the southwestern Yellow Sea during spring to summer. *Marine Pollution Bulletin* 156, 111139.

Wang, J., Yu, Z., Wei, Q., and Yao, Q. (2019). Long-term nutrient variations in the Bohai Sea over the past 40 years. *Journal of Geophysical Research: Oceans* 124(1), 703-722. doi: https://doi.org/10.1029/2018JC014765.

Wang, W., Yu, Z., Song, X., Wu, Z., Yuan, Y., Zhou, P., et al. (2016). The effect of Kuroshio Current on nitrate dynamics in the southern East China Sea revealed by nitrate isotopic composition. *Journal of Geophysical Research: Oceans* 121(9), 7073-7087. doi: https://doi.org/10.1002/2016JC011882.

Wang, W., Yu, Z., Song, X., Wu, Z., Yuan, Y., Zhou, P., et al. (2017). Characteristics of the $\delta^{15} N_{NO_3}$ $\delta15NNO3$ distribution and its drivers in the Changjiang River estuary and adjacent waters. *Chinese Journal of Oceanology and Limnology* 35(2), 367-382. doi: 10.1007/s00343-016-5276-x.

Wang, X., Li, H., Jiao, J.J., Barry, D.A., Li, L., Luo, X., et al. (2015). Submarine fresh groundwater discharge into Laizhou Bay comparable to the Yellow River flux. *Scientific Reports* 5, 8814. doi: https://doi.org/10.1038/srep08814.

Wang, X., Ma, H., Li, R., Song, Z., and Wu, J. (2012). Seasonal fluxes and source variation of organic carbon transported by two major Chinese Rivers: The Yellow River and Changjiang (Yangtze) River. *Global Biogeochemical Cycles* 26(2).

Wankel, S.D., Kendall, C., Francis, C.A., and Paytan, A. (2006). Nitrogen sources and cycling in the San Francisco Bay Estuary: A nitrate dual isotopic composition approach. *Limnology and Oceanography* 51(4), 1654-1664. doi: https://doi.org/10.4319/lo.2006.51.4.1654.

Wankel, S.D., Kendall, C., Pennington, J.T., Chavez, F.P., and Paytan, A. (2007). Nitrification in the euphotic zone as evidenced by nitrate dual isotopic composition: Observations from Monterey Bay, California. *Global Biogeochemical Cycles* 21(2). doi: https://doi.org/10.1029/2006GB002723.

Wei, Q.-S., Yu, Z.-G., Wang, B.-D., Fu, M.-Z., Xia, C.-S., Liu, L., et al. (2016). Coupling of the spatial–temporal distributions of nutrients and physical conditions in the southern Yellow Sea. *Journal of Marine Systems* 156, 30-45.

Wei, Q., Yao, Q., Wang, B., Wang, H., and Yu, Z. (2015). Long-term variation of nutrients in the southern Yellow Sea. *Continental Shelf Research* 111, 184-196.

Wei, Q., 周明, 魏修华, 臧家业, and 战闰 (2010a). 冬季南黄海海水化学要素的分布特征及变化趋势. *海洋科学进展* 28(3), 11.

Wei, Q.S., Wei, X.H., Xie, L.P., Zang, J.Y., and Zhan, R. (2010b). Features of Dissolved Oxygen

Distribution and Its Effective Factors in the Southern Yellow Sea in Spring,2007. *Advances in Marine Science*.

Wong, G.T. (2012). Removal of nitrite interference in the Winkler determination of dissolved oxygen in seawater. *Marine Chemistry* 130, 28-32. doi: https://doi.org/10.1016/j.marchem.2011.11.003.

Wu, J., Calvert, S.E., and Wong, C.S. (1997). Nitrogen isotope variations in the subarctic northeast Pacific: relationships to nitrate utilization and trophic structure. *Deep Sea Research Part I: Oceanographic Research* 44, 287. doi: 10.1016/s0967-0637(96)00099-4.

Wu, S. (1991). Oxygen isotope compositions of seawaters in the Huanghai (Yellow) Sea and the Bohai Sea. *Science in China, Ser. B* (3), 8. doi: CNKI:SUN:JBXG.0.1991-03-008.

Wu, Z., Yu, Z., Song, X., Wang, W., Zhou, P., Cao, X., et al. (2019). Key nitrogen biogeochemical processes in the South Yellow Sea revealed by dual stable isotopes of nitrate. *Estuarine, Coastal and Shelf Science* 225, 106222. doi: https://doi.org/10.1016/j.ecss.2019.05.004.

Xiao, X., Agustí, S., Pan, Y., Yu, Y., Li, K., Wu, J., et al. (2019). Warming Amplifies the Frequency of Harmful Algal Blooms with Eutrophication in Chinese Coastal Waters. *Environmental Science & Technology* 53(22), 13031-13041. doi: 10.1021/acs.est.9b03726.

Xin, M., Wang, B., Xie, L., Sun, X., Wei, Q., Liang, S., et al. (2019). Long-term changes in nutrient regimes and their ecological effects in the Bohai Sea, China. *Marine Pollution Bulletin* 146, 562-573. doi: https://doi.org/10.1016/j.marpolbul.2019.07.011.

Xiong, T.-q., Wei, Q.-s., Zhai, W.-d., Li, C.-l., Wang, S.-y., Zhang, Y.-x., et al. (2020). Comparing Subsurface Seasonal Deoxygenation and Acidification in the Yellow Sea and Northern East China Sea Along the North-to-South Latitude Gradient. *Frontiers in Marine Science* 7(686). doi: 10.3389/fmars.2020.00686.

Xu, S., Song, J., Li, X., Yuan, H., Li, N., Duan, L., et al. (2010). Changes in nitrogen and phosphorus and their effects on phytoplankton in the Bohai Sea. *Chinese Journal of Oceanology and Limnology* 28(4), 945-952. doi: 10.1007/s00343-010-0005-3.

Xu, Z., Liu, S., Xiang, R., and Song, G. (2017). Live benthic foraminifera in the Yellow Sea and the East China Sea: vertical distribution, nitrate storage, and potential denitrification. *Marine Ecology Progress Series* 571, 65-81. doi: 10.3354/meps12135.

Xue, A.L., Ming, X.B., Lz, B., Ts, B., Zhao, G.B., and Jw, B. (2012). Surface partial pressure of CO 2 and air–sea exchange in the northern Yellow Sea. *Journal of Marine Systems* s 105–108, 194-206.

Xue, D., Botte, J., De Baets, B., Accoe, F., Nestler, A., Taylor, P., et al. (2009). Present limitations and future prospects of stable isotope methods for nitrate source identification in surface-and groundwater. 43(5), 1159-1170.

Yang, F., Wei, Q., Chen, H., and Yao, Q. (2018a). Long-term variations and influence factors of nutrients in the western North Yellow Sea, China. *Marine Pollution Bulletin* 135, 1026-1034. doi: https://doi.org/10.1016/j.marpolbul.2018.08.034.

Yang, Z., Chen, J., Li, H., Jin, H., Gao, S., Ji, Z., et al. (2018b). Sources of nitrate in Xiangshan Bay (China), as identified using nitrogen and oxygen isotopes. *Estuarine, Coastal and Shelf Science* 207, 109-118. doi: https://doi.org/10.1016/j.ecss.2018.02.019.

Yellow River Conservancy Commission of MWR, C. (2019). "Yellow River Sediment Bulletin 2018 (in Chinese)". (Zhengzhou: Yellow River Conservancy Commission of MWR, China).

Yu, G., Jia, Y., He, N., Zhu, J., Chen, Z., Wang, Q., et al. (2019). Stabilization of atmospheric nitrogen

deposition in China over the past decade. *Nature Geoscience* 12(6)**,** 424-429. doi: 10.1038/s41561-019-0352-4.

Yu, H., Yu, Z., Song, X., Cao, X., Yuan, Y., and Lu, G. (2015). Seasonal variations in the nitrogen isotopic composition of dissolved nitrate in the Changjiang River estuary, China. *Estuarine, Coastal and Shelf Science* 155**,** 148-155. doi: https://doi.org/10.1016/j.ecss.2015.01.017.

Yu, J., Zhang, W., Tan, Y., Zong, Z., Hao, Q., Tian, C., et al. (2021). Dual-isotope-based source apportionment of nitrate in 30 rivers draining into the Bohai Sea, north China. *Environmental Pollution* 283**,** 117112. doi: https://doi.org/10.1016/j.envpol.2021.117112.

Yu, Q., Lou, A., Zhang, X., and Li, N. (2018). Numerical Analysis on the Impact of Main River Runoff on the Plain Distribution in the Low-Salinity Area at North Liaodong Bay. *Transactions of Oceanology and Limnology (in CHinese)* (2)**,** 88-96.

Yu, X., Guo, X., and Gao, H. (2020). Detachment of Low-Salinity Water From the Yellow River Plume in Summer. *Journal of Geophysical Research: Oceans* 125(10)**,** e2020JC016344. doi: https://doi.org/10.1029/2020JC016344.

Yuan, C., Wang, Y., and Wei, H. (2014). Estimating the budgets of nutrients for phytoplankton bloom in the central Yellow Sea using a modified lower tropic ecosystem model. *Journal of Ocean University of China* 13(1)**,** 1-12.

Yue, F.-J., Li, S.-L., Liu, C.-Q., Zhao, Z.-Q., and Hu, J. (2013). Using dual isotopes to evaluate sources and transformation of nitrogen in the Liao River, northeast China. *Applied Geochemistry* 36**,** 1-9. doi: https://doi.org/10.1016/j.apgeochem.2013.06.009.

Zhai, W.d., Zhao, H.d., Su, J.l., Liu, P.f., Li, Y.w., and Zheng, N. (2019). Emergence of summertime hypoxia and concurrent carbonate mineral suppression in the central Bohai Sea, China. *Journal of Geophysical Research: Biogeosciences* 124(9)**,** 2768-2785.

Zhang, G., Zhang, J., and Liu, S. (2007). Characterization of nutrients in the atmospheric wet and dry deposition observed at the two monitoring sites over Yellow Sea and East China Sea. *Journal of Atmospheric Chemistry* 57(1)**,** 41-57. doi: 10.1007/s10874-007-9060-3.

Zhang, J., Huang, W.W., Létolle, R., and Jusserand, C. (1995). Major element chemistry of the Huanghe (Yellow River), China - weathering processes and chemical fluxes. *Journal of Hydrology* 168(1)**,** 173-203. doi: https://doi.org/10.1016/0022-1694(94)02635-O.

Zhang, J., Yu, Z., Raabe, T., Liu, S., Starke, A., Zou, L., et al. (2004). Dynamics of inorganic nutrient species in the Bohai seawaters. *Journal of marine systems* 44(3-4)**,** 189-212. doi: https://doi.org/10.1016/j.jmarsys.2003.09.010.

Zhang, L., Song, L., Zhang, L., Shao, H., Chen, X., and Yan, K. (2013). Seasonal dynamics in nitrous oxide emissions under different types of vegetation in saline-alkaline soils of the Yellow River Delta, China and implications for eco-restoring coastal wetland. *Ecological engineering* 61**,** 82-89. doi: https://doi.org/10.1016/j.ecoleng.2013.09.065.

Zhang, S., Wang, Q., Lü, Y., Cui, H., and Yuan, Y. (2008a). Observation of the seasonal evolution of the Yellow Sea Cold Water Mass in 1996–1998. *Continental Shelf Research* 28(3)**,** 442-457.

Zhang, X., Ward, B.B., and Sigman, D.M. (2020). Global Nitrogen Cycle: Critical Enzymes, Organisms, and Processes for Nitrogen Budgets and Dynamics. *Chemical Reviews*.

Zhang, X., Zhang, Q., Yang, A., Hou, L., Zheng, Y., Zhai, W., et al. (2018). Incorporation of Microbial Functional Traits in Biogeochemistry Models Provides Better Estimations of Benthic Denitrification and Anammox Rates in Coastal Oceans. *Journal of Geophysical Research: Biogeosciences* 123(10)**,** 3331-3352. doi: https://doi.org/10.1029/2018JG004682.

Zhang, Y., Liu, X., Fangmeier, A., Goulding, K., and Zhang, F. (2008b). Nitrogen inputs and isotopes in precipitation in the North China Plain. *Atmospheric Environment* 42(7)**,** 1436-1448. doi: https://doi.org/10.1016/j.atmosenv.2007.11.002.

Zhang, Y., Yu, Q., Ma, W., and Chen, L. (2010). Atmospheric deposition of inorganic nitrogen to the eastern China seas and its implications to marine biogeochemistry. *Journal of Geophysical Research: Atmospheres* 115(D7).

Zhang, Z., Zheng, N., Zhang, D., Xiao, H., Cao, Y., and Xiao, H. (2019). Rayleigh based concept to track NOx emission sources in urban areas of China. *Science of The Total Environment*, 135362. doi: https://doi.org/10.1016/j.scitotenv.2019.135362.

Zhao, L., Wei, H., and Feng, S. (2002). *Annual Cycle and Budgets of Nutrients in the bohai Sea.*

Zhao, Y., Zhang, L., Chen, Y., Liu, X., Xu, W., Pan, Y., et al. (2017). Atmospheric nitrogen deposition to China: A model analysis on nitrogen budget and critical load exceedance. *Atmospheric Environment* 153**,** 32-40. doi: https://doi.org/10.1016/j.atmosenv.2017.01.018.

Zheng, L.-w., and Zhai, W.-d. (2021). Excess nitrogen in the Bohai and Yellow seas, China: Distribution, trends, and source apportionment. *Science of The Total Environment* 794**,** 148702. doi: https://doi.org/10.1016/j.scitotenv.2021.148702.

Zhong, X., Yan, M., Ning, X., Yan, Z., and Xin, Y. (2020). Nitrate processing traced by nitrate dual isotopic composition in the early spring in the Changjiang (Yangtze River) Estuary and adjacent shelf areas. *Marine Pollution Bulletin* 161**,** 111699. doi: https://doi.org/10.1016/j.marpolbul.2020.111699.

Zhou, J., Zhu, Z.-Y., Hu, H.-T., Zhang, G.-L., and Wang, Q.-Q. (2021). Clarifying Water Column Respiration and Sedimentary Oxygen Respiration Under Oxygen Depletion Off the Changjiang Estuary and Adjacent East China Sea. *Frontiers in Marine Science* 7(1229). doi: 10.3389/fmars.2020.623581.

Zong, Z., Wang, X., Tian, C., Chen, Y., Fang, Y., Zhang, F., et al. (2017). First Assessment of NOx Sources at a Regional Background Site in North China Using Isotopic Analysis Linked with Modeling. *Environmental Science & Technology* 51(11)**,** 5923-5931. doi: 10.1021/acs.est.6b06316.

Appendix

Appendix A1 Dissolved oxygen and apparent oxygen utilization

For comparing the spatial and seasonal variability of DO, we use AOU to eliminate the temperature effect on solubility. In spring, the average AOU was -0.77 ± 0.26 mg L^{-1} ($n = 57$) and ranged from -1.47 mg L^{-1} to -0.48 mg L^{-1}, respectively. The AOU pattern was homogeneous over the water column (Figure A1.1) and decreased in southeast and eastward direction to the BH strait (Figure A1.2).

In summer, the average AOU was 0.82 ± 1.58 mg L^{-1} ($n = 76$) and ranged between -1.89 to $+3.58$ mg L^{-1}. AOU vertical distribution mirrored stratification with significant negative values below the thermocline caused by respiration processes such as remineralization and nitrification.
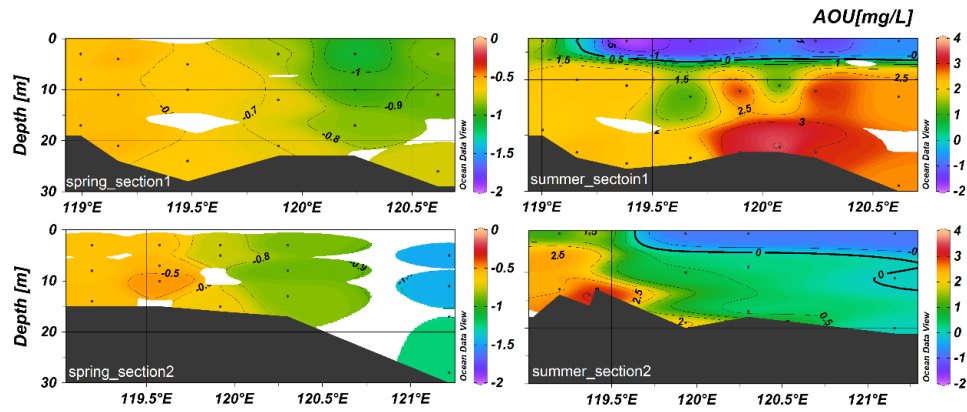
Figure A1.1. Profiles of AOU in spring and summer in the BHS (note that the eastern most station of section 2 in spring was changed from site B36 to site B35 due to missing DO data at B36)
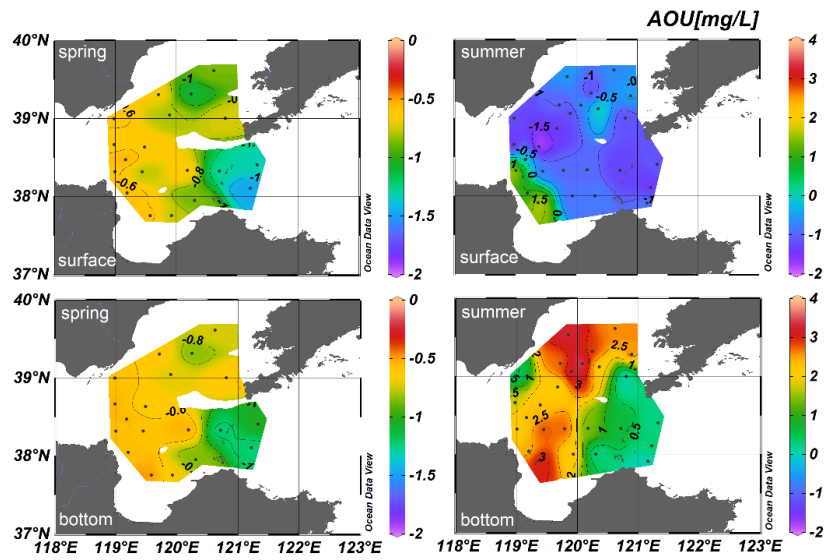

Figure A1.2. Horizontal distributions of AOU in spring and summer in the BHS

Appendix A2 Summary of results of the Bohai Sea

Table A2.1 Summary of results of Chapter 2

	Spring		Summer	
	Range	Average± Std Dev	Range	Average± Std Dev
Salinity/psu	29.9-32.8	32.3±0.5 (n=72)	28.5-32.5	31.6±0.8 (n=88)
Temperature/°C	2.9-6.7	4.7±0.8°C (n=72)	9.5-30.1	22.4±4.2 (n=88)
NO_3^-/μmol/L	0.3-31.1	6.5±5.8 (n=72)	0.1-13.6	1.9±2.7 (n=85)
NO_2^-/μmol/L	0.0-1.0	0.2±0.2 (n=72)	0.0-4.6	0.8±1.1 (n=85)
NH_4^+/μmol/L	0.2-2.7	0.8±0.5 (n=72)	0.1-7.8	1.6±1.9 (n=85)
PO_4^{3-}/μmol/L	0.1-0.7	0.4±0.2 (n=72)	0.0-0.3	0.1±0.1 (n=85)
SiO_3^-/μmol/L	0.2-13.9	5.3±3.1 (n=72)	1.3-17.0	7.7±3.2 (n=85)
δ^{15}N/‰	5.7-9.7	7.5±1.3 (n=52)	3.5 – 23.9	9.9±3.5 (n=23)
δ^{18}O/‰	5.0-19.8	11.3±2.5 (n=52)	3.1 – 18.4	8.7±3.3 (n=23)
SPM/ mg/L	2.3 - 44.3	10.6±8.0 (n=72)	5.7 - 82.9	22.2±16.5 (n=85)
TOC/%	0.6 - 6.9	2.7±1.7 (n=72)	0.8 - 6.3	2.1±1.2 (n=83)
TN/%	0.1 - 1.8	0.5±0.4 (n=72)	0.1 - 1.4	0.4±0.3 (n=83)
δ^{15}N-SPM/‰	3.2 - 6.2	4.8±0.9 (n=14)	3.9 - 7.2	5.7±0.8 (n=34)
DO/mg/L	10.27 - 11.47	10.84±0.35 (n=57)	3.84 - 8.86	6.22±1.37 (n=57)
AOU/mg/L	-0.48 - -1.47	0.77±0.26 (n=57)	-1.89 - +3.58	0.82±1.58 (n=76)

Appendix A3 The distribution of SPM and its nitrogen isotope
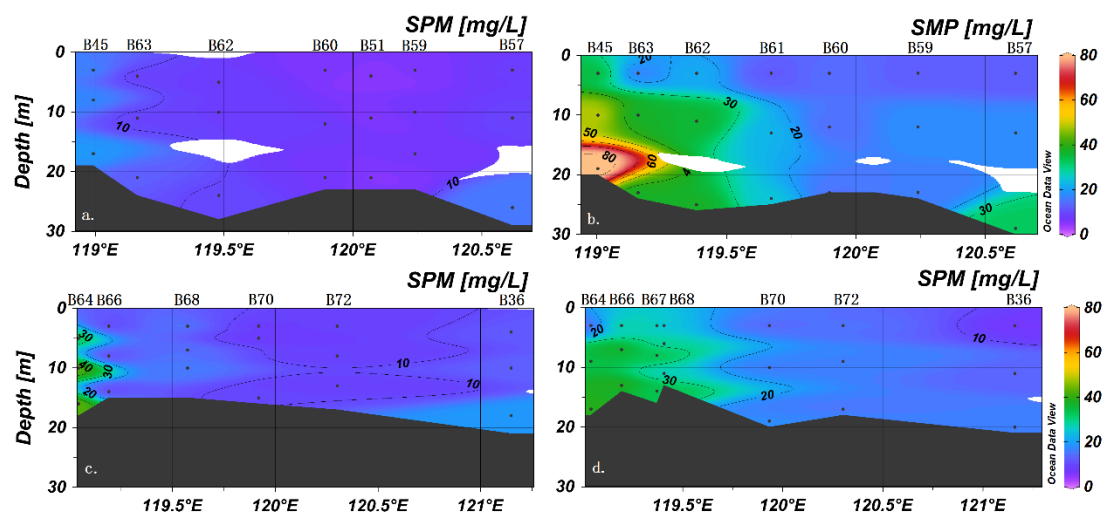

Figure A3.1. Suspended particulate matter concentrations of section 1 (a) and section 2 (c) of spring and section 1 (b) and section 2 (d) of summer.
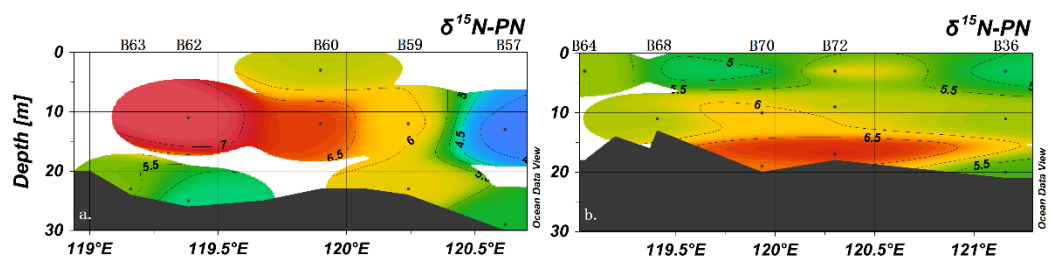

Figure A3.2. Profiles of δ^{15}N of particulate nitrogen in summer (a. section 1, b. section 2)

Appendix A4 The estimate of two end member mixing of nitrate and impact of underestimate of isotopes in summer

Only a subset of samples could be analyzed due to the low nitrate concentrations in summer, and most of these are from the Yellow River Diluted Water that had $[NO_3^-]$ >1.7μmol L^{-1}. The average values of δ^{15}N and δ^{18}O of the Bohai Sea in summer were 9.9 ± 3.5 ‰ (n = 23) and 8.7 ± 3.3 ‰ (n = 23). Although no measurements are available that could better constrain the seasonal range of nitrate isotope values, the lacking isotope data can be roughly estimated:

According to the T-S patten in summer, the Bohai Sea water can be considered as a two-end member mixture between fresh water discharged from Yellow River (YR) and sea water of central Bohai Sea, the nitrate concentration only affected by physically mixing hence can be calculated. The YR provides warm, fresh and nitrate enriched water whereas cold, saline and nitrate depleted water was observed near the area of the outer Liaodong Bay in both spring and summer. Thus, there were two end members to be considered in a mixing model. One should be aware that a contribution of atmospheric nitrogen is included in the marine end member as well.
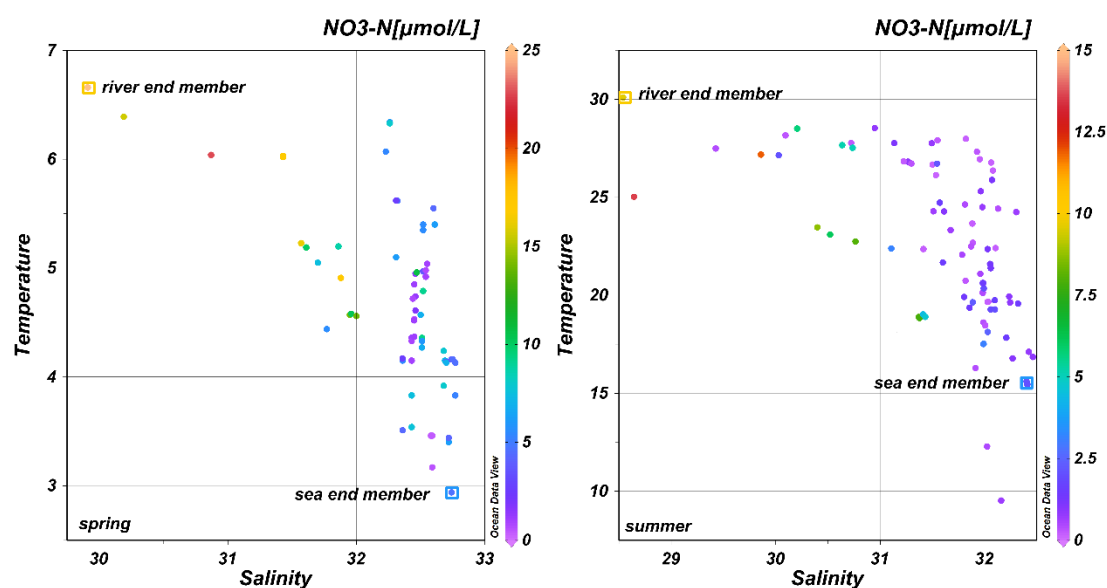

Figure A4.1. Temperature vs. salinity in Bohai Sea in spring (left) and summer (right). The values adopted for the two nitrate end members were mainly based on this pattern

The values of these two end members are shown in Table A4.1. The summer basic pattern of temperature and salinity was similar to that of spring. Thus, the fraction of water originating from YR and the BHS during the mixing process can be calculated follow A4.1 and A4.2:

$$S = S_r \times f_r + S_s \times f_s \quad (A4.1)$$

$$f_r + f_s = 1 \quad (A4.2)$$

where S, S_r and S_s refers to the observed salinity in study area, the end member value of river and sea, respectively. f_r and f_s refers to the fraction of river and sea water, respectively. The modeled nitrate concentration and modeled $\delta^{15}N$ and $\delta^{18}O$ values can be calculated following equations A4.3, A4.4 and A4.5:

$$[NO_3^-]_m = [NO_3^-]_r \times f_r + [NO_3^-]_s \times f_s \quad (A4.3)$$

$$\delta^{15}N_m[NO_3^-]_m = \delta^{15}N_r[NO_3^-]_r + \delta^{15}N_s[NO_3^-]_s \quad (A4.4)$$

$$\delta^{18}O_m[NO_3^-]_m = \delta^{18}O_r[NO_3^-]_r + \delta^{18}O_s[NO_3^-]_s \quad (A4.5)$$

where $[NO_3^-]_m$, $[NO_3^-]_r$ and $[NO_3^-]_r$ refers to the modeled nitrate concentration and the end member nitrate concentration values of river and sea, respectively. $\delta^{15}N_m/\delta^{18}O_m$, $\delta^{15}N_r/\delta^{18}O_r$ and $\delta^{15}N_s/\delta^{18}O_s$ refer to the modeled $\delta^{15}N$ and $\delta^{18}O$ values, and the end member $\delta^{15}N$ and $\delta^{18}O$ values of river and sea, respectively.

Table A4.1. Two end member values in Bohai Sea

		Riverine	Marine
spring	Salinity	29.9	33.0
	Nitrate/$\mu mol\ L^{-1}$	31.1	6.0
	$\delta^{15}N$‰	9.5	6.0
	$\delta^{18}O$‰	6.8	12.5
summer	Salinity	28.5	32.5
	Nitrate/$\mu mol\ L^{-1}$	13.6	2.0
	$\delta^{15}N$‰	9.9	9.5
	$\delta^{18}O$‰	5.3	8.2

The isotope effect of assimilation for nitrate in the Bohai Sea follows the "steady-state model" rather than the Rayleigh model because the Yellow River supplies nitrate continuously (Sigman and Fripiat, 2019). Thus, the estimated dual nitrate isotope values can be calculated according to equation A4.6 and A4.7:

$$\delta^{15}N_{reactant} = \delta^{15}N_{initial} + {}^{15}\varepsilon(1 - f) \quad (A4.6)$$

$$\delta^{18}O_{reactant} = \delta^{18}O_{initial} + {}^{18}\varepsilon(1 - f) \quad (A4.7)$$

In Eq. A4.6 and Eq. A4.7, f is equal to the observed nitrate concentration divided by of result of the two-end member model, $\delta^{15}N_{initrial}$ is equal to the end member of YR, and $\delta^{15}N_{reactant}$ is the estimated value of the residual nitrate, the value we need. The average of $^{15}\varepsilon$ and $^{18}\varepsilon$ adopted here are 5 ‰ (DiFiore et al., 2009; Granger et al., 2010; Umezawa

et al., 2013; Wang et al., 2016; Liu et al., 2017c; Wu et al., 2019).

The readjusted values of $\delta^{15}N$ and $\delta^{18}O$ for the Bohai Sea in summer is 12.8 ± 2.7 ‰ (n = 85) and 9.1 ± 1.9‰ (n = 85), respectively, resulting in seasonally averaged values of $\delta^{15}N$ and $\delta^{18}O$ of 10.3 ‰ and 10.6 ‰, respectively. These values induce about -36% to 21% deviations of the mass fluxes in our reference box model.
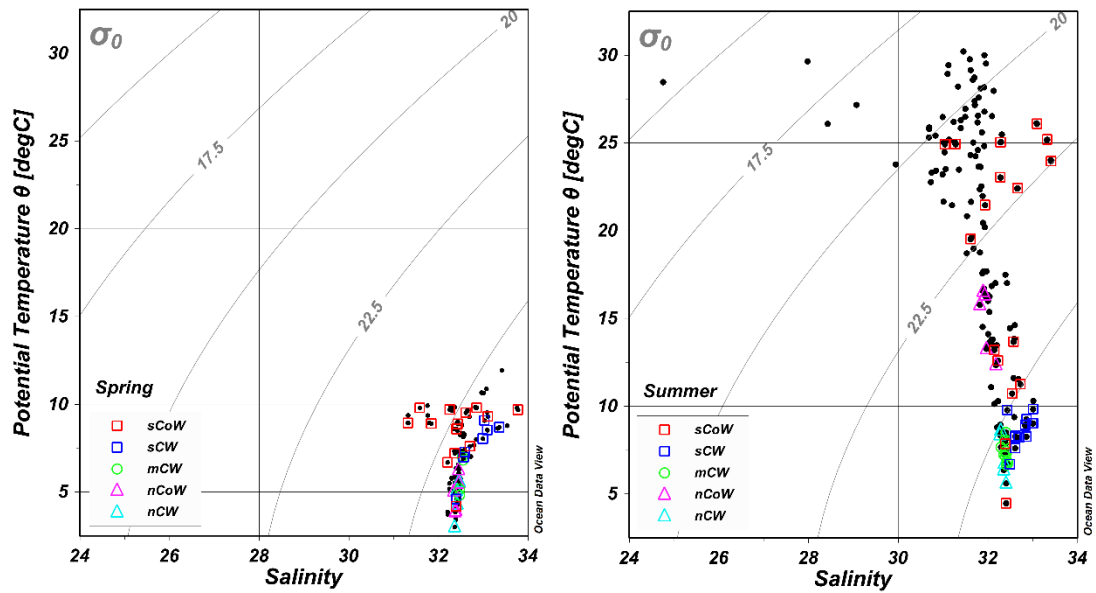
Appendix A5 The T-S diagram of Yellow Sea in spring and summer.

Figure A5.1. The T-S diagram of Yellow Sea in spring and summer. sCoW: south Coastal Water, sCW: south Cold Water, mCW: middle Cold Water, nCoW: north Coastal Water, nCW: north Cold Water. These water masses are all bottom water and grouped according to the temperature and locations. It is apparent that temperature and salinities for sCW, mCW and nCW are very similar in spring and summer.

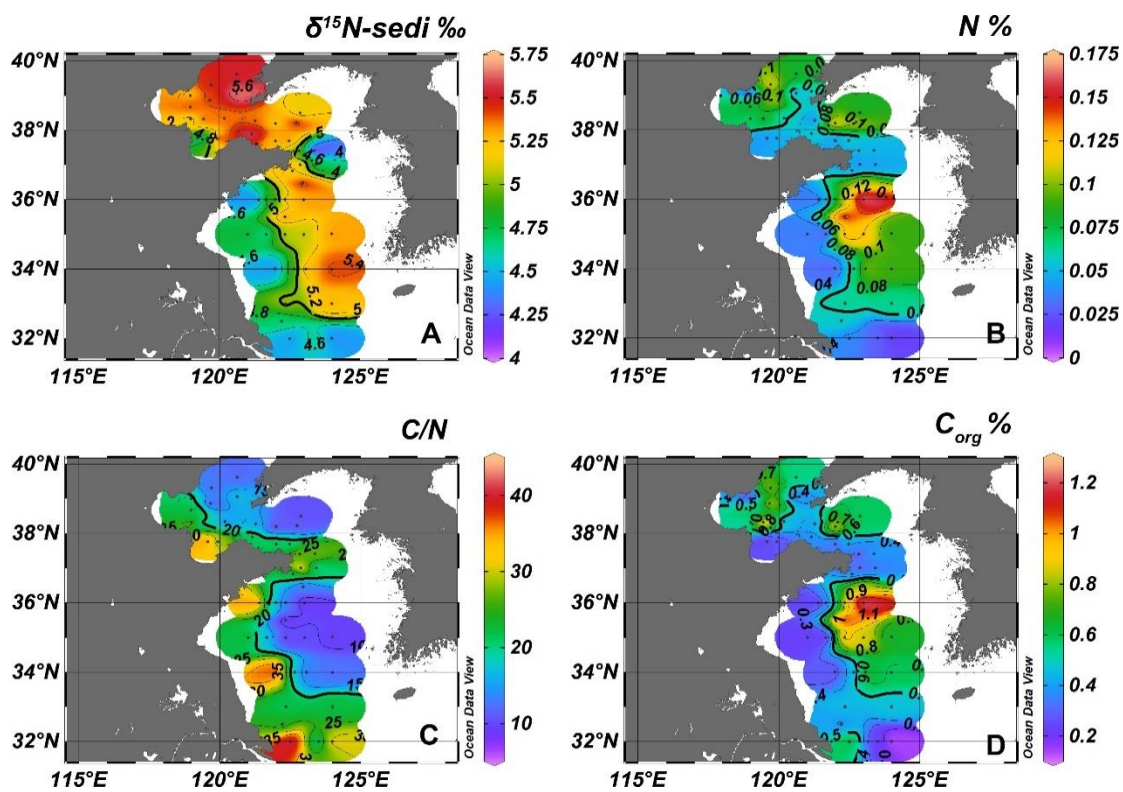## Appendix A6 Distributions of different parameters of the sediment

Figure A6.1. Distribution of $\delta^{15}N$ (A), N % (B), C/N ratio (C) and C_{org} (weight %) (D) in surface sediment of the Bohai Sea and Yellow Sea.

Acknowledgement

I would like to thank my supervisor Prof. Dr. Kay-Christian Emeis for giving me the opportunity to study with the group of Biogeochemistry. His professional and timely support developing the ideas for the papers, constructive discussions and revising my manuscripts were of tremendous help to me.

I am extending my thanks to my co-supervisor Dr. Birgit Gaye for the continuous support. She was always patient and helped with my manuscripts and meeting abstracts. She gave me encouragement every time, which lighted up my hardest moments.

I also thank Dr. Niko Lahajnar for his reliable support. He was always there offering the assistances on not only the laboratory work and cruise preparations, but also about how to live in Hamburg.

I further thank the whole Biogeochemistry working group. Frauke Langenberg and Marc Metzke helped a lot with measuring my samples and preparing my cruises. The results cannot be received without the help of the team. Dr. Natalie Harms also helped me with the doctoral issues of the university and is a nice office roommate. Carolin Perkuhn kindly helps a lot especially when I'm not in Hamburg.

I thank Dr. Kirstin Dähnke, Dipl.-Ing. Markus Ankele, Leon Schmidt, Dr. Tina Sanders, and Dr. Justus E. E. van Beusekom for the guidance, support, and discussion when I was analyzing nutrients and stable isotopes of nitrate at the Helmholtz-Zentrum Hereon, Geesthacht. I spent several months in Geesthacht and I very much appreciate the support by Markus Ankele who helped a lot with both, my experiments and my daily traveling between Geesthacht and Hamburg. Leon Schmidt also measured part of my nutrient samples and I enjoyed the conversations with him.

I would like to especially thank to Prof. Dr. Haiyan Jin and Prof. Dr. Jianfang Chen from Hangzhou, Dr. Zhiyong Xie from Geesthacht who recommended me to join part of the long-history Sino-German cooperating project. It is my great honor to be part of the friendship of scientists from China and Germany which had been rooted in the last century. I also thank to Prof. Dr. Yongming Luo, Prof. Dr. Jianhui Tang, Dr. Yuan Li and Dr. Chuancheng Fu from Yantai who helped so much on my cruises and field expedition in China. The crew and friends of Chinese research vessel *Dongfanghong 2* and German research vessel *Sonne* were so lovely and I appreciate their great help.

Finally, I thank my parents and my families who were always standing with me. My wife Huiru Liu supported me without doubt although she had to suffer from the separation. She is also the first and best audience of my scientific ideas. I also would

like to thank my dear friends in Hamburg and China, their company made my life more colorful.

To study in Germany is like my own Odyssey, I came to Hamburg four years ago with lots of concerns about unknowns, but I met great people here and opened my mind again. The numerous difficulties and happiness in science and life comprised my travel of gain, this memory will always be shining in my lifetime.

Publications

The attached article corresponding to Chapter 2 has been accepted in *Biogeosciences*:

> **Tian, S.**, Gaye, B., Tang, J., Luo, Y., Li, W., Lahajnar, N., Dähnke, K., Sanders, T., Xiong, T., Zhai, W., and Emeis, K.-C.: A reactive nitrogen budget of the Bohai Sea based on an isotope mass balance model, *Biogeosciences* Discuss. [preprint], https://doi.org/10.5194/bg-2020-471, accepted, 2020.

Author contributions:

> BG and KCE designed the study. ST collected the samples on board. JT and YL supported the sampling on cruises and field trips. ST, NL, and TS analyzed samples. TX and WZ supplied thses dissolved oxygen data. WL ran the HAMSOM model and calculated water mass exchanges. ST, BG, KCE and KD interpreted the data. ST prepared the manuscript with input from all co-authors.

The attached article corresponding to Chapter 3 has been published in *Frontiers of Marine Science*:

> **Tian, S.**, Gaye, B., Tang, J., Luo, Y., Lahajnar, N., Dähnke, K., et al. (2022). Nitrate Regeneration and Loss in the Central Yellow Sea Bottom Water Revealed by Nitrogen Isotopes. *Frontiers in Marine Science* 9. doi: 10.3389/fmars.2022.834953.

Author contributions:

> BG and K-CE designed the study. ST collected the samples on board. JT and YL supported the sampling on cruises and field trips. ST, NL, and TS analyzed samples. TX and WZ supplied the dissolved oxygen data. ST, BG, K-CE, and KD interpreted the data. ST prepared the manuscript with input from all co-authors. All authors contributed to the article and approved the submitted version.